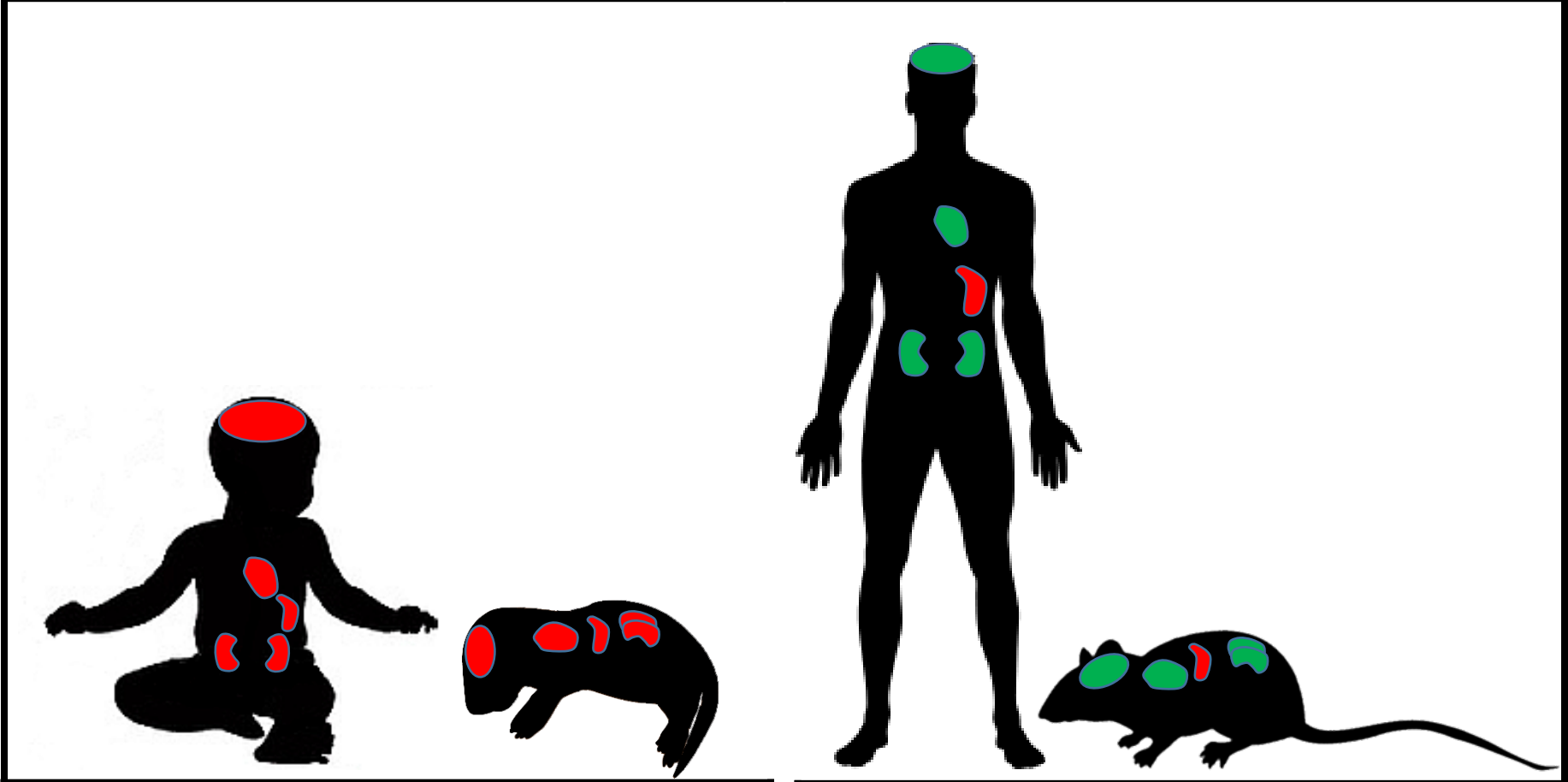


Developmental regulation of apoptosis in healthy tissues



Children/Pups	
Brain, Heart, Kidneys	Hematopoietic Organs
Status of apoptosis pathway:	
Primed for Apoptosis	Primed for Apoptosis
Expression of apoptotic machinery:	
High	High
Sensitivity to radiation or chemotherapy:	
High	High

Adults	
Brain, Heart, Kidneys	Hematopoietic Organs
Status of apoptosis pathway:	
Apoptosis Refractory	Primed for Apoptosis
Expression of apoptotic machinery:	
Low	High
Sensitivity to radiation or chemotherapy:	
Low	High

Developmental regulation of mitochondrial apoptosis by c-Myc governs age- and tissue-specific sensitivity to cancer therapeutics

Kristopher A. Sarosiek^{1,2}, Cameron Fraser¹, Nathiya Muthalagu³, Patrick D. Bhola^{1,2}, Weiting Chang^{2,4}, Samuel K. McBrayer^{1,2}, Adam Cantlon^{2,4}, Sudeshna Fisch^{2,4}, Gail Golomb-Mello⁵, Jeremy M. Ryan^{1,2}, Jing Deng^{1,2}, Brian Jian⁶, Chris Corbett⁷, Marti Goldenberg⁷, Joseph R. Madsen^{2,7}, Ronglih Liao^{2,4}, Dominic Walsh^{2,4}, John Sedivy⁵, Daniel J. Murphy^{3,8}, Daniel Ruben Carrasco^{1,2}, Shenandoah Robinson^{2,7}, Javid Moslehi^{9,10,11}, Anthony Letai^{1,2}

¹Dept of Medical Oncology, Dana-Farber Cancer Institute, Boston, MA 02215, USA

²Harvard Medical School, Boston, MA 02115, USA

³Cancer Research UK Beatson Institute, Glasgow, Scotland

⁴Brigham and Women's Hospital, Boston, MA 02115, USA

⁵Dept of Molecular Biology, Cell Biology and Biochemistry, Brown University, Providence, RI, 02912 USA

⁶Kaiser Permanente, Sacramento, CA 95815, USA

⁷Dept of Neurosurgery, Boston Children's Hospital, Boston, MA 02115, USA

⁸Institute of Cancer Sciences, University of Glasgow, Glasgow, Scotland

⁹Division of Cardiovascular Medicine, ¹⁰Division of Hematology-Oncology, ¹¹Cardio-Oncology Program, Dept of Medicine, Vanderbilt-Ingram Cancer Center, Vanderbilt University School of Medicine, Nashville, TN 37232, USA

For correspondence:

Anthony Letai M.D., Ph.D.,

Sarosiek, et al.

Dana Farber Cancer Institute

450 Brookline Avenue

Mayer 430

Boston, MA 02115

Tel: 617-582-7254

Fax: 617-582-8160

anthony_letai@dfci.harvard.edu

RUNNING TITLE: Apoptosis regulation in healthy tissues

SUMMARY

It is not understood why healthy tissues can exhibit varying levels of sensitivity to the same toxic stimuli. Using BH3 Profiling, we find that mitochondria of many adult somatic tissues, including brain, heart and kidneys, are profoundly refractory to pro-apoptotic signaling, leading to cellular resistance to cytotoxic chemotherapies and ionizing radiation. In contrast, mitochondria from these tissues in young mice and humans are primed for apoptosis, predisposing them to undergo cell death in response to genotoxic damage. While expression of the apoptotic protein machinery is nearly absent by adulthood, in young tissues its expression is driven by c-Myc, linking developmental growth to cell death. These differences may explain why pediatric cancer patients have a higher risk of developing treatment-associated toxicities.

SIGNIFICANCE

Pediatric cancer patients treated with ionizing radiation or cytotoxic chemotherapy have a high risk of developing devastating toxicities including cognitive decline and chronic heart failure, limiting the use of potentially curative therapies. These treatments, which rely on the preferential induction of an apoptotic cell death in cancer cells over healthy tissues, are comparatively well tolerated in adults, yet the molecular basis for this difference in sensitivity is unknown. Herein, we make the discovery that apoptosis is dynamically regulated during postnatal development in healthy tissues, altering cell fate in response to genotoxic damage induced by anti-cancer therapies. Importantly, we use mouse models to show that these pathways may be modulated to potentially prevent treatment-associated toxicities.

INTRODUCTION

The intrinsic, or mitochondrial, pathway of apoptosis is an evolutionarily-conserved and highly regulated form of cell death that is critical for development and homeostasis of multicellular organisms. The deregulation of apoptosis is associated with many pathologies including cancer (Hanahan and Weinberg, 2000). Apoptosis is triggered when a pro-apoptotic effector protein (BAX or BAK) is activated by an activator BH3-only protein, of which BIM and BID are most potent (Tait and Green, 2013). This results in the oligomerization of BAX or BAK, causing mitochondrial outer membrane permeabilization (MOMP) and consequent release of cytochrome *c* into the cytosol, where it complexes with APAF-1 to form the apoptosome. This complex activates downstream cysteine proteases, including caspase 3, that dismantle the cell and promote phagocytosis (Galluzzi et al., 2009; Taylor et al., 2008). However, anti-apoptotic proteins in this family (BCL-2, BCL-X_L, MCL-1, etc.) can block apoptosis by binding and sequestering monomeric BAX/BAK or BH3-only proteins (Czabotar et al., 2013). In order for apoptosis to occur, anti-apoptotic proteins within the cell must be overwhelmed and BAX and/or BAK activated.

The mitochondrial apoptosis pathway can be activated by a wide variety of cellular stressors including growth factor or nutrient deprivation as well as genotoxic damage from cytotoxic chemotherapies and radiation. In each of these cases, the basal state of the mitochondrial apoptotic pathway can alter the eventual fate of the cell (Sarosiek and Letai, 2016). To directly measure the functional state of the mitochondrial apoptotic pathway in cells, we developed the BH3 Profiling assay, which measures apoptotic priming (proximity of cellular mitochondria to the apoptotic threshold) by delivering titrated doses of distinct pro-apoptotic signals (BH3 peptides) to mitochondria while monitoring MOMP (Ryan and Letai, 2013). In this

assay, mitochondria bearing only a small reserve of unbound anti-apoptotic proteins undergo MOMP in response to even relatively low doses of pro-apoptotic peptides and are thus classified as “primed” for apoptosis; primed cells readily die when pro-death signals are generated in response to cellular damage or stress (Ni Chonghaile et al., 2011). In contrast, cells that contain a large reserve of unbound anti-apoptotic proteins are less sensitive to BH3 peptides and are classified as “unprimed;” unprimed cells must experience higher levels of damage or stress to trigger MOMP. Finally, cells that block apoptosis by not expressing sufficient levels of critical components of the cell death machinery (such as BAX and BAK) are classified as “apoptosis refractory.” We have previously shown that patients with primed cancers respond more favorably to chemotherapy than patients with unprimed cancers (Davids et al., 2012; Ni Chonghaile et al., 2011; Vo et al., 2012).

Chemotherapy and radiation treatments have cured cancer in millions of patients (American Cancer Society, 2014), yet the apoptotic cell death that these agents can induce in healthy tissues limits their use. This is especially true in pediatric patients who experience considerably higher levels of treatment-associated toxicity and morbidity from genotoxic agents. For example, brain irradiation is a critical component of the potentially curative treatment for brain tumors. However, radiation can also trigger cell death in healthy neurons in very young patients, resulting in permanent and devastating cognitive deficits with severity being inversely correlated with age (Merchant et al., 2010; Silber et al., 1992). Similarly, children with many types of cancers are commonly treated with anthracyclines including doxorubicin. However, doxorubicin treatment in children can cause thinning of the cardiac ventricular walls, a reduction in ventricular mass and consequent heart failure, with the youngest children again being most at risk (Lipshultz et al., 1995; Trachtenberg et al., 2011). Currently, parents and clinicians must balance the curative potential of these treatments with their potential for causing devastating

toxicities. It is unclear why young children are more at risk of developing these toxicities than adults.

Much of the study of apoptosis has been devoted to cancer and hematopoietic tissues, with relatively little study of other healthy somatic tissues. It is currently unknown whether cells that make up distinct tissues have varying levels of apoptotic priming, which could potentially contribute to their different sensitivities to classical apoptosis-inducing agents.

RESULTS

Many adult tissues are apoptosis refractory

We first performed BH3 Profiling on a comprehensive set of adult mouse tissues to detect any potential differences in their apoptotic priming. Cells of the hematopoietic lineage from the periphery (peripheral blood mononuclear cells [PBMCs]), thymus, spleen and bone marrow are the most primed cells in the body among those we studied, as indicated by high mitochondrial depolarization in response to BIM or BID BH3 peptides or full length proteins (Figures 1A-B and S1A). Cells (excluding blood) constituting the large intestine, small intestine, lungs and liver were relatively unprimed, as they required higher doses of BIM or BID BH3 peptides and a longer time period to trigger depolarization. Strikingly, we found adult brain, heart and kidney tissues are far less primed, and nearly completely insensitive to concentrations of BIM and BID BH3 (100 μ M) that are sufficient to induce MOMP in nearly every cancer cell line or primary cancer cell we have tested.

We previously found that apoptotic priming is a strong determinant of cancer cell fate in response to cytotoxic chemotherapies. We hypothesized that healthy tissue sensitivity to

genotoxic agents would be dependent on their degree of priming. To test this hypothesis, we exposed live adult mice to 8 Gray of gamma radiation and found that the degree of apoptosis induced in the tissues corresponded to their level of apoptotic priming (Figure 1C-D, S1B-C).

We next asked whether the profound differences in mitochondrial priming in adult tissues could be due to differences in expression of BCL-2 family proteins. While we might have expected to find reduced expression of pro-apoptotic proteins or increased expression of their anti-apoptotic counterparts, we instead found that both pro- and anti-apoptotic proteins were lacking in apoptosis refractory tissues (Figure 1E). BAX and BAK, two proteins that are required for mitochondrial apoptosis, were nearly undetectable in refractory tissues. These tissues also expressed lower levels of Caspases 3 and 8 to potentially further suppress cell death. We did not observe major differences in the expression of XIAP, a potent inhibitor of caspase activity, across adult tissues.

We next examined the levels of these proteins in human tissues by mining mass-spectrometry-based proteome data (Kim et al., 2014) and found that adult human tissues exhibit a similar pattern of protein expression to that of mice (Figure 1F, Tables S1 and S2), suggesting that mouse and human tissues regulate apoptosis similarly, which is consistent with previous work (Reed et al., 2003).

To test whether the lack of BAX and BAK in apoptosis refractory tissues was preventing activator-induced MOMP, we tested whether addition of recombinant BAX to mitochondria would restore sensitivity to BH3 peptides. While recombinant BAX alone did not induce MOMP, we detected efficient and complete MOMP in adult brain, heart and kidney tissues when administering BAX concurrently with even minute amounts of BIM (Figure 1G). These data indicate that neither BAX nor BAK are expressed at levels sufficient for MOMP in adult brain, heart and kidney tissues. Moreover, in these tissues there is lower expression of nearly all

proteins comprising the mitochondrial apoptotic machinery, both pro- and anti-apoptotic, and pre- and post-mitochondrial. This apoptotic resistance presumably protects vital, long-lived cells constituting these largely post-mitotic tissues from aberrant cell death. Operationally, we defined cells as apoptosis refractory when MOMP is not induced by BIM or BID BH3 at even 100 μ M, yet efficiently induced by low doses (1 μ M) of BIM BH3 in the presence of exogenous BAX. It is important to note that although cells may be designated as apoptosis refractory based on the BH3 Profiling assay, this designation is made at a single time point and in the absence of stress. There may exist conditions under which apoptosis refractory cells upregulate critical pro-apoptotic proteins to acquire apoptotic sensitivity.

Early in life, tissues are primed for apoptosis

Young children frequently experience neuro- and cardiotoxicity when treated with radiation or genotoxic chemotherapies. We therefore hypothesized that the apoptotic pathway may be more active in these tissues in young mammals as compared to adults. To test this, we measured levels of apoptotic priming in newborn mice and found that brain, heart and kidney mitochondria in embryonic and very young mice are extremely primed for apoptosis (Figure 2A). In fact, mitochondria in neonatal brain cells were almost as primed for apoptosis as adult splenocytes. We next sought to delineate the transition between being highly primed and apoptosis refractory in relevant tissues by making serial measurements over time. Each tissue exhibited a distinct temporal program to transition from being primed to being apoptosis refractory with the sharpest decreases occurring shortly after birth (P0-P5) (Figure 2B). In contrast, the spleen maintained a high level of priming throughout development and into adulthood (Figure 2B).

We next sought to test the functional consequences of these developmental changes in apoptotic priming. We chose to again stress cells with gamma radiation, which applies an equal and reproducible level of genotoxic damage across tissues and models radiation therapy in pediatric cancer patients. Mice at various stages of postnatal development were treated with whole-body gamma irradiation and apoptosis was quantified. We detected extensive caspase 3/7 activation post radiation, at doses of 0.50 - 8 Gy, in brain, heart and kidney tissues in P0-P2 mice, which was measurably reduced each day of postnatal development and finally silenced (insensitivity to 8 Gy) by P13, P15 and P12 in brain, heart and kidney, respectively (Figure 2C and S2A). Splenocytes, which are primed throughout life, consistently activated caspases in response to damage. We utilized immunohistochemical (IHC) staining for cleaved caspase 3 and TUNEL to confirm that the cells undergoing apoptosis in each tissue in response to radiation are not blood cells (Figure 2D-F and S2B-F).

Very young patients suffer increased iatrogenic cardiotoxicity from anthracyclines compared with non-elderly adults. To determine whether the dynamic levels of apoptotic priming during postnatal development may contribute to this difference, we injected mice at various postnatal stages with the anthracycline doxorubicin and measured caspase activation in the heart, again modeling pediatric cancer treatment in humans. In neonatal heart tissue, we detected caspase activation, which decreases with age in a manner similar to that following radiation damage (Figure 2C).

Finally, we sought to determine whether the changes in apoptotic priming were dependent on an in vivo milieu or whether they could be driven by cell-autonomous mechanisms. To test this, we isolated hippocampal neurons from embryonic day 19 (E19) rat brains and measured apoptotic priming and chemosensitivity of these cells at regular intervals as they matured in vitro (Figure 3A-C). These non-proliferating (Figure 3D) neurons underwent

the same developmentally-defined transition from high apoptotic priming to apoptotic resistance that was evident *in vivo*. Their sensitivity to the classical apoptosis inducers staurosporine and doxorubicin followed a similar pattern (Figure 3E).

Age-related apoptotic priming is regulated via BAX and BAK

The contrast in apoptotic priming in vital tissues between young and adult mice prompted us to explore the age-related expression of BCL-2 family proteins. Because we had previously shown that exogenous BAX supplementation is sufficient to reverse mitochondrial resistance to pro-apoptotic signals, we focused on the developmental regulation of BAX and BAK. In the spleen, we found the critical effectors BAX and BAK and potent activator BH3-only proteins BIM and BID to be consistently expressed during the entire lifespan of the animals (Figure 4A). Major anti-apoptotic proteins were also expressed in the spleen consistently throughout life, although a downregulation of BCL-XL and MCL-1 and upregulation of BCL-2 with age was noted. Expression of caspase 3 and APAF-1 was unchanged over time. These results were consistent with BH3 profiling data showing high levels of priming throughout life.

In contrast to the spleen, we found the expression of BCL-2 family members in the mouse brain during postnatal development to be dynamic. BAX was highly expressed in the mouse brain at P0-P5, but continually reduced into adulthood (Figure 4A). BAK was reduced in a similar manner yet expression levels were lower overall (relative to adult spleen). BCL-XL, as well as caspases 8 and 9 were consistently expressed while BIM, BID, MCL-1 and BCL-2 were also reduced during postnatal brain development. Finally, both caspase 3 and APAF-1 were strongly downregulated during postnatal development, further contributing to the suppression of apoptosis in adult brain tissue.

Similar results to the brain were also observed in heart, kidney and liver with BAX and BAK being rapidly downregulated following birth (Figure 4A). We confirmed this downregulation occurs in the non-blood cells that comprise these tissues via IHC (Figure S3). We also found that adult liver tissue expresses low, yet detectable, levels of BAK (Figure S3B), which is consistent with the higher sensitivity of adult hepatocytes to BID over BIM (Figure 1B) due to their activation preferences (Sarosiek et al., 2013). It is notable that anti-apoptotic proteins tended to be downregulated in these tissues as well, further demonstrating that adult tissues are not protected from apoptosis by high expression of anti-apoptotic proteins. Instead, there appears to be a wholesale dismantling of the apoptotic machinery to render these cells apoptosis refractory, preserving their survival. The expression levels of VDAC, which can facilitate cytochrome c release from mitochondria during MOMP, and IAP proteins (XIAP, CIAP1) also remained largely unchanged across all tissues.

We also found BAX and BAK, along with other key components of the apoptotic machinery, to be strongly downregulated in human adult brain, heart and liver tissues relative to fetal tissues (Figure 4B and Tables S1-S2).

Healthy tissues differ in utilizing BAX versus BAK to undergo apoptosis

BAX and BAK have non-overlapping roles in regulating apoptosis and their activity can be modulated selectively (Sarosiek et al., 2013; Shamas-Din et al., 2014). Our results showed that BAX and BAK are downregulated in tissue-specific manners as they transition from being apoptotically primed to refractory. We therefore utilized mouse models to determine the distinct contributions of BAX and BAK to the activation of apoptosis in healthy tissues. Neonatal brain tissue in WT mice was efficiently depolarized by the BIM (~80%) and, to a lesser extent, BID

(40%) peptides (Figures 5A-B and S4). In *Bax*^{-/-} neonates, however, we found the responses to BIM and BID significantly reduced, which was not evident in *Bak1*^{-/-} mice. We therefore hypothesized that loss of *Bax* would protect brain tissue from radiation-induced apoptosis while loss of *Bak1* would not. In agreement with the BH3 Profiling data, we found that loss of *Bax* prevented nearly all caspase 3 activation post radiation while loss of *Bak1* had no effect (Figure 5C). Thus, in the early postnatal brain, BAX and not BAK is the dominant effector that is engaged to trigger apoptosis.

We then found that each tissue exhibits its own pattern of effector dependence. Splenocytes can execute apoptosis via BAX or BAK and although loss of BAX is somewhat protective, both must be lost in order to prevent all radiation-induced apoptosis (Figure 5C). In the neonatal heart, loss of either BAX or BAK reduced responses to peptides and radiation, indicating that both effectors are present, yet at limited levels, consistent with our immunoblotting results (Figure 4A). Cells within the neonatal kidney also contain both BAX and BAK, and loss of either reduced peptide responses. However, loss of BAX meaningfully reduced caspase activation after irradiation while loss of BAK did not. Finally, we found that neonatal hepatocytes contained both BAX and BAK and required the loss of both in order to significantly reduce apoptosis post radiation. In all cases, the knockout of *Bax* preferentially dulled responses to the BIM BH3 peptide while loss of *Bak1* preferentially dulled responses to the BID BH3 peptide, which is in agreement with reported specificity of activator/effector interactions (Sarosiek et al., 2013). These results may enable the prevention of damage-induced apoptosis in neonatal tissues by inhibiting BAX alone (brain) or both BAX and BAK (heart, kidney, liver, spleen).

Higher apoptotic priming in young mice contributes to doxorubicin-induced cardiotoxicity

Young hearts are considerably more sensitive to doxorubicin than non-elderly adult hearts. Clinically, the degree of cardiotoxicity observed correlates with age, with the youngest children being most at risk for developing symptoms including decreased ejection fraction (EF), thinning of ventricular walls, and an overall reduction in heart size (ventricular mass), sometimes referred to as “Grinch syndrome” (Lipshultz et al., 2014). We hypothesized that the differences in apoptotic priming in cardiomyocytes from young versus adult hearts may contribute to the heightened risk of developing cardiotoxicity in young patients.

We developed a mouse model of doxorubicin-induced cardiotoxicity by injecting mice with 3 doses of doxorubicin (5 mg/kg) over the course of one week, starting at days P5/6 (primed for apoptosis), P11/12 (unprimed), or P60-80 (apoptosis refractory) (Figure 6A). Our dosing schedule is reduced in intensity (3 doses instead of 5) from one previously used to model chronic doxorubicin cardiotoxicity in adult mice (Zhang et al., 2012), which, when tested in young mice induced prohibitively high levels of cardiotoxicity as evidenced by arrhythmias and death (data not shown). Using echocardiograms at day 14, we found significant thinning of the interventricular septal (IVS;d) and posterior ventricular walls (LVPW;d) in M-mode echocardiogram tracings at diastole in animals that began receiving injections at P5/6, but not those that began as adults (Figure 6B-D, Movies S1-S2). Moreover, animals treated at a young age exhibited a profound decrease in EF and left ventricular mass while adults did not. Masson’s Trichrome staining (MTS) of hearts after treatment showed focal areas of altered myocyte architecture with signs of early injury (loss of cross striations, disorganization of

myofilaments resulting in abnormal staining, and hypochromatic nuclei) in mice treated starting at P5/6 but not adults (Figure S5A).

We next asked if suppression of the intrinsic apoptotic pathway could reverse these effects of doxorubicin. Using knockout mice to model pharmacologic inhibition, we found that loss of both *Bax* and *Bak1* was required to consistently reverse doxorubicin-induced damage in neonatal mouse hearts (Figure 6E). In addition, knockout of *Bax* and *Bak1* in P5/6 mice treated with doxorubicin showed dramatically reduced, although not completely lost, evidence of early injury in MTS histology (Figure S5B). Therefore, young heart tissue expresses both BAX and BAK at sufficient levels to activate apoptosis and thus inhibition of both of these effectors is needed to mitigate doxorubicin-induced thinning of ventricular walls and reduction in ventricular mass. In addition, there may also be a non-apoptotic component of doxorubicin-induced cardiotoxicity since the BAX/BAK double knockout mice still exhibited some signs of early injury based on MTS histology, although symptoms were greatly reduced. Taken together, our results show that hearts in young mice exhibit more severe clinically-relevant symptoms of doxorubicin cardiotoxicity than adults, potentially due to the increased BAX and BAK expression in apoptotically primed young hearts (Figure 2B) that renders them hypersensitive to doxorubicin (Figure 2C).

Apoptotic priming is modulated by c-Myc

The concerted loss of several genes responsible for regulating apoptosis suggested that a master developmental program or transcription factor may be regulating multiple members of this pathway. One such potential modulator is c-Myc (hereafter Myc), a transcription factor that drives cellular growth and proliferation in normal as well as cancerous cells (Dang et al., 2006).

Several links between Myc and apoptosis have been reported, including the sensitization of Myc over-expressing cells to a variety of pro-apoptotic stimuli (Bissonnette et al., 1992; Egle et al., 2004; Evan et al., 1992; Murphy et al., 2008) and its direct regulation of BAX expression (Mitchell et al., 2000). We thus hypothesized that tissues early in development express Myc at levels that are sufficient to drive the expression of BAX and potentially other apoptosis-related genes, making them primed for apoptosis, and that loss of BAX expression in adulthood is related to loss of Myc.

Consistent with our hypothesis, we found that Myc is expressed at higher levels in young brain, heart and kidney tissues as compared to adult (Figure 4A). The human proteome database did not contain sufficient data for Myc expression. If Myc was driving expression of pro-apoptotic genes, we would expect Myc-expressing cells to be more primed. To test, we utilized flow cytometry-based BH3 Profiling, which allows for single-cell measurements of priming concurrently with evaluation of extracellular or intracellular factors. We measured priming and nuclear Myc expression (indicative of activation) in cells from P0 tissues and found that Myc-positive brain, kidney and liver cells were, as expected, more primed than Myc negative cells (Figure 7A). We did not detect any Myc-positive cells within the respective adult tissues, which we again found to be dramatically less primed than neonatal tissues. In heart tissues, the extended processing necessary for this analysis resulted in prohibitively high levels of cytochrome *c* loss in even untreated cells, thus preventing analysis in that tissue.

Expression of Myc was associated with higher apoptotic priming, but this relationship may not be causal, prompting us to test whether Myc expression was necessary to maintain high priming in neonatal tissues. We therefore measured priming in the cerebral cortex of either WT or *Myc*^{+/-} mice (Hofmann et al., 2015). As expected, the loss of one allele of *Myc* resulted in reduced sensitivity to BIM as compared to WT littermates (Figure 7B).

Next, we sought to determine whether activating Myc in adult tissues would be sufficient to reactivate apoptosis in refractory cells. We first utilized the well-characterized Gt(ROSA)26Sor^{tm1.1(MYC/ERT2)GEV} (hereafter MycER) mouse model that was developed to study the physiological effects of acute Myc activation in adult tissues (Murphy et al., 2008). These mice express a cDNA encoding human c-Myc fused at its C terminus to the hormone-binding domain of 4-hydroxytamoxifen (4-OHT)-responsive mutant murine estrogen receptor, enabling us to activate Myc systemically with injections of tamoxifen. Activation of Myc in normally apoptosis refractory brain and kidney tissue, or unprimed liver tissue increased sensitivity to genotoxic damage (Figure 7C). Notably, we found that Myc-positive cells within these tissues were more primed for apoptosis than their Myc-negative counterparts as measured via flow cytometry-based BH3 Profiling (Figure 7D). Our data suggests that Myc activation may re-enable the apoptotic pathway in apoptosis refractory tissues.

After acute liver damage, hepatocytes are able to re-enter the cell cycle and proliferate in order to replace dead cells (Tzung et al., 1997). Based on our previous data, we hypothesized that hepatocytes from adult liver tissue that are actively expressing Myc and proliferating would become more primed for apoptosis. We tested this by inducing immune-mediated liver damage via injection of Concanavalin A (ConA), which triggers active liver regeneration and hepatocyte proliferation (Trautwein et al., 1998). After injection with ConA, we observed a profound increase in Myc-positive cells within the liver (~0% Myc-positive in untreated animals) (Figure 7E), as hepatocytes proliferated to replace dead cells. We directly compared the level of priming in Myc-positive versus Myc-negative hepatocytes and found the former to be significantly more sensitive to BIM and BID BH3 peptides (Figure 7F). Thus, using both genetic and physiologic models, we found that activation of Myc increases mitochondrial priming.

Because modulation of Myc was sufficient to alter priming in the expected manner, we next sought to test whether Myc directly drives the expression of apoptosis-regulating genes in neonatal tissues. Myc activates the transcription of its target genes by binding specific E-box (Enhancer box) elements in gene promoters (Mitchell et al., 2000). We therefore used chromatin immunoprecipitation followed by quantitative polymerase chain reaction (ChIP-qPCR) to test for Myc occupancy in the E-boxes present in the promoters of various BCL-2 family member genes. In agreement with our hypothesis that Myc may be modulating BAX expression in neonatal tissues, we detected the *Bax* promoter being bound by Myc in neonatal brain, kidney, liver and spleen tissues (Figure 7G). Furthermore, Myc binding to the *Bax* promoter was lost in the adult brain and kidney but not the spleen, consistent with the spleen maintaining a high level of priming throughout life (note that adult heart and liver tissues were not tested). We also detected E-boxes in the promoters of pro-apoptotic *Bcl2l11* (*Bim*), which is consistent with previous reports (Campone et al., 2011; Muthalagu et al., 2014), and *Bid*, and confirmed that Myc bound to these promoters. Taken together, these data indicate that Myc drives an apoptotically primed state by directly activating transcription of pro-apoptotic genes *Bax*, *Bim*, and *Bid*.

Human brain regulates apoptosis during development similarly to mouse

The dynamic regulation of apoptosis in murine tissues dramatically affected responses to genotoxic damage and prompted us to ask whether the same temporal regulation could be directly observed in human tissues. One source of non-malignant, viable human brain tissue is from pediatric and adult patients that undergo removal of seizure foci to control otherwise intractable seizures caused by epilepsy, trauma or other pathology. Seizure foci are mapped in

the human brain and resected, inevitably along with some ostensibly healthy brain tissue (Bittigau et al., 2003). We obtained fresh, healthy brain tissue from over 20 such patients from 4 months to 21 years of age for BH3 Profiling analysis (Table S3). As with mice, we found human brain tissue from young patients to be significantly more sensitive to BIM and BID BH3 peptides than those from adults (Figure 7H-I). There existed a consistent downregulation of apoptotic priming during postnatal human brain development, predisposing the youngest children to radiation- and chemotherapy-induced neurotoxicity. In our study, there was a period of higher heterogeneity in apoptotic priming among patients between 2 and 6 years old, after which, the brain transitions to full apoptotic resistance. Finally, we mined mRNA expression data in the human brain during prenatal and postnatal development (Miller et al., 2014) and found that *BAX* expression is dramatically reduced during development, starting even prenatally (Figure 7I), which we confirmed at the protein level in our samples (Figure 7J). The highest mRNA expression of BAX was found in fetal brain, suggesting that the highest levels of apoptotic priming, perhaps similar to those observed in the youngest (P0-P2) mice, would be found in fetuses and pre-term infants.

DISCUSSION

The study of apoptosis has been traditionally dominated by the study of cancer cells and lymphocytes, the ubiquitous presence of functioning machinery of the mitochondrial apoptotic pathway in which has led to a general acceptance that this pathway is present in all cells. We were surprised to find that heart, kidney, and brain in adult mice lacked the proteins that regulate the mitochondrial apoptotic pathway. It appears that the mitochondrial apoptotic machinery is largely absent in these adult tissues, which we designate as being “apoptosis

refractory.” This apoptosis refractory state is achieved as part of a regulated postnatal developmental program in both mice and humans and is apparently reversible, as stress can restore apoptotic sensitivity to cells previously apoptosis refractory. A common feature of embryonic, immediately postnatal, and regenerating tissues is a greater degree of proliferation. We believe that in all of these tissues, enhanced priming is the price that cells pay for the capacity to proliferate. Cancer cells often share many features of embryonal cells, including lack of differentiation, enhanced proliferation, and stem-like function (Daley, 2009). The relatively primed nature of cancer cells may be thought of as re-establishment of yet another embryonic program in cancer cells.

Previous studies have shown that ectopically expressed Myc can foster pro-apoptotic signaling (Bissonnette et al., 1992; Evan et al., 1992; Murphy et al., 2008). We demonstrate here that endogenous, physiological Myc regulates apoptosis sensitivity across a range of tissues during mammalian development. Myc therefore provides one important mechanistic link between developmental proliferation, expression of pro-apoptotic genes, and apoptotic priming. However, we suspect that there are additional modulators of properties of this significance. In addition, our findings raise the question of whether other programmed cell death pathways including extrinsic (cell death receptor mediated) apoptosis, necroptosis (Zhou and Yuan, 2014), and ferroptosis (Dixon et al., 2012) are also dynamically regulated during postnatal development.

Very young pediatric cancer patients are subject to severe side effects of radiation and chemotherapy from which older children and adults are relatively spared. We show that the apoptotic responses of heart and brain tissues depend on the developmentally regulated priming of the mitochondria. It is possible that this regulation is a major contributor to the hypersensitivity of very young tissues to genotoxic agents. We find this correlation holds in the

brains of very young humans. Moreover, we find we can reverse this phenotype by un-priming mitochondria of young tissues by genetic means, potentially modeling pharmacologic inhibition.

Earlier work in this field reported the seemingly contrasting findings that individual BCL-2 family members were modulated with time in select tissues (Kole et al., 2013; Polster et al., 2003a) (Kole et al., 2013; Polster et al., 2003; Shi et al., 2012; Soane et al., 2008) and that BAX and BAK were highly and broadly expressed in somatic tissues including the brain (Brustovetsky et al., 2003; Krajewski et al., 1994). Our work aims to clarify how apoptosis is regulated in healthy tissues and also highlight the challenges in inferring phenotypic changes due to changes in levels of individual BCL-2 family proteins. The large number of proteins within this family and their nuanced pro- and anti-apoptotic effects, which can be further modulated by post-translational modifications, requires the use of a functional test of apoptotic priming to measure the net integration of these signals.

It is important to note that BH3 Profiling does not assess the state of post-MOMP regulators of apoptosis such as IAP proteins or caspases, which are also known to affect cell fate (Holly et al., 1999; Martin, 2002). In addition, the abilities of cells to die via the extrinsic apoptotic pathway (Fulda and Debatin, 2006) or inflammation-associated pathways (Martin et al., 2012) in response to genotoxic damage are not directly probed by BH3 Profiling. Finally, we acknowledge that even in a primed cell, whether apoptotic machinery is actually engaged following genotoxic damage depends on factors such as DNA damage responses and p53 competence (Kandioler-Eckersberger et al., 2000; Loewer et al., 2010; Rich et al., 2000). Combining BH3 Profiling with tests of the expression or adequacy/activity of these other factors/pathways, as we have attempted to do to some extent here, would provide the most complete understanding of the pretreatment state of the cell or tissue and how that impacts cell fate in response to damage or stress.

While our results show that many healthy tissues are apoptosis refractory in the adult, we do not mean to rule out the possibility that various chronic injuries or disease states might restore apoptotic sensitivity in these tissues. In fact, increased levels of neuronal BAX and/or BAK have been reported in patients with Alzheimer's disease (MacGibbon et al., 1997; Shimohama, 2000), which would be expected to contribute to the neuronal death that characterizes this pathology. BAX expression has also been observed to increase in different liver pathologies, including hepatitis and cirrhosis (Jr et al., 2000; Liang et al., 2007) and is increased following *Mc11* deletion in mouse cardiomyocytes, potentially contributing to the apoptosis reported in that model (Wang et al., 2013). Indeed, we found that chemical liver injury and the resulting regenerative proliferation increased apoptotic priming in adult mice. Such findings suggest that the program we observe is reversible, as we observed with the increased priming post activation of Myc in the regenerating liver or MycER mouse model. More study is needed to understand how disease states may impact apoptotic priming.

Our analysis shows that virtually all cells within neonatal brain, heart and kidney are primed for apoptosis while in adults virtually all cells within these tissues are apoptosis refractory. We did not measure priming levels or changes in priming among different types of cells within each tissue. It remains possible, however, that apoptotic priming of cell subsets are differentially regulated in development. Future work will focus on mapping how individual cell types within organs regulate apoptosis.

Our findings suggest that there may potentially be ways to improve the therapeutic index of cancer treatments through the use of agents that selectively modulate BCL-2 family member function. For example, because of the developing brain's dependence on BAX and not BAK for apoptosis, clinicians could utilize a BAX inhibitor or RNAi-based knockdown of BAX while administering brain irradiation for the treatment or prophylaxis of acute lymphocytic leukemia

(ALL) with CNS involvement. This strategy would potentially prevent apoptosis in neurons, which express only BAX, while still allow ALL cells, which express both BAX and BAK (Haferlach et al., 2010), to undergo apoptosis via BAK. It may also be possible to modulate developmental programs or Myc levels via recently developed strategies (Delmore et al., 2011) to induce transient apoptotic resistance in healthy tissues prior to administering radiation or chemotherapy. Beyond cancer, our data have implications for medical conditions such as head trauma in pediatric patients, which induces neuronal death via apoptotic and excitotoxic pathways, while in adults only the excitotoxic pathway is engaged (Pohl et al., 1999). A BAX (or BAX/BAK) inhibitor could prevent the apoptotic component of this neuronal death, potentially rescuing some of the ill effects of these injuries in young children. Although no inhibitors of BAX and/or BAK have reached the clinic, efforts are currently underway to develop such agents (Hetz et al., 2005; Lessene, 2015).

Our findings may also impact the development of anti-cancer agents targeting cell death. Efforts to develop small molecule direct activators of BAX for cancer therapy have begun (Gavathiotis et al., 2012). The BIM BH3 peptide is itself a BAX activator. Our finding that the mitochondria of most adult somatic tissues are relatively insensitive to BIM BH3 makes the direct activation of BAX for cancer therapy more attractive. However, based on our findings these same tissues in pediatric patients could prove to be exquisitely sensitive, and thus efforts to utilize such agents in very young children should be accompanied by consideration of the apoptotic sensitivity of their normal tissues.

EXPERIMENTAL PROCEDURES

Animals: Mice were housed and bred in accordance with the policies and regulations set forth by the Dana-Farber Cancer Institute's Institutional Animal Care and Use Committee (IACUC). All animal experiments were approved by IACUC under DFCI protocols 11-008, 12-049 and UK Home Office licenses 70-7950 and 70-8645.

Human brain specimens: All specimens were collected under IRB-approved tissue collection protocol #09-02-0043 at Boston Children's Hospital and transferred to DFCI via Office for Human Research Studies exemption 13-545. Patients underwent surgery for removal of seizure foci at Boston Children's Hospital (Table S3) and resected tissues were first delivered to a neuropathologist for evaluation. If available, a de-identified sample (0.2-0.5g) of brain tissue was provided to study investigators in PBS on ice and was immediately processed for BH3 Profiling. Part of the sample (0.1g) was excluded for cryopreservation and was subsequently prepared for immunoblotting as outlined above. The remaining brain tissue was dissociated by repeated pipetting until a single cell suspension was achieved and BH3 Profiled with JC1.

Fluorescence-based BH3 Profiling: Briefly, BH3 peptides or recombinant proteins in T-EB buffer were deposited into each well in a black 384-well plate, 1 treatment per well, in triplicate for each independent experiment. Single cells isolated from indicated tissues were resuspended in T-EB buffer and mixed 1:1 with a dye solution containing digitonin and JC-1 in T-EB. Cells were kept at room temperature for 5 min to allow for cell permeabilization and dye equilibration. Cells were then added to each treatment well in the 384-well plate and fluorescence at 590 nm was measured every 5 min at 32°C for a total of 120 min. Relative mitochondrial depolarization was

defined as the magnitude of mitochondrial potential loss resulting from BH3 peptide treatments as compared to negative control DMSO and positive control FCCP.

Flow cytometry-based BH3 Profiling: Briefly, BH3 peptides in T-EB buffer with digitonin were deposited into each well in a 384-well plate. Single cells were resuspended in T-EB buffer and added to each treatment well and incubated for 60 min at 28°C. Peptide exposure was terminated with formaldehyde and cells were stained overnight with an antibody to cytochrome c conjugated to AF647. Cytochrome c positivity was measured on a BD Biosciences LSR II flow cytometer.

Additional experimental procedures can be found in the Extended Experimental Procedures.

AUTHOR CONTRIBUTIONS

K.A.S., C.F., N.M., P.D.B., W.C., S.K.M., A.C., S.F., G.G-M., J.M.R. and J.D. conducted the experiments. K.A.S. and A.L. conceptualized the study and wrote the manuscript. K.A.S., C.C., M.G., J.R.M, B.J., R.L., D.W., J.S., D.J.M., D.R.C., S.R., J.M. and A.L. assisted with the acquisition and analysis of the data. All authors revised the manuscript and approved its content.

ACKNOWLEDGEMENTS

We thank J. Sims, P. Sorger, X. Chi, L. Walensky, D. Andrews, C. Unitt, T. Bowman, O. Pozdnyakova and S. White for providing assistance and B. Mar, J. Montero, G. Joshi and L. Boise for critical review of our manuscript. We gratefully acknowledge funding from the American Cancer Society Postdoctoral Fellowship 121360-PF-11-256-01-TBG (K.A.S.), Alex's Lemonade Stand Foundation for Childhood Cancers Young Investigator Award (K.A.S), as well as NIH grants K99CA188679 (K.A.S) and RO1CA129974 (A.L). A.L. was a Leukemia and Lymphoma Society Scholar. The authors have no conflict of interest to declare.

FIGURE LEGENDS

Figure 1: Adult brain, heart, and kidney tissues are apoptosis refractory, protected from genotoxic damage. (A) Tissues were isolated from adult mice (>P60) and BH3 Profiled.

Mitochondrial potential under each treatment condition was measured every 5 min during the experimental time course and plotted relative to maximum value of negative control (DMSO).

Percent depolarization (indicative of MOMP) is calculated for each BH3 peptide treatment relative to DMSO (0%) and FCCP (100%). Representative traces are shown (mean \pm SD, ≥ 3 independent experiments [IEs]). (B) Summary BH3 Profiling data across healthy adult mouse

tissues. ≥ 3 IEs. (C) After whole body gamma irradiation, apoptosis was measured via a caspase 3 activity assay. Data were compiled from 5 animals for each treatment across 3 IEs

with bars representing means. (D) After whole body irradiation, apoptosis was detected via immunohistochemistry for cleaved caspase 3. Data were compiled from 2 animals for each treatment across 2 IEs with bars representing means. (E) Tissues were collected from adult

mice and immunoblotting was performed. Densitometry was performed across immunoblots from 3 IEs and averaged (blue heatmap on right). GAPDH is loading control. Relative molecular weight markers are shown on left. (F) Expression of indicated proteins in adult human tissues was assessed via the Kim et al. (2014) mass spectrometry dataset. (G) Tissues were isolated from adult mice and BH3 Profiled in the presence of recombinant BAX. Representative traces are shown (mean \pm SD, ≥ 3 IEs). See Figure S1 and Tables S1-S2

Figure 2: Embryonic and early postnatal brain, heart, kidney and liver tissues are primed for apoptosis and sensitive to genotoxic damage. (A) Tissues were isolated from postnatal day 0 mice (P0) and BH3 Profiled. Representative traces are shown (mean \pm SD, ≥ 3 IEs). (B)

Summary BH3 Profiling data across tissues during embryonic and postnatal development. Each point represents an average of 3 measurements in each mouse tissue across at least 5 IEs. (C) After whole body irradiation or doxorubicin injection, tissues were collected and caspase activity was measured via an enzymatic assay. Each point represents an average of 3 measurements in each mouse tissue across at least 5 IEs. (D) After whole body irradiation, apoptosis was detected via IHC for cleaved caspase 3. Representative images, 2 IEs. Olfactory bulb (OB) and cerebral cortex (CC) are indicated. Scale bars are 200 μ m. (E-F) Cleaved caspase 3-positive (E) or TUNEL-positive (F) cells were counted per 40X field in sham-treated or irradiated tissues from young (P0-P2) or adult (P60+) mice processed via IHC. Data are compiled from 2 IEs with bars representing means. See Figure S2.

Figure 3: Apoptotic priming and chemosensitivity decrease as primary rat hippocampal neurons mature in vitro. (A) Primary neurons were isolated from E19 rat embryos and allowed to mature in vitro, with representative images shown at indicated time points (days in vitro). Note that the same cells (those inside box on low magnification) are shown across the 4 time points in the higher magnification window. Scale bars are 200 μ m. (B) Primary neurons were BH3 Profiled at indicated days in vitro. Representative traces are shown (mean \pm SD, 2 IEs). (C) Summary of BH3 Profiling data of primary neurons at indicated time points. (D) Neuron nuclei were counted at indicated time points. (E) Chemosensitivity of rat hippocampal neurons in vitro. Each point represents an average of 3 measurements at each time point across 2 IEs.

Figure 4: Key components of the apoptotic machinery are lost during postnatal development. (A) Healthy tissues were collected from mice at indicated ages and

immunoblotted. (B) Expression of indicated proteins in fetal and adult human tissues assessed via proteome data (Kim et al., 2014). See Figure S3.

Figure 5: BAX and BAK dependence in early postnatal mouse tissues. (A) Tissues were collected from P0 mice of indicated genotypes and BH3 Profiled. Representative traces are shown (mean \pm SD, ≥ 3 IEs). (B) Summary BH3 Profiling data from P0-P2 mouse tissues. Each point represents an average of 3 measurements in each tissue across 4 IEs. Bars represent means (C) Summary caspase 3 activity data from P0-P2 mouse tissues after whole body irradiation. Each point represents an average of 3 measurements in each tissue across 11 IEs. Bars represent means. See Figure S4.

Figure 6: Mouse model of pediatric doxorubicin cardiotoxicity. (A) Schematic representation of the experiment. WT mice of different ages were injected intraperitoneally with 3 doses of doxorubicin at 5 mg/kg on days 0, 4 and 7. Echocardiograms to assess heart function were performed on day 14. (B) Representative M-mode echocardiogram tracings are shown from WT mice treated at P5 or P60+. (C) Representative parasternal long-axis views at the level of the papillary muscle are shown from WT mice treated at P5. (D) Summary echocardiogram data. Each point represents an average of 2 measurements in each animal across ≥ 5 IEs. Bars represent means. (E) P5-P6 mice of indicated genotypes were treated as in (A). Bars represent means. See Figure S5 and Movies S1-S2.

Figure 7: Apoptotic priming is modulated by Myc and priming is dynamically regulated in human brain tissue. (A) Flow cytometry-based BH3 Profiling was performed on indicated tissues collected from neonatal or adult mice and loss of cytochrome *c* (indicative of apoptosis)

was measured after treatment with negative control (DMSO), positive control alamethicin (AlaM), or BH3 peptides. For neonatal tissues, each point represents a flow cytometry-based measurement of either Myc negative or positive cells (as determined by co-staining for nuclear Myc) from a single tissue sample. For adult tissues, each point represents a flow cytometry-based measurement of Myc negative cells. All cells analyzed by flow cytometry were CD45 negative to exclude blood cells from analysis. Data shown are for either 3 (neonatal) or 2 (adult) IEs. (B) Fluorescence-based BH3 Profiling was performed on brain tissue (neocortex) of litter-matched, neonatal Myc WT or heterozygous mice. Each point represents analysis of a single animal across 2 IEs. (C) MycER mice were treated with vehicle (oil) or tamoxifen (tam) to activate Myc for 3 days and then irradiated (8 Gy). TUNEL⁺ cells were counted per 20X field. (D) Flow cytometry-based BH3 Profiling was performed on tissues from (C) and each point represents the loss of cytochrome *c* in cells that are nuclear Myc-positive vs -negative from each tamoxifen-treated animal across 2 IEs. (E) After injection with vehicle or concanavalin A, liver tissue was collected from mice at indicated time points and Myc positivity was measured in hepatocytes via flow cytometry. Each point represents one animal across 2 IEs. (F) 96 hours after injection with concanavalin A, liver tissue was collected and flow cytometry-based BH3 Profiling was performed on hepatocytes while monitoring nuclear Myc expression. Each point represents one animal across 3 IEs. (G) ChIP-qPCR was performed to measure Myc occupancy on promoters for positive control (*Mybbp1a*) and negative control (*Untr6*) genes, along with genes of interest. Values shown are binding events detected per μ g chromatin. In (A-G), bars represent means. (H) Representative BH3 Profile traces (mean \pm SD) from healthy human brain tissue obtained during resection of seizure foci. (I) Summary of fluorescence-based BH3 Profiling data from human brain tissues. Each point represents an average of 3 measurements in each human brain specimen across at least 5 IEs. *BAX* mRNA expression across human

brain regions were assessed at indicated ages. (J) Immunoblotting for BAX across healthy human brain specimens tested in (H-I). Numbers indicate months post conception. Heatmap represents expression of BAX normalized to GAPDH levels. See Table S3.

REFERENCES

- American Cancer Society (2014). Cancer Treatment & Survivorship Facts and Figures 2014-2015. Atlanta Am. Cancer Soc. 44.
- Bissonnette, R.P., Echeverri, F., Mahboubi, A., and Green, D.R. (1992). Apoptotic cell death induced by c-myc is inhibited by bcl-2. *Nature* 359, 552–554.
- Bittigau, P., Sifringer, M., and Ikonomidou, C. (2003). Antiepileptic drugs and apoptosis in the developing brain. *Ann. N. Y. Acad. Sci.* 993, 103–114; discussion 123–124.
- Brustovetsky, N., Dubinsky, J.M., Antonsson, B., and Jemmerson, R. (2003). Two pathways for tBID-induced cytochrome c release from rat brain mitochondria: BAK- versus BAX-dependence. *J. Neurochem.* 84, 196–207.
- Campone, M., Noël, B., Couriaud, C., Grau, M., Guillemain, Y., Gautier, F., Gouraud, W., Charbonnel, C., Campion, L., Jézéquel, P., et al. (2011). c-Myc dependent expression of pro-apoptotic Bim renders HER2-overexpressing breast cancer cells dependent on anti-apoptotic Mcl-1. *Mol. Cancer* 10, 110.
- Czabotar, P.E., Lessene, G., Strasser, A., and Adams, J.M. (2013). Control of apoptosis by the BCL-2 protein family: implications for physiology and therapy. *Nat. Rev. Mol. Cell Biol.* 15, 49–63.
- Daley, G.Q. (2009). Common Themes of Dedifferentiation in Somatic Cell Reprogramming and Cancer Common Themes of Dedifferentiation in Somatic Cell Reprogramming and Cancer. Cold Spring Harb. Symp. Quant. Biol. LXXIII.
- Dang, C. V., O'Donnell, K.A., Zeller, K.I., Nguyen, T., Osthus, R.C., and Li, F. (2006). The c-Myc target gene network. *Semin. Cancer Biol.* 16, 253–264.
- Daids, M.S., Deng, J., Wiestner, A., Lannutti, B.J., Wang, L., Wu, C.J., Wilson, W.H., Brown, J.R., and Letai, A. (2012). Decreased mitochondrial apoptotic priming underlies stroma-mediated treatment resistance in chronic lymphocytic leukemia. *Blood*.
- Delmore, J.E., Issa, G.C., Lemieux, M.E., Rahl, P.B., Shi, J., Jacobs, H.M., Kastiris, E., Gilpatrick, T., Paranal, R.M., Qi, J., et al. (2011). BET bromodomain inhibition as a therapeutic strategy to target c-Myc. *Cell* 146, 904–917.
- Dixon, S.J., Lemberg, K.M., Lamprecht, M.R., Skouta, R., Zaitsev, E.M., Gleason, C.E., Patel, D.N., Bauer, A.J., Cantley, A.M., Yang, W.S., et al. (2012). Ferroptosis: An Iron-Dependent Form of Nonapoptotic Cell Death. *Cell* 149, 1060–1072.
- Egle, A., Harris, A.W., Bouillet, P., and Cory, S. (2004). Bim is a suppressor of Myc-induced mouse B cell leukemia. *Proc. Natl. Acad. Sci. U. S. A.* 101, 6164–6169.
- Evan, G.I., Wyllie, A.H., Gilbert, S., Littlewood, T.D., Land, H., Brooks, M., Waters, C.M., Penn, L., and Hancock, D.C. (1992). Induction of Apoptosis by c-myc Protein in Fibroblasts. 69, 119–128.
- Fulda, S., and Debatin, K.-M. (2006). Extrinsic versus intrinsic apoptosis pathways in anticancer chemotherapy. *Oncogene* 25, 4798–4811.
- Galluzzi, L., Aaronson, S. a, Abrams, J., Alnemri, E.S., Andrews, D.W., Baehrecke, E.H., Bazan, N.G., Blagosklonny, M. V, Blomgren, K., Borner, C., et al. (2009). Guidelines for the use and interpretation of assays for monitoring cell death in higher eukaryotes. *Cell Death Differ.* 16,

1093–1107.

Gavathiotis, E., Reyna, D.E., Bellairs, J. a, Leshchiner, E.S., and Walensky, L.D. (2012). Direct and selective small-molecule activation of proapoptotic BAX. *Nat. Chem. Biol.* 1–7.

Haferlach, T., Kohlmann, A., Wiczorek, L., Basso, G., Te Kronnie, G., Béné, M.C., De Vos, J., Hernández, J.M., Hofmann, W.K., Mills, K.I., et al. (2010). Clinical utility of microarray-based gene expression profiling in the diagnosis and subclassification of leukemia: Report from the international microarray innovations in leukemia study group. *J. Clin. Oncol.* 28, 2529–2537.

Hanahan, D., and Weinberg, R. (2000). The hallmarks of cancer. *Cell* 100, 57–70.

Hetz, C., Vitte, P.-A., Bombrun, A., Rostovtseva, T.K., Montessuit, S., Hiver, A., Schwarz, M.K., Church, D.J., Korsmeyer, S.J., Martinou, J.-C., et al. (2005). Bax channel inhibitors prevent mitochondrion-mediated apoptosis and protect neurons in a model of global brain ischemia. *J. Biol. Chem.* 280, 42960–42970.

Hofmann, J.W., Zhao, X., De Cecco, M., Peterson, A.L., Pagliaroli, L., Manivannan, J., Hubbard, G.B., Ikeno, Y., Zhang, Y., Feng, B., et al. (2015). Reduced expression of MYC increases longevity and enhances healthspan. *Cell* 160, 477–488.

Holly, T., Drincic, A., and Byun, Y. (1999). Caspase Inhibition Reduces Myocyte Cell Death Induced by Myocardial Ischemia and Reperfusion In Vivo. *J. Mol. ...* 1715, 1709–1715.

Jr, E., Galuszkova, D., Ehrmann, J., Ek, B.V., Murray, P.G., and Kolao, Z. (2000). Apoptosis-related proteins, BCL-2, BAX, FAS, FAS-L and PCNA in liver biopsies of patients with chronic Hepatitis B virus infection. 6.

Kandioler-Eckersberger, D., Ludwig, C., Rudas, M., Kappel, S., Janschek, E., Wenzel, C., Schlagbauer-Wadl, H., Mittlböck, M., Gnant, M., Steger, G., et al. (2000). TP53 mutation and p53 overexpression for prediction of response to neoadjuvant treatment in breast cancer patients. *Clin. Cancer Res.* 6, 50–56.

Kim, M.-S., Pinto, S.M., Getnet, D., Nirujogi, R.S., Manda, S.S., Chaerkady, R., Madugundu, A.K., Kelkar, D.S., Isserlin, R., Jain, S., et al. (2014). A draft map of the human proteome. *Nature* 509, 575–581.

Kole, a J., Annis, R.P., and Deshmukh, M. (2013). Mature neurons: equipped for survival. *Cell Death Dis.* 4, e689.

Krajewski, S., Krajewska, M., Shabaik, a, Miyashita, T., Wang, H.G., and Reed, J.C. (1994). Immunohistochemical determination of in vivo distribution of Bax, a dominant inhibitor of Bcl-2. *Am. J. Pathol.* 145, 1323–1336.

Lessene, G. (2015). Targeting cell death pathways with small molecules: playing with life and death at the cellular level to treat diseases. *Future Med. Chem.*

Liang, X., Liu, Y., Zhang, Q., Gao, L., Han, L., Ma, C., Zhang, L., Chen, Y.H., and Sun, W. (2007). Hepatitis B virus sensitizes hepatocytes to TRAIL-induced apoptosis through Bax. *J. Immunol.* 178, 503–510.

Lipshultz, S.E., Lipsitz, S.R., Mone, S.M., Goorin, a M., Sallan, S.E., Sanders, S.P., Orav, E.J., Gelber, R.D., and Colan, S.D. (1995). Female sex and drug dose as risk factors for late cardiotoxic effects of doxorubicin therapy for childhood cancer. *N. Engl. J. Med.* 332, 1738–1743.

Lipshultz, S.E., Scully, R.E., Stevenson, K.E., Franco, V.I., Neuberg, D.S., Colan, S.D.,

- Silverman, L.B., Moslehi, J.J., Cheng, S., and Sallan, S. (2014). Hearts too small for body size after doxorubicin for childhood ALL: Grinch syndrome. *J Clin Oncol* 32, suppl; abstr 10021.
- Loewer, A., Batchelor, E., Gaglia, G., and Lahav, G. (2010). Basal dynamics of p53 reveal transcriptionally attenuated pulses in cycling cells. *Cell* 142, 89–100.
- MacGibbon, G., Lawlor, P., Sirimanne, E., Walton, M., Connor, B., Young, D., Williams, C., Gluckman, P., Faull, R.L., Hughes, P., et al. (1997). Bax expression in mammalian neurons undergoing apoptosis, and in Alzheimer's disease hippocampus. *Brain Res.* 750, 223–234.
- Martin, S.J. (2002). Destabilizing influences in apoptosis: Sowing the seeds of IAP destruction. *Cell* 109, 793–796.
- Martin, S.J., Henry, C.M., and Cullen, S.P. (2012). A Perspective on Mammalian Caspases as Positive and Negative Regulators of Inflammation. *Mol. Cell* 46, 387–397.
- Merchant, T.E., Pollack, I.F., and Loeffler, J.S. (2010). Brain tumors across the age spectrum: biology, therapy, and late effects. *Semin. Radiat. Oncol.* 20, 58–66.
- Miller, J. a, Ding, S.-L., Sunkin, S.M., Smith, K. a, Ng, L., Szafer, A., Ebbert, A., Riley, Z.L., Royall, J.J., Aiona, K., et al. (2014). Transcriptional landscape of the prenatal human brain. *Nature* 508, 199–206.
- Mitchell, K.O., Ricci, M.S., Miyashita, T., Dicker, D.T., Jin, Z., Reed, J.C., and El-Deiry, W.S. (2000). Bax is a transcriptional target and mediator of c-Myc-induced apoptosis. *Cancer Res.* 60, 6318–6325.
- Murphy, D.J., Junttila, M.R., Pouyet, L., Karnezis, A., Shchor, K., Bui, D. a, Brown-Swigart, L., Johnson, L., and Evan, G.I. (2008). Distinct thresholds govern Myc's biological output in vivo. *Cancer Cell* 14, 447–457.
- Muthalagu, N., Junttila, M.R., Wiese, K.E., Wolf, E., Morton, J., Bauer, B., Evan, G.I., Eilers, M., and Murphy, D.J. (2014). Report BIM Is the Primary Mediator of MYC-Induced Apoptosis in Multiple Solid Tissues. *CellReports* 1–7.
- Ni Chonghaile, T., Sarosiek, K. a, Vo, T.-T., Ryan, J. a, Tammareddi, A., Moore, V.D.G., Deng, J., Anderson, K.C., Richardson, P., Tai, Y.-T., et al. (2011). Pretreatment mitochondrial priming correlates with clinical response to cytotoxic chemotherapy. *Science* 334, 1129–1133.
- Pohl, D., Bittigau, P., Ishimaru, M.J., Stadthaus, D., Hübner, C., Olney, J.W., Turski, L., and Ikonomidou, C. (1999). N-Methyl-D-aspartate antagonists and apoptotic cell death triggered by head trauma in developing rat brain. *Proc. Natl. Acad. Sci. U. S. A.* 96, 2508–2513.
- Polster, B.M., Basañez, G., Young, M., Suzuki, M., and Fiskum, G. (2003a). Inhibition of Bax-induced cytochrome c release from neural cell and brain mitochondria by dibucaine and propranolol. *J. Neurosci.* 23, 2735–2743.
- Polster, B.M., Robertson, C.L., Bucci, C.J., Suzuki, M., and Fiskum, G. (2003b). Postnatal brain development and neural cell differentiation modulate mitochondrial Bax and BH3 peptide-induced cytochrome c release. *Cell Death Differ.* 10, 365–370.
- Reed, J.C., Doctor, K., Rojas, A., Zapata, J.M., Stehlik, C., Fiorentino, L., Damiano, J., Roth, W., Matsuzawa, S., Newman, R., et al. (2003). Comparative Analysis of Apoptosis and Inflammation Genes of Mice and Humans Comparative Analysis of Apoptosis and Inflammation Genes of Mice and Humans. 1376–1388.
- Rich, T., Allen, R.L., and Wyllie, a H. (2000). Defying death after DNA damage. *Nature* 407,

777–783.

Ryan, J., and Letai, A. (2013). BH3 profiling in whole cells by fluorimeter or FACS. *Methods*.

Sarosiek, K.A., and Letai, A. (2016). Directly targeting the mitochondrial pathway of apoptosis for cancer therapy with BH3 mimetics: recent successes, current challenges and future promise. *FEBS J.* n/a – n/a.

Sarosiek, K.A., Chi, X., Bachman, J.A., Sims, J.J., Montero, J., Patel, L., Flanagan, A., Andrews, D.W., Sorger, P., and Letai, A. (2013). BID preferentially activates BAK while BIM preferentially activates BAX, affecting chemotherapy response. *Mol. Cell* 51, 751–765.

Shamas-Din, A., Binder, S., Chi, X., Leber, B., Andrews, D.W., and Fradin, C. (2014). Distinct lipid effects on tBid and Bim activation of membrane permeabilization by pro-apoptotic Bax. Submitted 505, 1–25.

Shi, J., Zhang, L., Zhang, Y.-W., Surma, M., Mark Payne, R., and Wei, L. (2012). Downregulation of doxorubicin-induced myocardial apoptosis accompanies postnatal heart maturation. *Am. J. Physiol. Heart Circ. Physiol.* 302, H1603–H1613.

Shimohama, S. (2000). Apoptosis in Alzheimer ' s disease — an update. 5, 9–16.

Silber, J.H., Radcliffe, J., Peckham, V., Perilongo, G., Kishnani, P., Fridman, M., Goldwein, J.W., and Meadows, a T. (1992). Whole-brain irradiation and decline in intelligence: the influence of dose and age on IQ score. *J. Clin. Oncol.* 10, 1390–1396.

Soane, L., Siegel, Z.T., Schuh, R. a, and Fiskum, G. (2008). Postnatal developmental regulation of Bcl-2 family proteins in brain mitochondria. *J. Neurosci. Res.* 86, 1267–1276.

Tait, S.W.G., and Green, D.R. (2013). Mitochondrial regulation of cell death. *Cold Spring Harb. Perspect. Biol.* 5.

Taylor, R.C., Cullen, S.P., and Martin, S.J. (2008). Apoptosis: controlled demolition at the cellular level. *Nat. Rev. Mol. Cell Biol.* 9, 231–241.

Trachtenberg, B.H., Landy, D.C., Franco, V.I., Henkel, J.M., Pearson, E.J., Miller, T.L., and Lipshultz, S.E. (2011). Anthracycline-associated cardiotoxicity in survivors of childhood cancer. *Pediatr. Cardiol.* 32, 342–353.

Trautwein, C., Rakemann, T., Malek, N.P., Plümpe, J., Tiegs, G., and Manns, M.P. (1998). Concanavalin A-induced liver injury triggers hepatocyte proliferation. *J. Clin. Invest.* 101, 1960–1969.

Tzung, S.P., Fausto, N., and Hockenbery, D.M. (1997). Expression of Bcl-2 family during liver regeneration and identification of Bcl-x as a delayed early response gene. *Am. J. Pathol.* 150, 1985–1995.

Vo, T.-T., Ryan, J., Carrasco, R., Neuberg, D., Ross, D.J., Stone, R., DeAngelo, D.J., Frattini, M.G., and Letai, A. (2012). Relative Mitochondrial Priming of Malignant Myeloblasts and Normal HSCs Determines Chemotherapeutic Success in AML. *Cell In Press*.

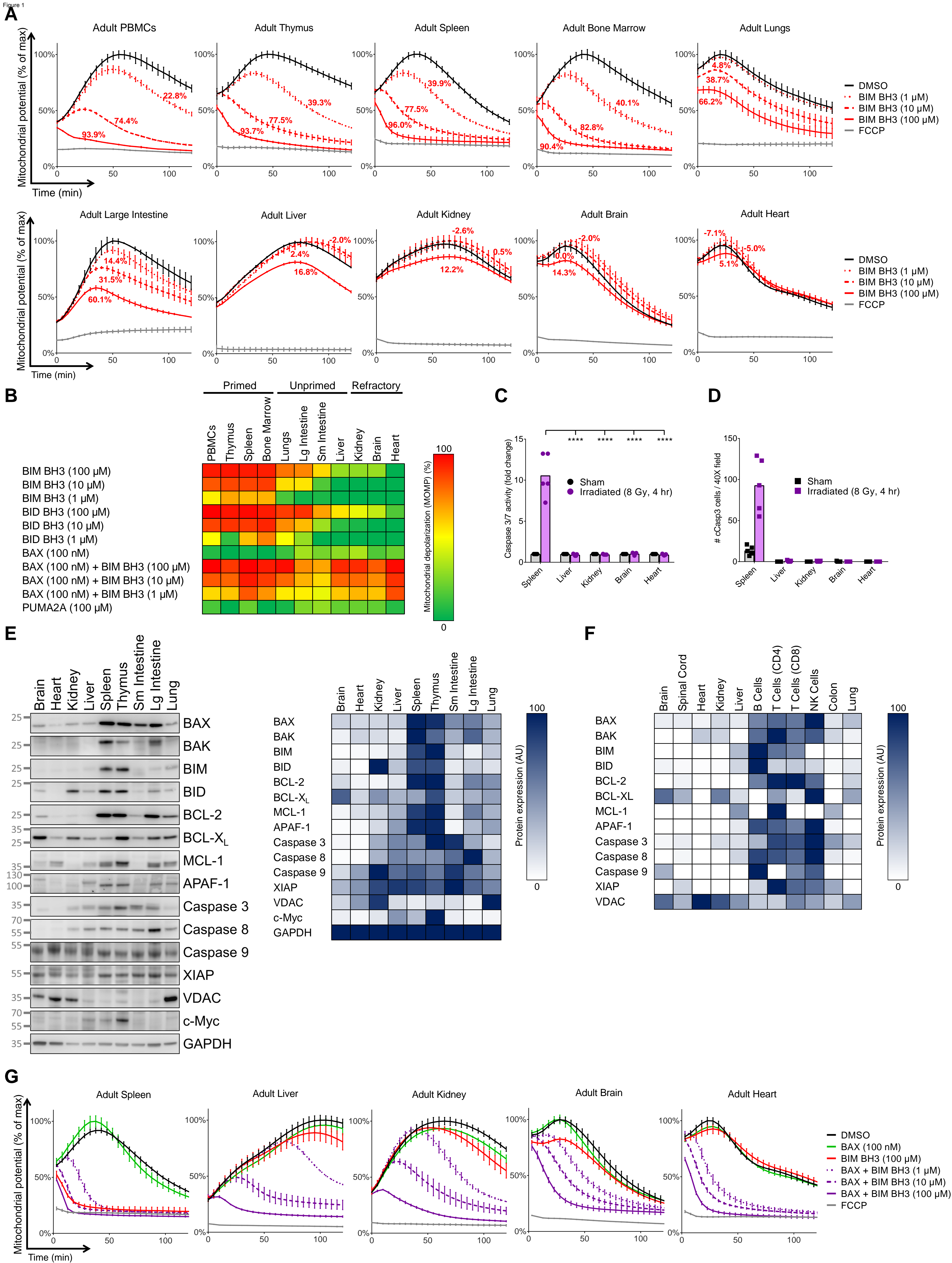
Wang, X., Bathina, M., Lynch, J., Koss, B., Calabrese, C., Frase, S., Schuetz, J.D., Rehg, J.E., and Opferman, J.T. (2013). Deletion of MCL-1 causes lethal cardiac failure and mitochondrial dysfunction. *Genes Dev.* 27, 1351–1364.

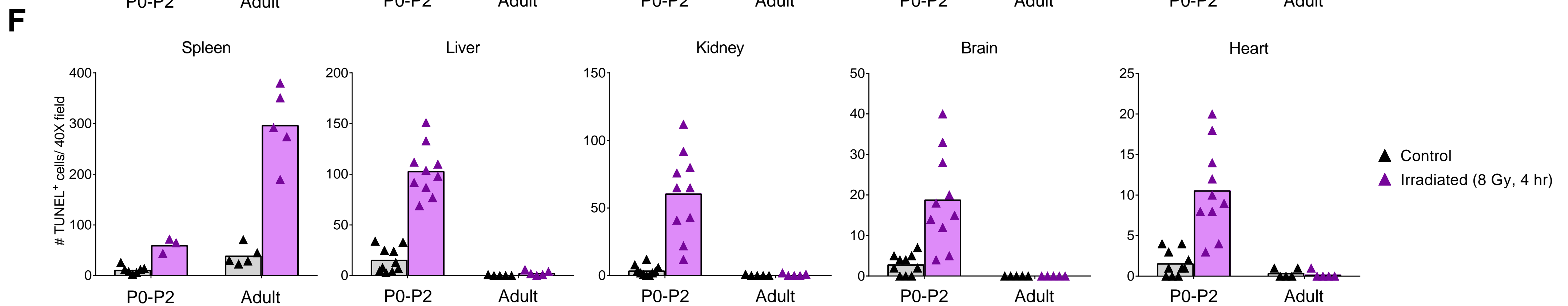
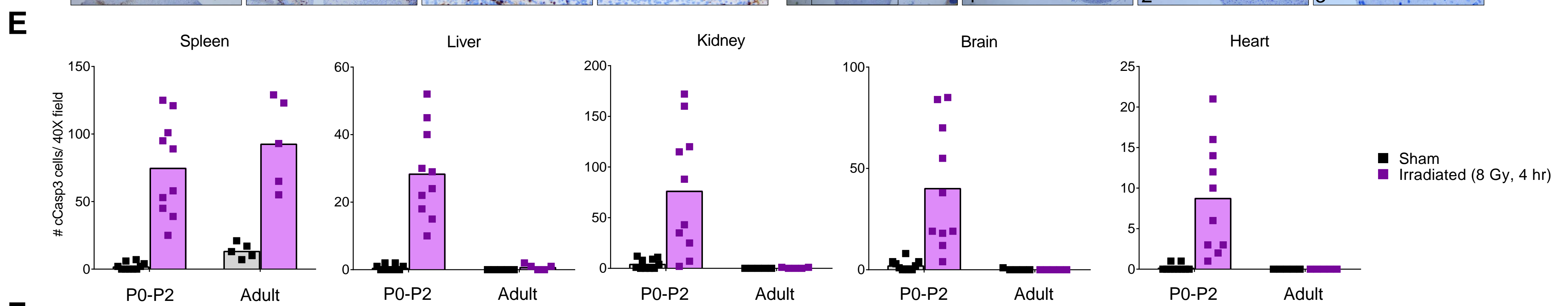
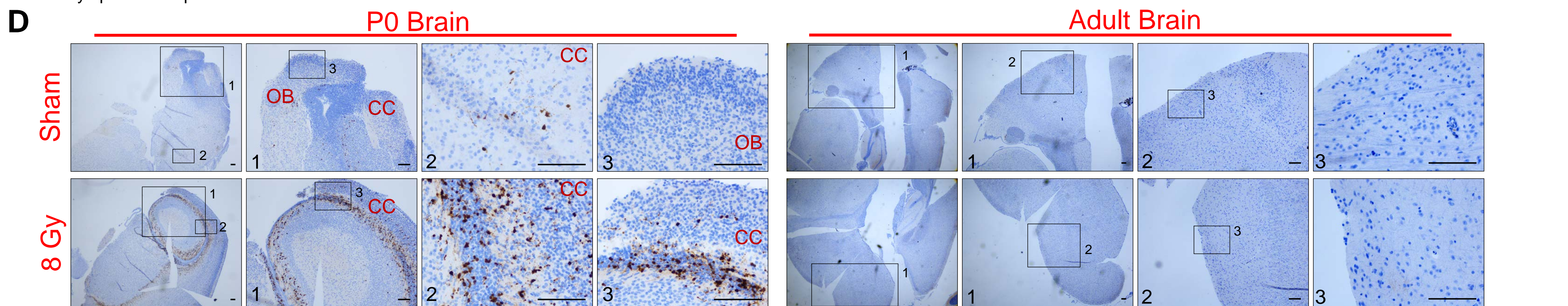
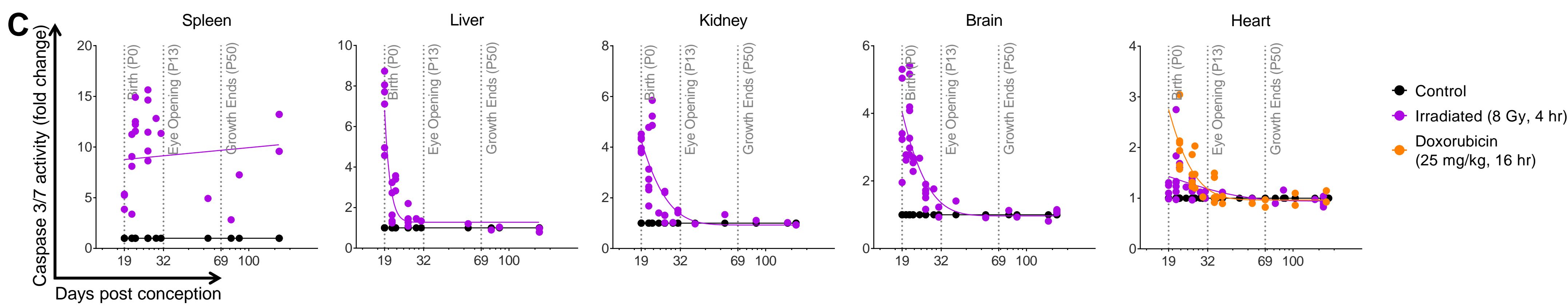
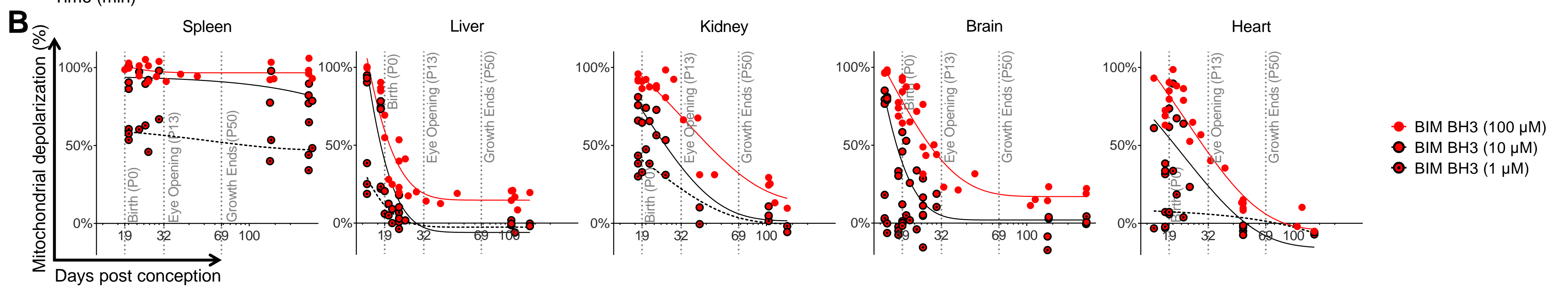
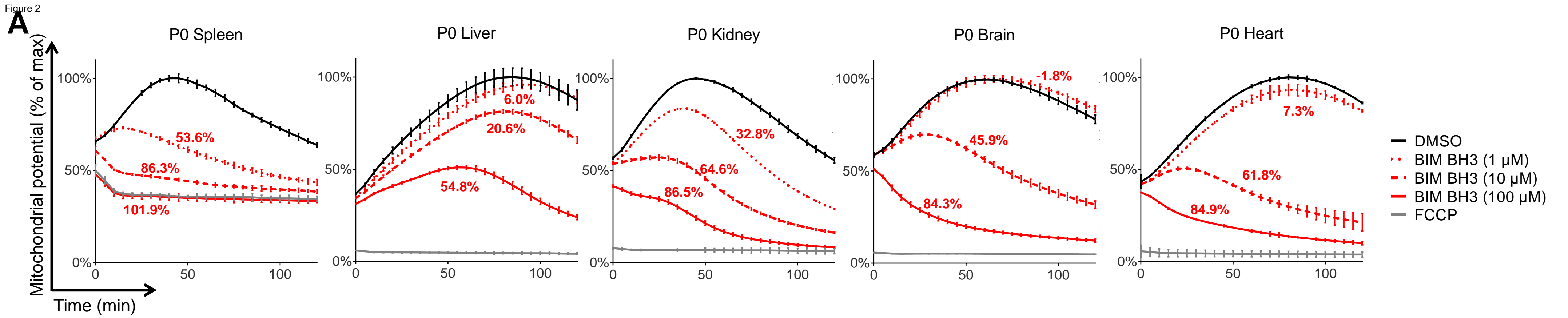
Zhang, S., Liu, X., Bawa-Khalfe, T., Lu, L.-S., Lyu, Y.L., Liu, L.F., and Yeh, E.T.H. (2012). Identification of the molecular basis of doxorubicin-induced cardiotoxicity. *Nat. Med.* 18, 1639–

Sarosiek, et al.

1642.

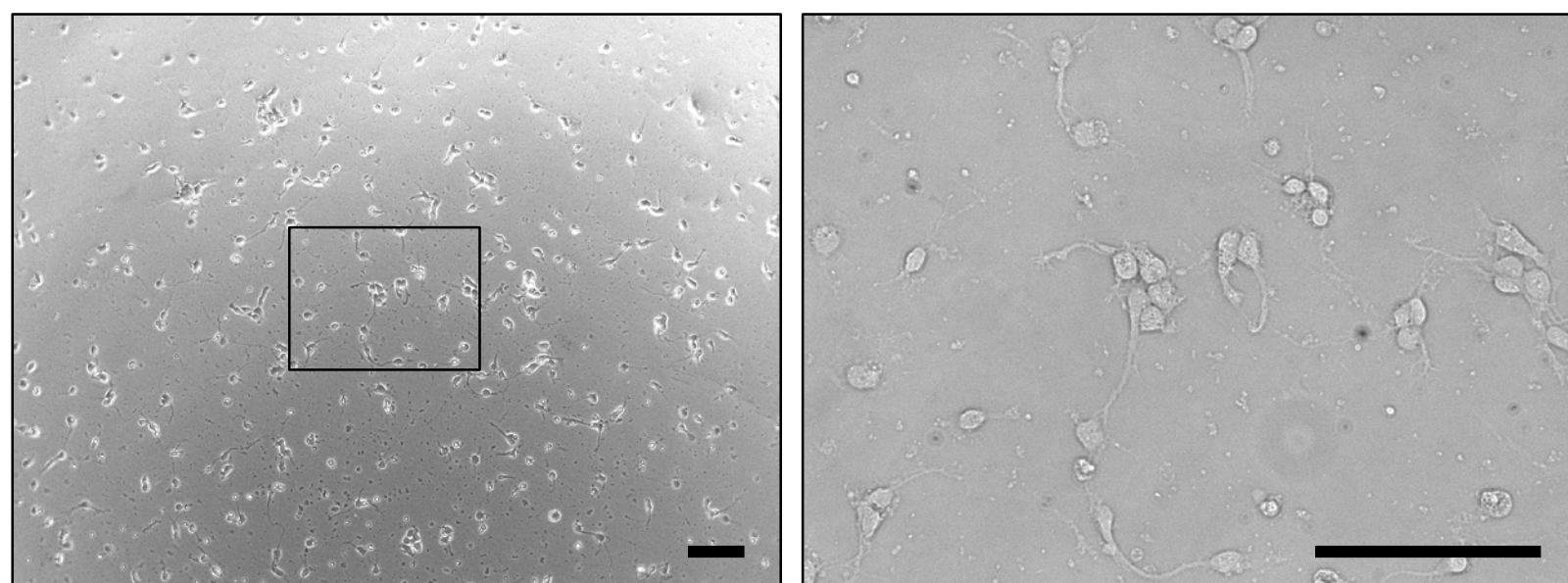
Zhou, W., and Yuan, J. (2014). SnapShot: Necroptosis. *Cell* 158, 464–464.e1.



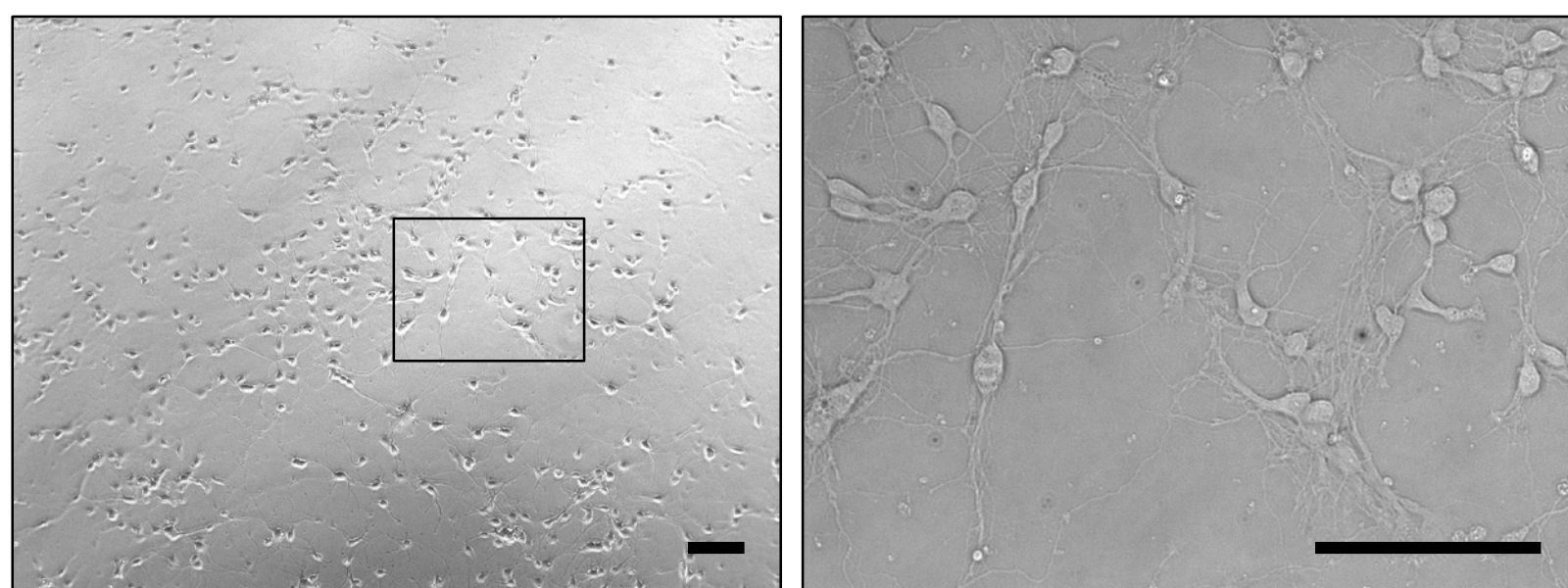


A

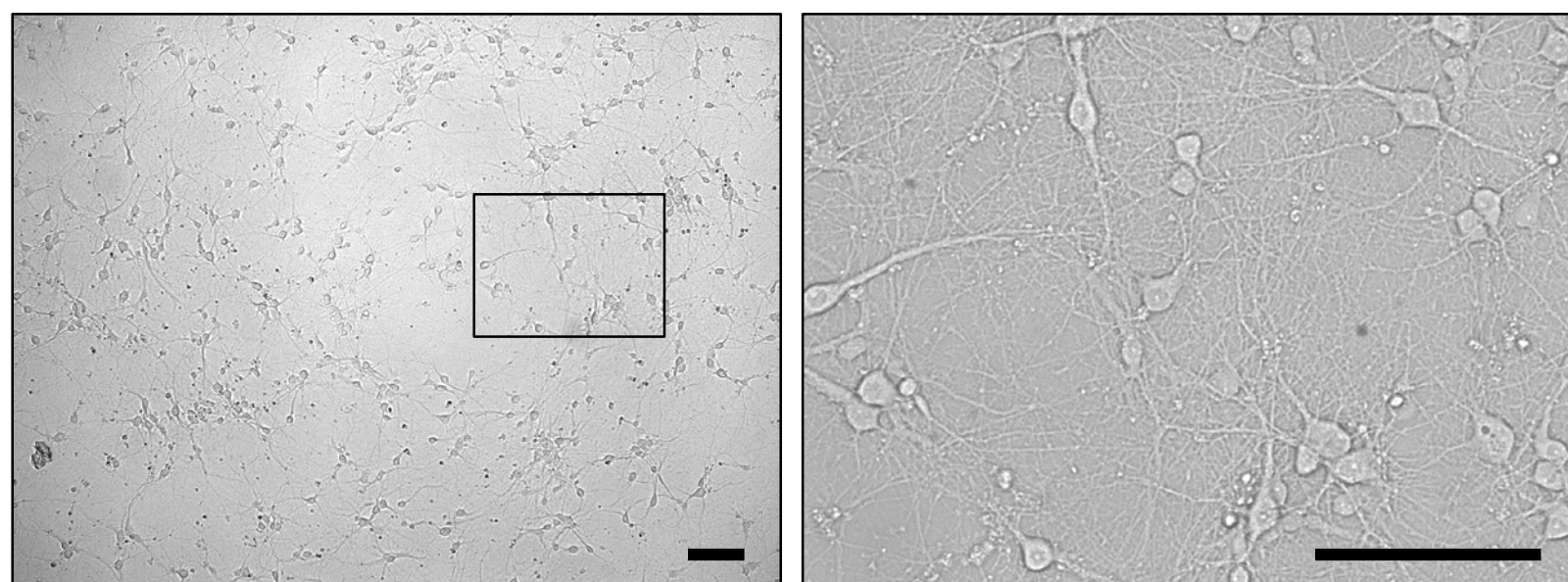
Day 1



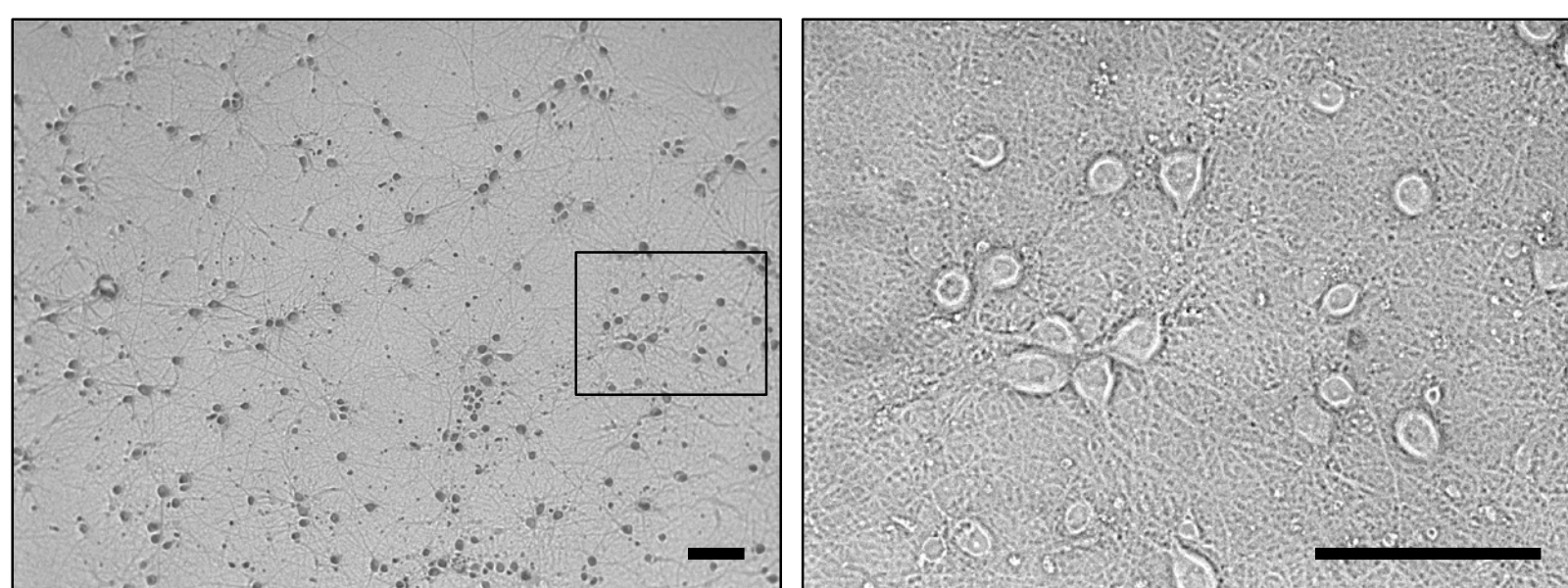
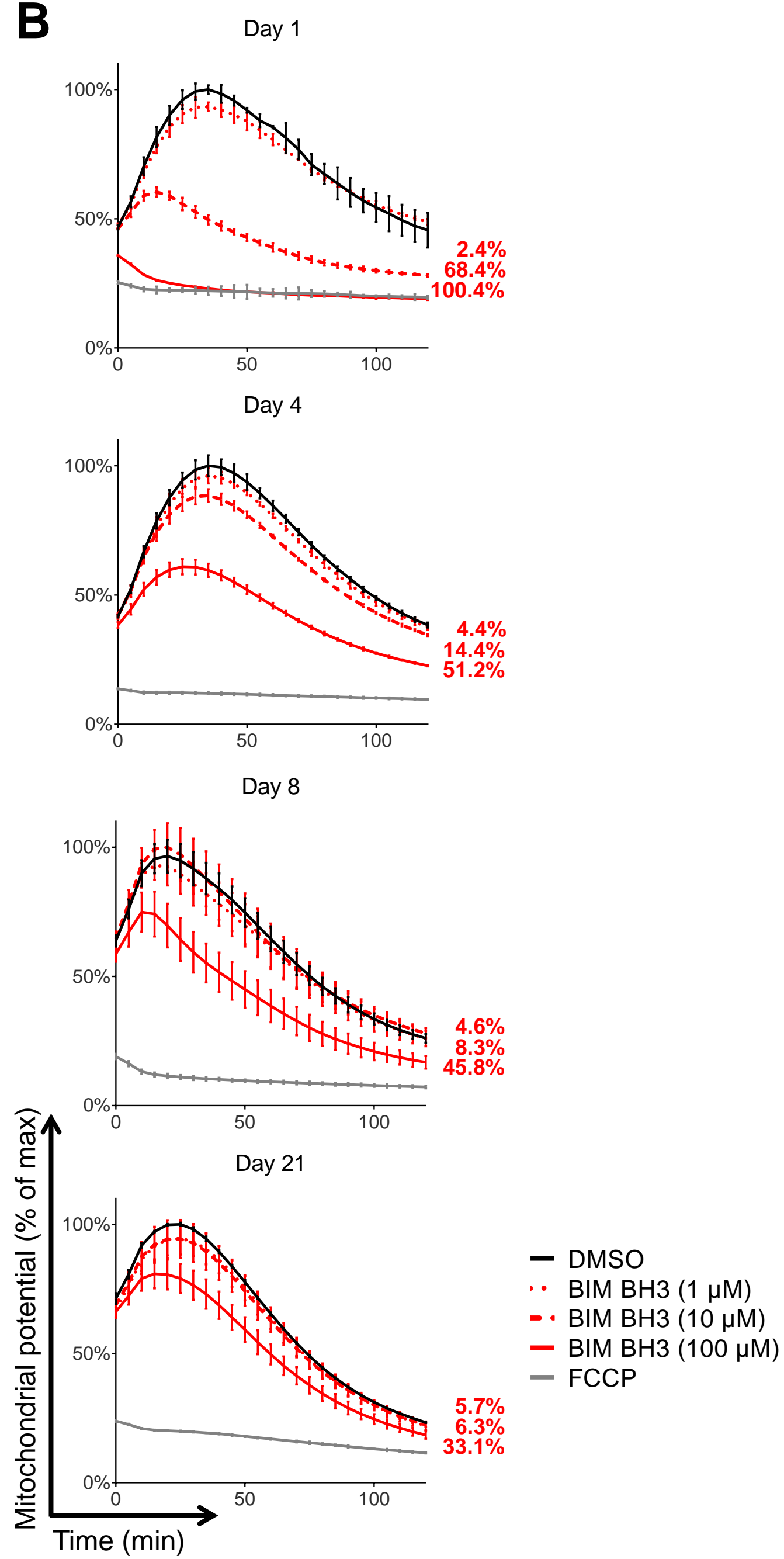
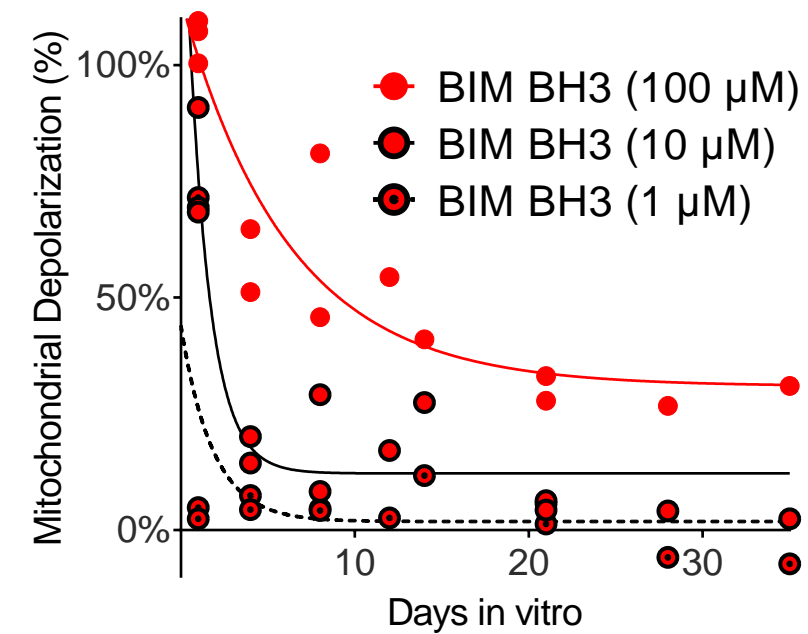
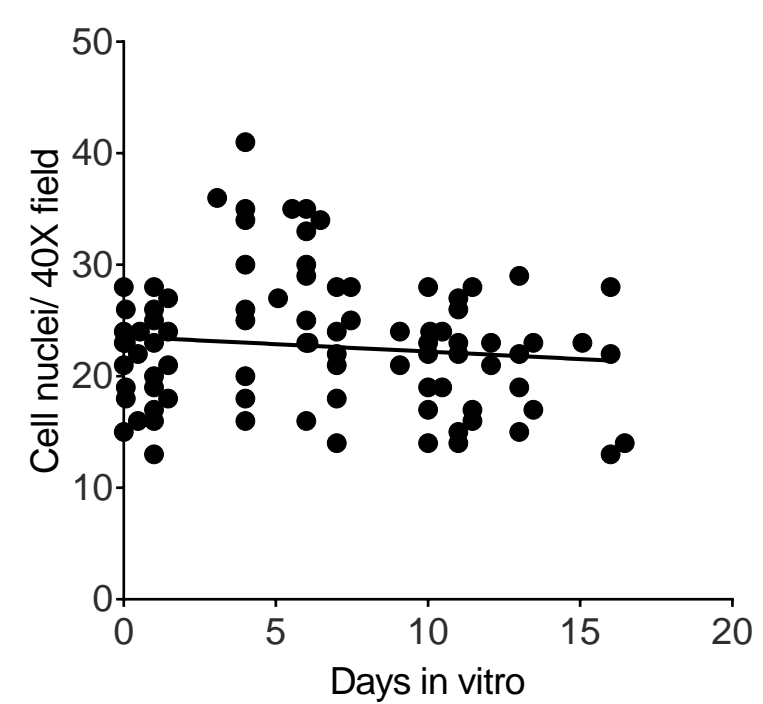
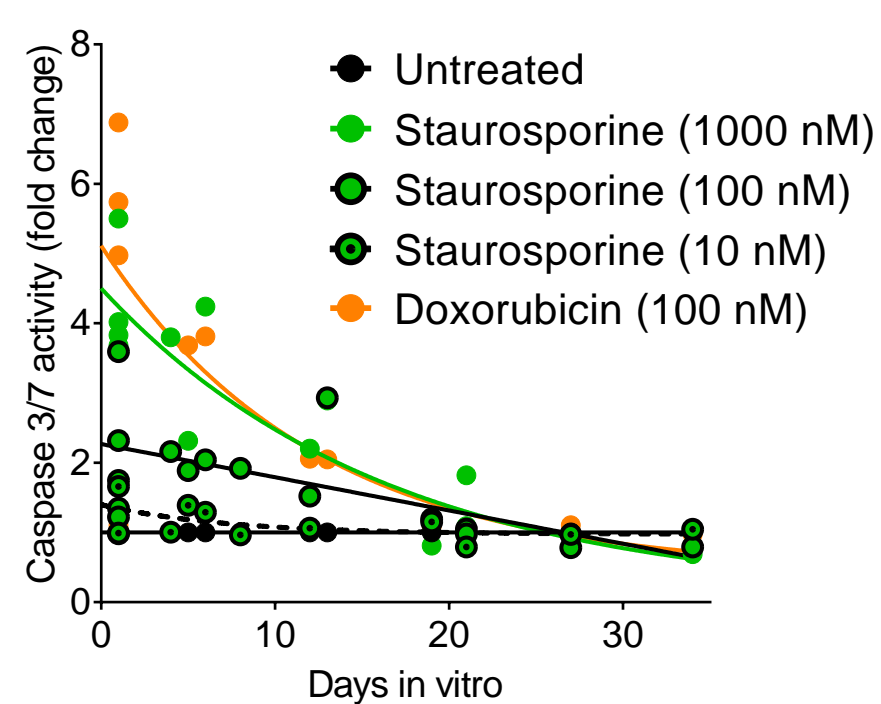
Day 4



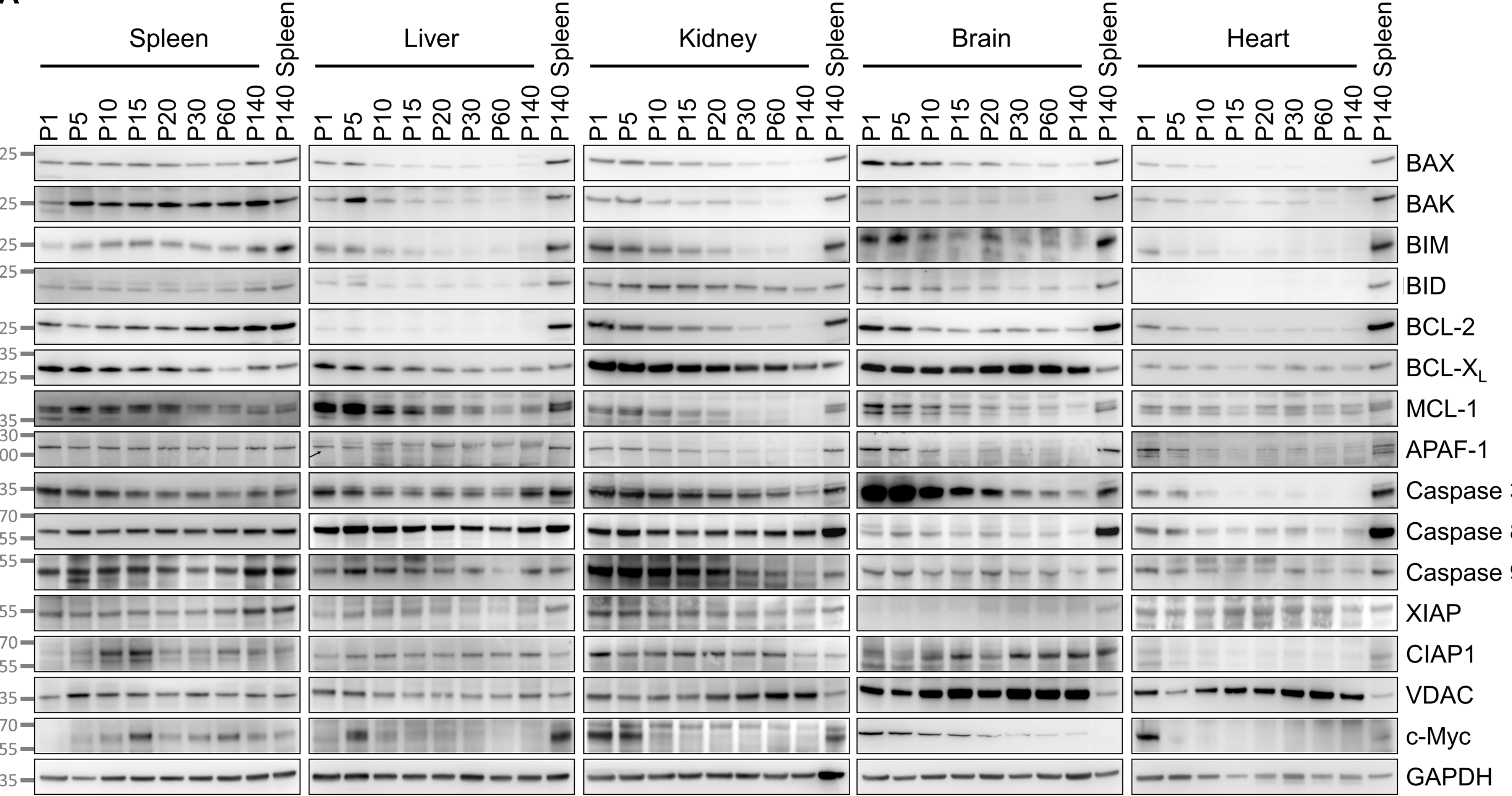
Day 7



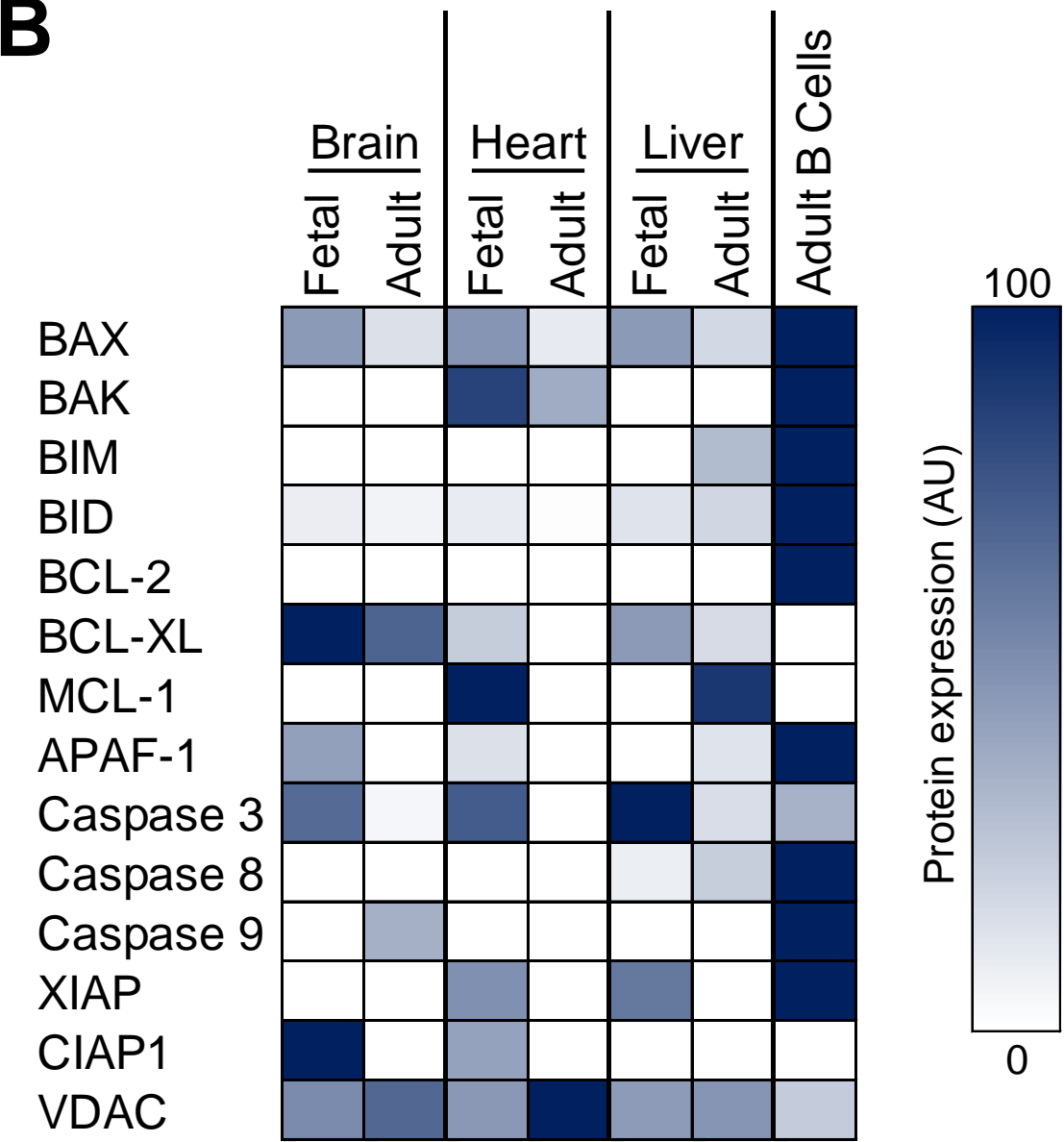
Day 19

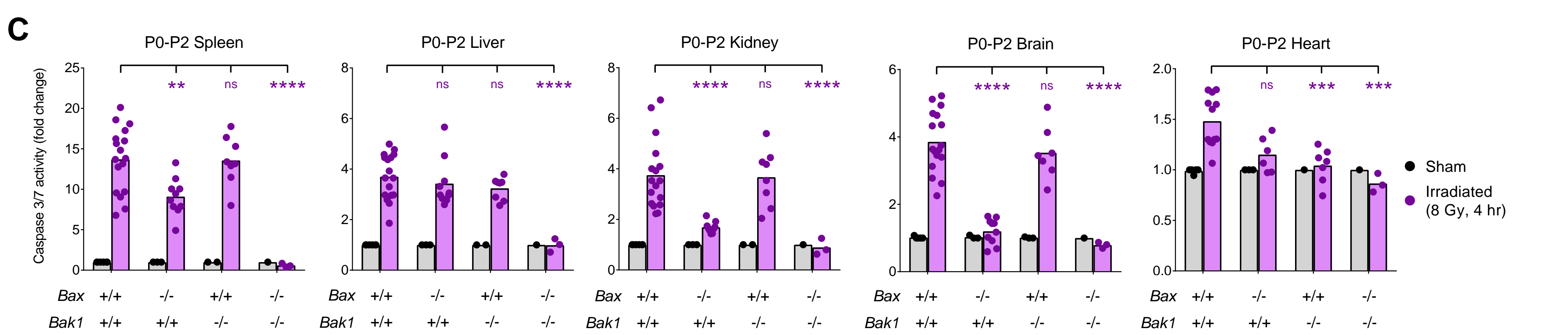
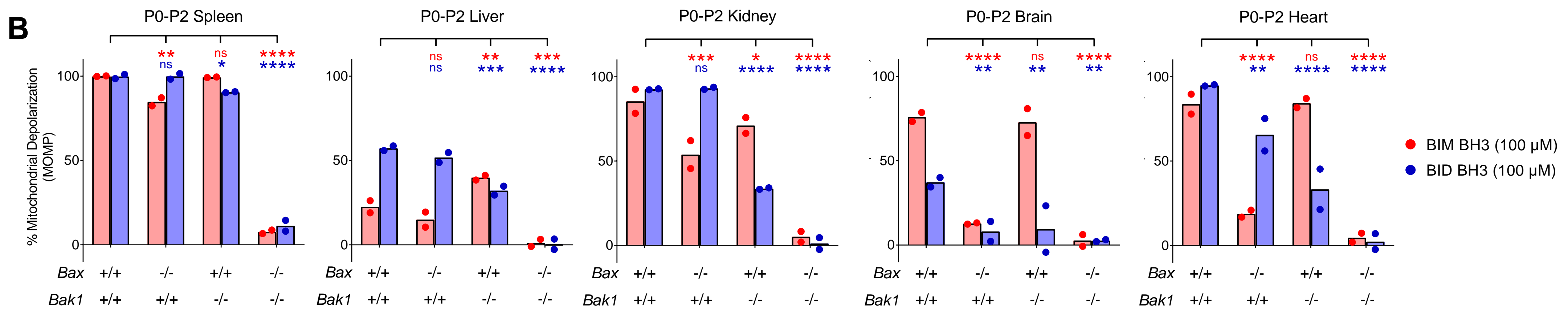
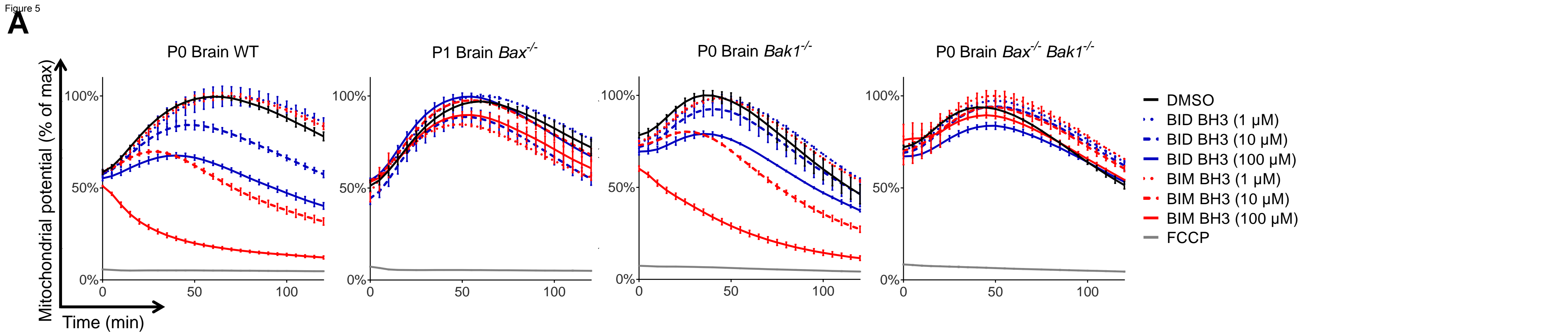
**B****C****D****E**

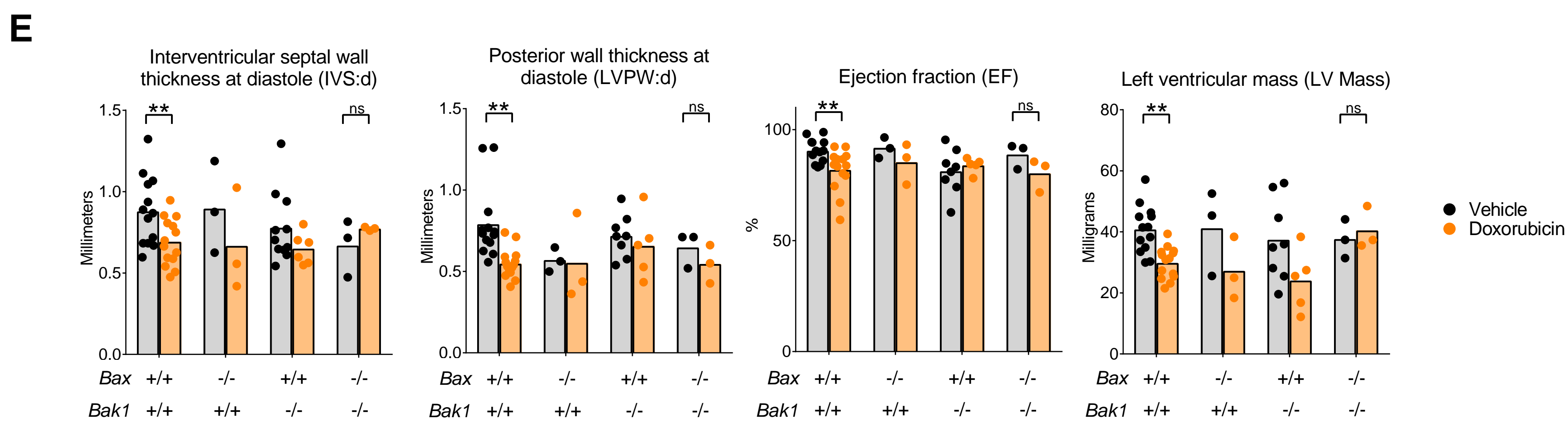
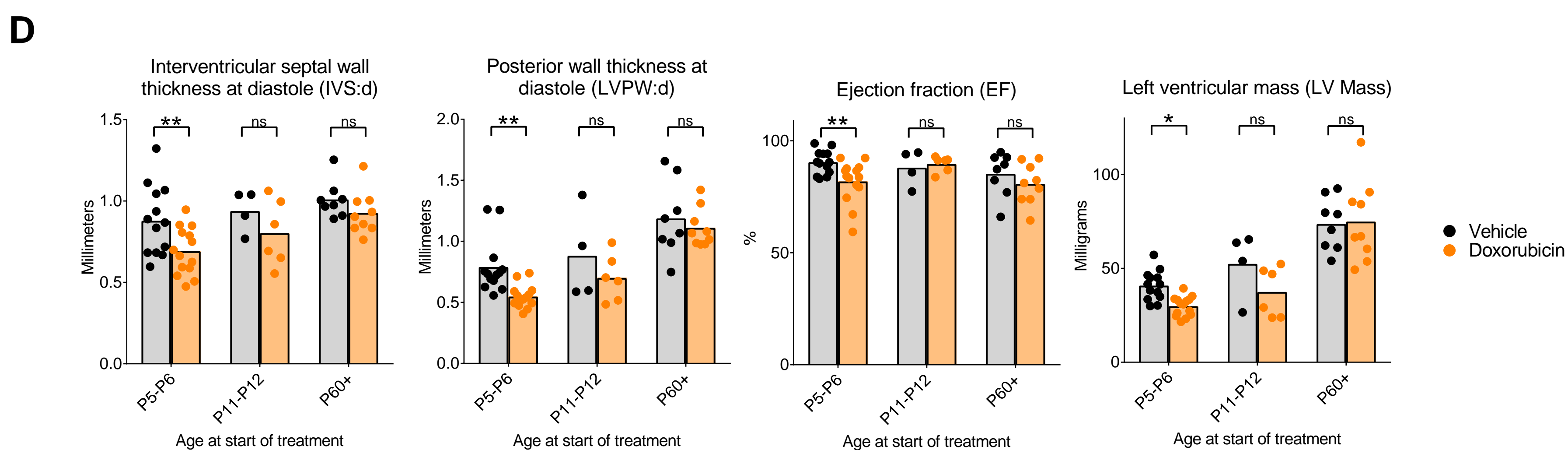
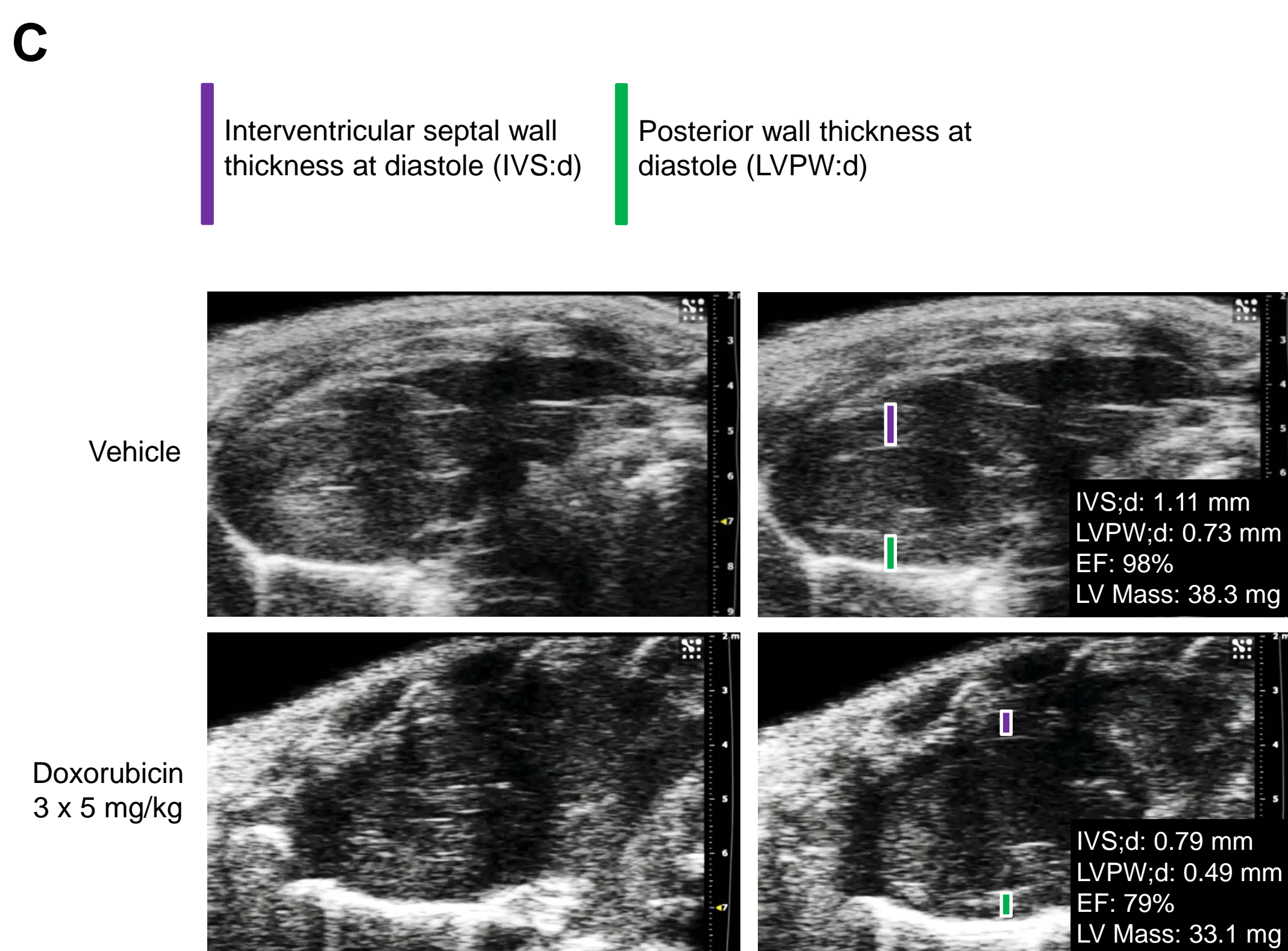
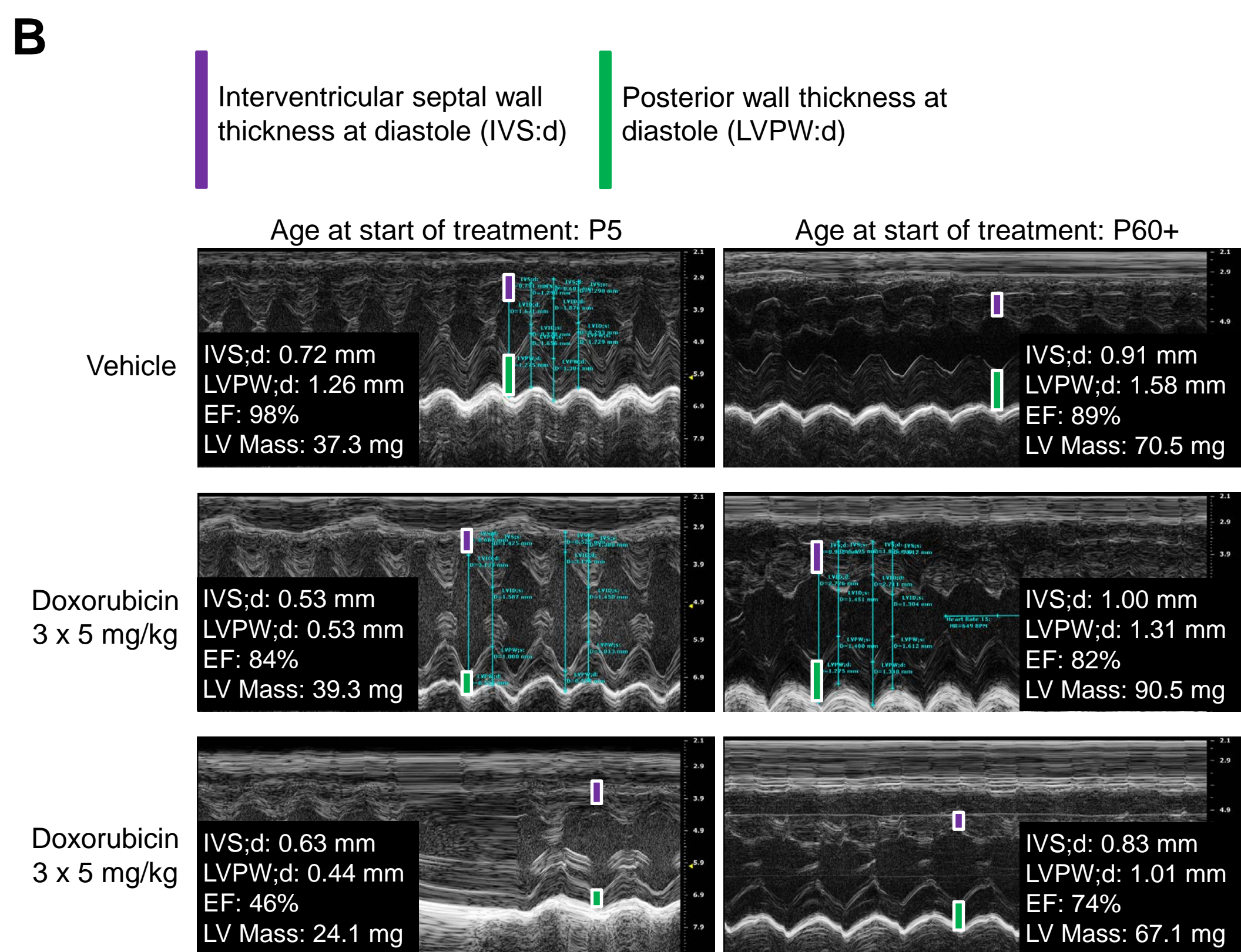
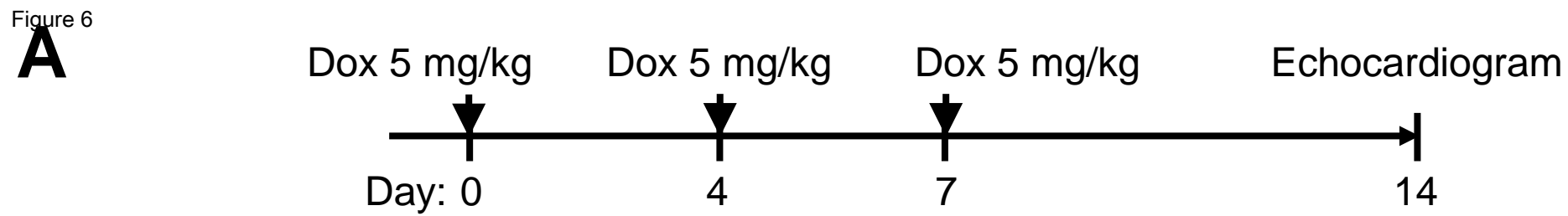
A

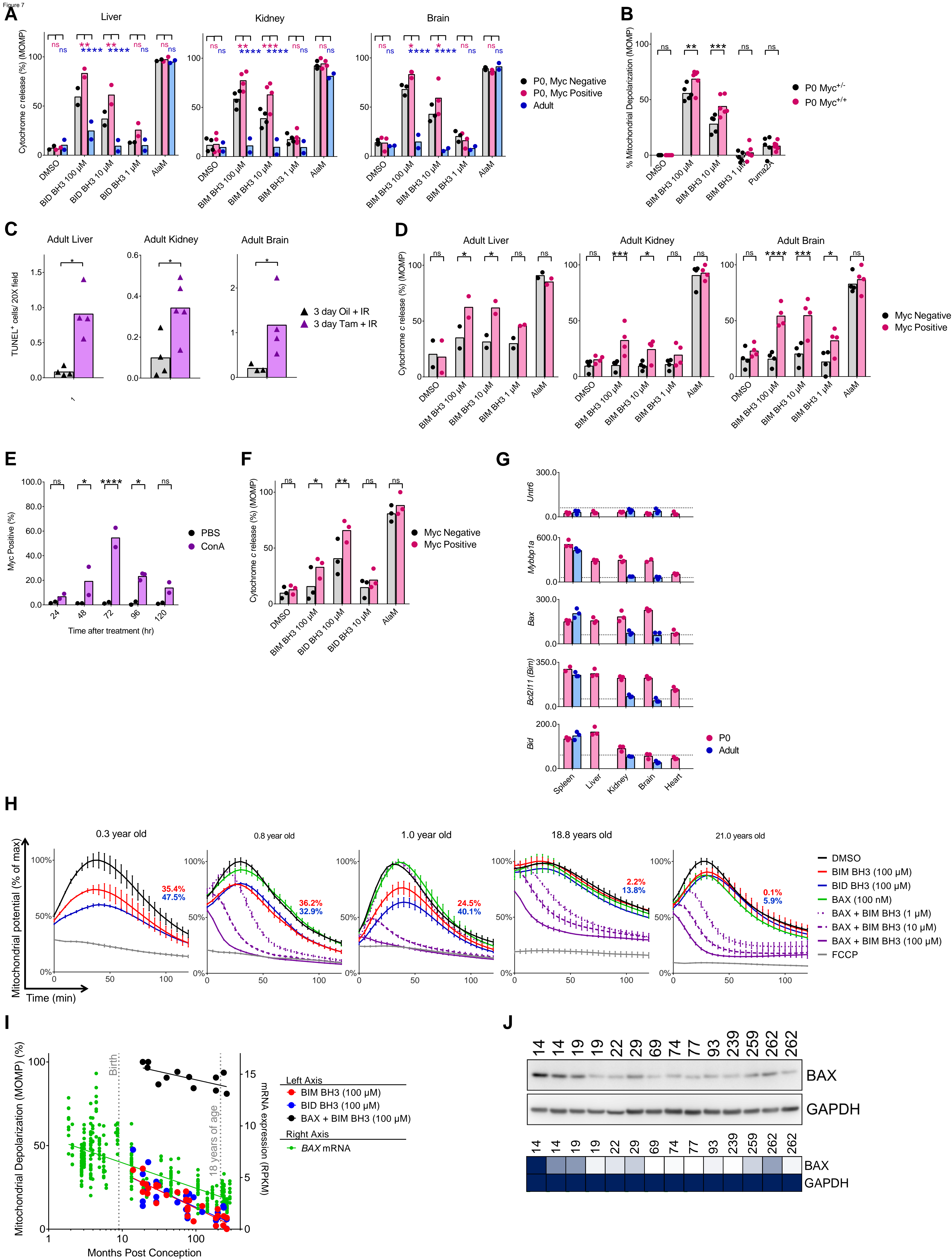


B

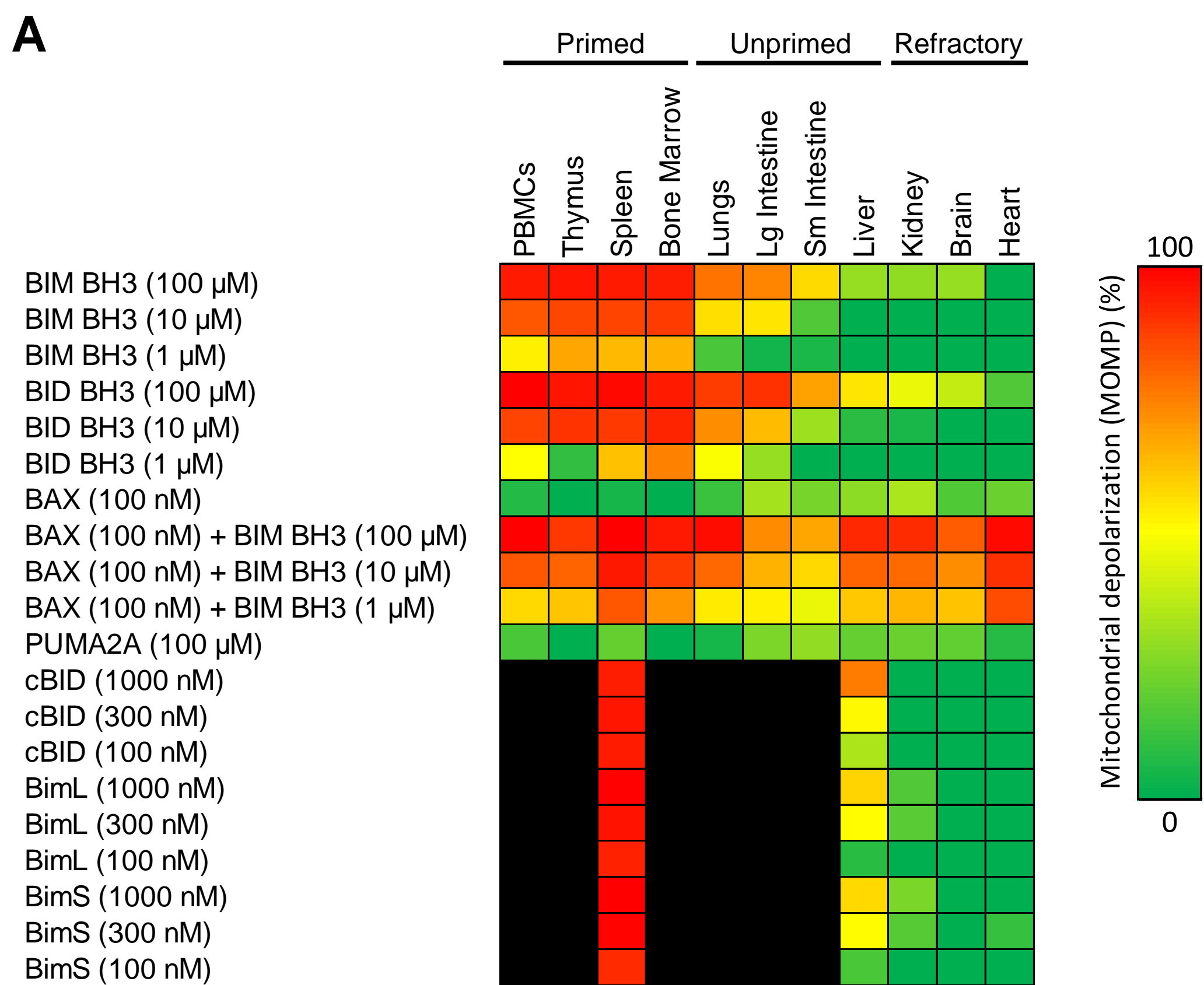




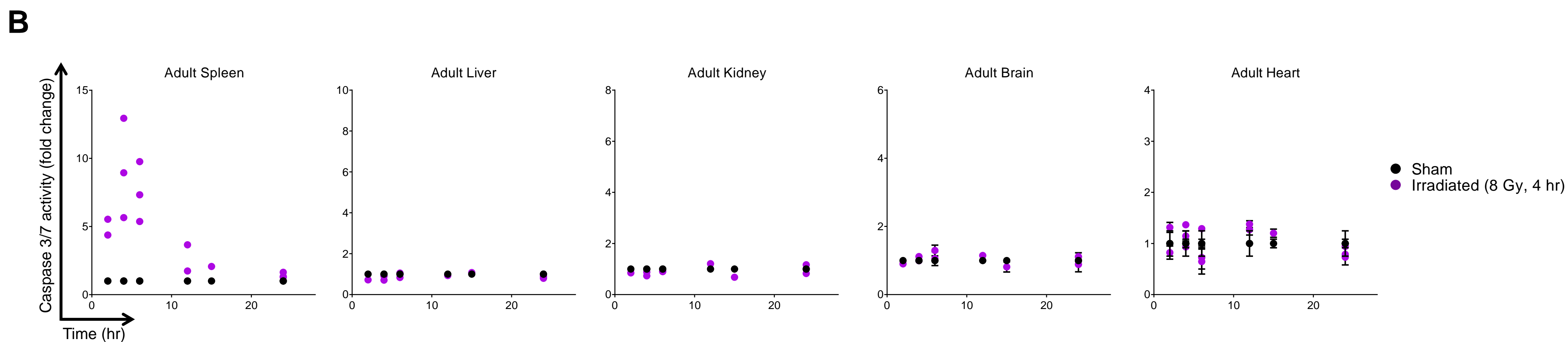




A



B



C

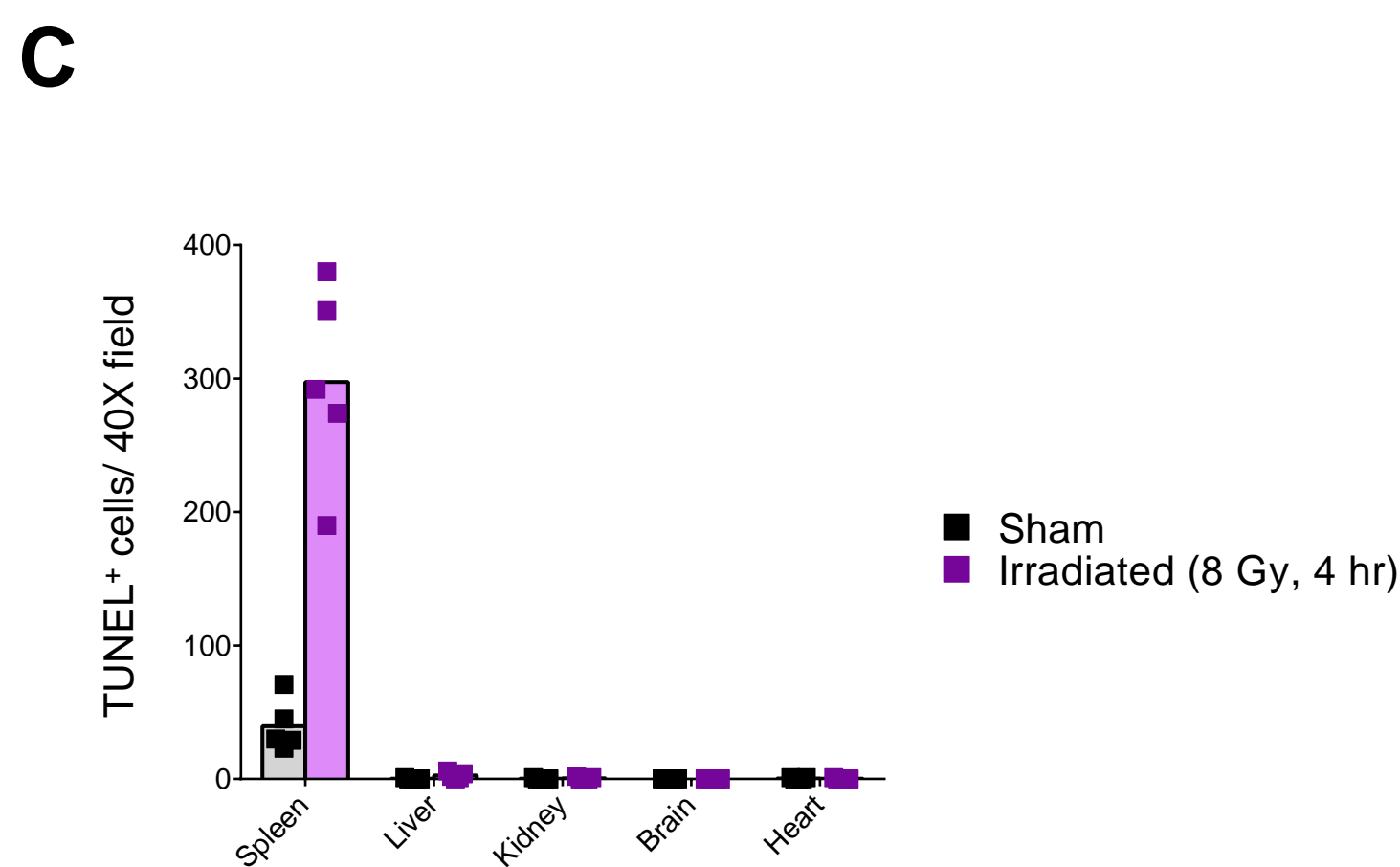


Figure S1: Measuring apoptotic priming with full-length proteins across adult mouse tissues (Related to Figure 1). (A) Summary BH3 Profiling data across healthy adult mouse tissues. Data were compiled from three indepenadent experiments. (B) Mice were irradiated and tissues were collected at the indicated time points and caspase 3/7 activity was measured. Data shown are mean \pm SD, 2 independent experiments (IEs). (C) Mice were irradiated and tissues were collected after four hours and processed for TUNEL staining. Each point represents the total TUNEL⁺ cells counted within a 40X field of view (FOV) in each tissue in one experiment. Bars represent means.

Table S1: Peptide-level mass spectrometry data for human protein expression (Related to Figure 1).

Protein	Peptide	Length	Protein Accession	Gene Symbol	GeneSpecific	IsoformSpecific	Shared
BAX	GGGPTSSEQIMK	12	gi 242117893 ref	BAX	True	False	True
	IGDELDSNMELQR	13	gi 242117893 ref	BAX	True	False	True
	KLSECLK	7	gi 242117893 ref	BAX	True	False	True
	KLSECLKR	8	gi 242117893 ref	BAX	True	False	True
	LLKPPHPHHR	10	gi 4757838 ref	BAX	True	True	False
	LSECLK	6	gi 242117893 ref	BAX	True	False	True
	LSECLKR	7	gi 242117893 ref	BAX	True	False	True
	MDGSGEQPRGGGPTSSEQIMK	21	gi 242117893 ref	BAX	True	False	True
	MDGSGEQPR	9	gi 242117893 ref	BAX	True	False	True
	MGGEAPELALDPVPQDASTK	20	gi 242117893 ref	BAX	True	False	True
	MGGEAPELALDPVPQDASTKK	21	gi 242117893 ref	BAX	True	False	True
	MIAAVDTDSPREVFFR	16	gi 242117893 ref	BAX	True	False	True
	MIAAVDTDSPR	11	gi 242117893 ref	BAX	True	False	True
	RIGDELDSNMELQR	14	gi 242117893 ref	BAX	True	False	True
	TGALLLQGFIQDR	13	gi 242117893 ref	BAX	True	False	True
	TIMGWTLDFLR	11	gi 242117893 ref	BAX	True	False	True
	VAADMFSDGNFNWGR	15	gi 242117893 ref	BAX	True	False	True
	VVALFYFASK	10	gi 242117893 ref	BAX	True	False	True
	VPELIR	6	gi 4502053 ref	ALOX12B;BAX;CLIP4	False	False	True
BAK	ASGQGP GPPR	10	gi 4502363 ref	BAK1	True	True	False
	FVVDFMLHHCIAR	13	gi 4502363 ref	BAK1	True	True	False
	HQQEQEAEGVAAPADPEMVTLP LQPSSTMGO	34	gi 4502363 ref	BAK1	True	True	False
	IATSLFESGINWGR	14	gi 4502363 ref	BAK1	True	True	False
	LALHVVYQHGLTGFLGQVTR	19	gi 4502363 ref	BAK1	True	True	False
	MASGQGP GPPR	11	gi 4502363 ref	BAK1	True	True	False
	QECGEPALPSASEEQVAQDTEEVFR	25	gi 4502363 ref	BAK1	True	True	False
	QLAIIGDDINR	11	gi 4502363 ref	BAK1	True	True	False
	QLAIIGDDINRR	12	gi 4502363 ref	BAK1	True	True	False
	SYVFYR	6	gi 4502363 ref	BAK1	True	True	False
	VVALLGFGYR	10	gi 4502363 ref	BAK1	True	True	False
	YDSEFQTMLQHLQPTAENAYEYFTK	25	gi 4502363 ref	BAK1	True	True	False
BCL-2	DFAEMSSQLHLTPFTAR	17	gi 72198189 ref	BCL2	True	False	True
	FATVVEELFR	10	gi 72198189 ref	BCL2	True	False	True
	GYEWDAGDVGAAPPGAAPAPGIFSSQPGHTP	42	gi 72198189 ref	BCL2	True	False	True
	GYEWDAGDVGAAPPGAAPAPGIFSSQPGHTP	37	gi 72198189 ref	BCL2	True	False	True
	QAGDDFSR	8	gi 72198189 ref	BCL2	True	False	True
	TSPLQTPAAPGAAAGPALSPVPPVH LTLR	30	gi 72198189 ref	BCL2	True	False	True
BCL-XL	AFSDLTSQLHITPGTAYQSFEQVVNELFR	29	gi 20336335 ref	BCL2L1	True	True	False
	EAGDEFELR	9	gi 4502381 ref	BCL2L1	True	False	True
	ELVVDFLSYK	10	gi 4502381 ref	BCL2L1	True	False	True
	EMQVLVSR	8	gi 20336335 ref	BCL2L1	True	True	False
	EVIPMAAVK	9	gi 4502381 ref	BCL2L1	True	False	True
	GYSWSQFSDVEENR	14	gi 4502381 ref	BCL2L1	True	False	True
	QALREAGDEFELR	13	gi 4502381 ref	BCL2L1	True	False	True
BCL-2/BCL-XL	DGVNWGR	7	gi 72198189 ref	BCL2L1;BCL2	False	False	True
MCL-1	LLFFAPTR	8	gi 11386165 ref	MCL1	True	False	True
	NHETAFQGMLR	11	gi 11386165 ref	MCL1	True	False	True
	TINQESCIEPLAESITDVLVR	21	gi 11386165 ref	MCL1	True	False	True
	VARPPPIGA EVPDVTATPAR	20	gi 11386165 ref	MCL1	True	False	True
	KALETLR	7	gi 19924129 ref	MCL1;RAD50	False	False	True
	ALETLR	6	gi 54792138 ref	RAD50;MCL1;HELZ	False	False	True
BIM	IGDEFNAYYAR	11	gi 5729740 ref	BCL2L11	True	False	True
	QAEPADMRPEIWIAQELR	18	gi 5729740 ref	BCL2L11	True	False	True
	QLQPAERPPQLRPGAP TSLQTEPQDRSPAPMSG	63	gi 323362973 ref	BCL2L11	True	True	False
	QPSDVSSECDR	11	gi 5729740 ref	BCL2L11	True	False	True
	VFLNNYQAAEDHPR	14	gi 5729740 ref	BCL2L11	True	False	True
BID	DLATALEQLLQAYPRDMEKEK	21	gi 347300410 ref	BID	True	False	True
	DLATALEQLLQAYPR	15	gi 347300410 ref	BID	True	False	True
	DVFHTTVNFINQNLR	15	gi 347300410 ref	BID	True	False	True
	ELDALGH ELPVLAPQWEGYDELQTDGNR	28	gi 347300410 ref	BID	True	False	True
	HLAQVGDSMDR	11	gi 347300410 ref	BID	True	False	True
	IEADSESQEDIIR	13	gi 347300410 ref	BID	True	False	True
	KVASHTPSLLR	11	gi 347300410 ref	BID	True	False	True
	LGRIEADSESQEDIIR	16	gi 347300410 ref	BID	True	False	True
	RELDALGH ELPVLAPQWEGYDELQTDGNR	29	gi 347300410 ref	BID	True	False	True
	SIPPGLVNGLALQLR	15	gi 347300410 ref	BID	True	False	True
	TMLVLALLAK	11	gi 347300410 ref	BID	True	False	True
	VASHTPSLLR	10	gi 347300410 ref	BID	True	False	True

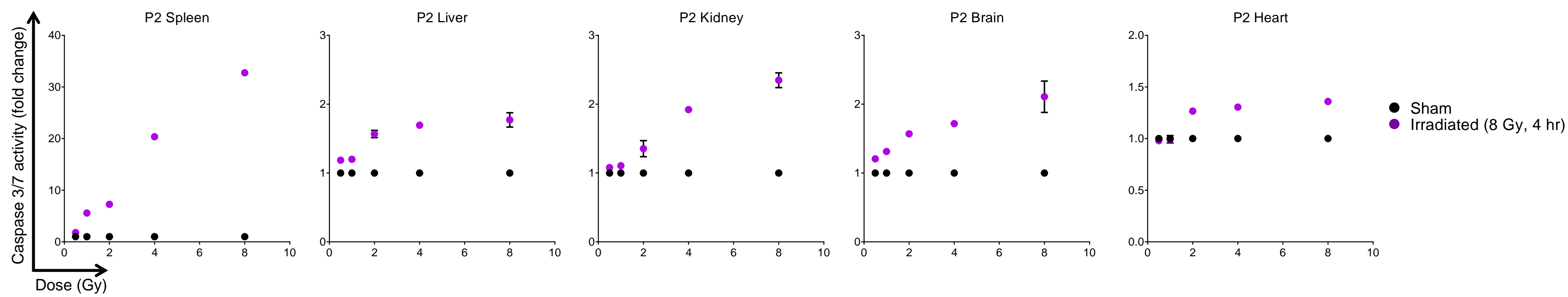
Protein	Peptide	Length	Protein Accession	Gene Symbol	Genespecific	IsoformSpecific	Shared
Caspase 3	DGSWFIQSLCAMLK	14	gi 14790119 ref	CASP3	True	False	True
	EEIVELMR	8	gi 14790119 ref	CASP3	True	False	True
	ELYFYH	6	gi 14790119 ref	CASP3	True	False	True
	GTELDCGIETDSGVDDDMACHK	22	gi 14790119 ref	CASP3	True	False	True
	GTELDCGIETDSGVDDDMACHKIPVEADFLYAY	43	gi 14790119 ref	CASP3	True	False	True
	IIHGSESMDSGISLDNSYK	19	gi 14790119 ref	CASP3	True	False	True
	IPVEADFLYAYSTAPGYYSWR	21	gi 14790119 ref	CASP3	True	False	True
	ITNFFR	6	gi 14790119 ref	CASP3	True	False	True
	KITNFFR	7	gi 14790119 ref	CASP3	True	False	True
	LEFMHILTR	9	gi 14790119 ref	CASP3	True	False	True
	LFIIQACR	8	gi 14790119 ref	CASP3	True	False	True
	MDYPEMGLCIINNKK	15	gi 14790119 ref	CASP3	True	False	True
	MENTENSVDISK	11	gi 14790119 ref	CASP3	True	False	True
	NKNDLTREEIVELMR	15	gi 14790119 ref	CASP3	True	False	True
	NKNDLTR	7	gi 14790119 ref	CASP3	True	False	True
	NLKYEVK	7	gi 14790119 ref	CASP3	True	False	True
	QIPCIVSMLTK	11	gi 14790119 ref	CASP3	True	False	True
	QYADKLEFMHILTR	14	gi 14790119 ref	CASP3	True	False	True
	SGTDVDAANLR	11	gi 14790119 ref	CASP3	True	False	True
	SLTGKPK	7	gi 14790119 ref	CASP3	True	False	True
	SSFVCVLLSHGEEGIIFGTNGPVDLKK	27	gi 14790119 ref	CASP3	True	False	True
	STGMTSR	7	gi 14790119 ref	CASP3	True	False	True
	VATEFESFSFDATFHAK	17	gi 14790119 ref	CASP3	True	False	True
XIAP	AGFLYTGEDTVK	13	gi 32528299 ref	XIAP	True	False	True
	AGFYALGEDGKVK	13	gi 32528299 ref	XIAP	True	False	True
	DHFALDRPSETHADYLLR	18	gi 32528299 ref	XIAP	True	False	True
	DSMQDESSQTSLQK	14	gi 32528299 ref	XIAP	True	False	True
	EEEFVEEFNR	10	gi 32528299 ref	XIAP	True	False	True
	EISTEEQLR	9	gi 32528299 ref	XIAP	True	False	True
	GQEYINNIHLTHSLEECLVR	20	gi 32528299 ref	XIAP	True	False	True
	IQISGSNYK	9	gi 32528299 ref	XIAP	True	False	True
	NPAMYSEEAK	10	gi 32528299 ref	XIAP	True	False	True
	NPSMADYEAK	10	gi 32528299 ref	XIAP	True	False	True
	SESDAVSSDR	10	gi 32528299 ref	XIAP	True	False	True
	SFQNWPDYAHLTPTK	14	gi 32528299 ref	XIAP	True	False	True
	SLEVLVADLVNAQK	14	gi 32528299 ref	XIAP	True	False	True
	TCVPADINKEEEFVEEFNR	19	gi 32528299 ref	XIAP	True	False	True
	TCVPADINKEEEFVEEFNRLK	21	gi 32528299 ref	XIAP	True	False	True
	TFANFPGSPVSASTLAR	18	gi 32528299 ref	XIAP	True	False	True
	TGQVVDISDTIYPTK	14	gi 32528299 ref	XIAP	True	False	True
	TPSLTR	6	gi 32528299 ref	XIAP	True	False	True
	VENYLGSR	8	gi 32528299 ref	XIAP	True	False	True
	WQYGDSAVGR	10	gi 32528299 ref	XIAP	True	False	True
APAF-1	HILDEK	6	gi 22749293 ref	FANCB;APAF1	False	False	True
	SVMGPK	6	gi 7108333 ref	HDLBP;APAF1	False	False	True
	GHLLGR	6	gi 13994259 ref	AF5;RPL13A;MRPS5;AGPS;AF5	False	False	True
	FSPDDK	6	gi 8922301 ref	VDR70;FER1L5;APAF1;NOP1	False	False	True
	ADLPEQAHSIIK	12	gi 7108333 ref	APAF1	True	False	True
	AFDSQCQILLTTR	13	gi 7108333 ref	APAF1	True	False	True
	AHEDEVLCCAFSTDDR	16	gi 7108333 ref	APAF1	True	False	True
	DFVCHQGTVLSCDISHDATK	20	gi 7108333 ref	APAF1	True	False	True
	DKSVTDSVMGPK	12	gi 7108333 ref	APAF1	True	False	True
	DLAALLHDGIPVVSSSSGK	19	gi 32483359 ref	APAF1	True	False	True
	DNDSYVSFYNALLHEGYK	18	gi 7108333 ref	APAF1	True	False	True
	DSVSGITSYVR	11	gi 32483359 ref	APAF1	True	False	True
	DYYTDLNILQK	11	gi 7108333 ref	APAF1	True	False	True
	ECKVVER	7	gi 32483363 ref	APAF1	True	True	False
	EDIKDYTTDLNILQK	15	gi 7108333 ref	APAF1	True	False	True
	FIATCSVDK	9	gi 7108333 ref	APAF1	True	False	True
	FIATCSVDKK	10	gi 7108333 ref	APAF1	True	False	True
	GHQETVKDFR	10	gi 7108333 ref	APAF1	True	False	True
	GSPLVSLIGALLR	14	gi 7108333 ref	APAF1	True	False	True
	HILDEKDCAVSENFQEFSLNQHLLGR	27	gi 7108333 ref	APAF1	True	False	True
	IHVSPDFK	8	gi 7108333 ref	APAF1	True	False	True
	IITQFQR	7	gi 7108333 ref	APAF1	True	False	True
	IWSFDLLLPLHELK	14	gi 7108333 ref	APAF1	True	False	True
	KADLPEQAHSIIK	13	gi 7108333 ref	APAF1	True	False	True
	KIHVSPDFK	9	gi 7108333 ref	APAF1	True	False	True
	KLVNAIQQK	9	gi 7108333 ref	APAF1	True	False	True
	LDQDESFQK	10	gi 7108333 ref	APAF1	True	False	True
	LLASCSADGTLK	12	gi 7108333 ref	APAF1	True	False	True
	LLSWSFDGTVK	11	gi 7108333 ref	APAF1	True	False	True
	LPLNIEEAKDR	11	gi 7108333 ref	APAF1	True	False	True
	LPLNIEEAK	9	gi 7108333 ref	APAF1	True	False	True
	LQNLCTR	7	gi 7108333 ref	APAF1	True	False	True
	LVNAIQQK	8	gi 7108333 ref	APAF1	True	False	True
	LVVRPHTDAVYHACFSEDGQR	21	gi 7108333 ref	APAF1	True	False	True
	LWDATSANER	10	gi 7108333 ref	APAF1	True	False	True
	LWDLNQK	7	gi 7108333 ref	APAF1	True	False	True
	NCLLQHR	7	gi 7108333 ref	APAF1	True	False	True
	NCSQLQDLHK	10	gi 7108333 ref	APAF1	True	False	True
	NEPTQQQR	8	gi 7108333 ref	APAF1	True	False	True
	NITNLSR	7	gi 7108333 ref	APAF1	True	False	True
	NTMFGHTNSVNHCR	14	gi 7108333 ref	APAF1	True	False	True
	QFFLNLEDPEQEDMEIVK	18	gi 7108333 ref	APAF1	True	False	True
	QFPFNIVQLGLCEPETSEVYQQAK	24	gi 7108333 ref	APAF1	True	False	True
	SLLFCDR	7	gi 7108333 ref	APAF1	True	False	True
	SVLAAEAVR	9	gi 7108333 ref	APAF1	True	False	True
	SVTDSVMGPK	10	gi 7108333 ref	APAF1	True	False	True
	TELVGPAHLIHEFVEYR	17	gi 7108333 ref	APAF1	True	False	True
	TLQVFK	6	gi 7108333 ref	APAF1	True	False	True
	TVLCEGGVPQRPVVVTR	18	gi 7108333 ref	APAF1	True	False	True
	VWNITGNK	9	gi 7108333 ref	APAF1	True	False	True
	WEYYLK	6	gi 7108333 ref	APAF1	True	False	True
	YVVPVESSLGKEK	13	gi 7108333 ref	APAF1	True	False	True
	YVVPVESSLGK	11	gi 7108333 ref	APAF1	True	False	True
	YYLHDLQVDFLTEK	14	gi 7108333 ref	APAF1	True	False	True

Protein	Peptide	Length	Protein Accession	Gene Symbol	Gene specific	Isoform specific	Shared
CIAP	ILTTGENYK	9 gi	4502141 ref	BIRC2	True	True	False
	LGDSPIQK	8 gi	4502141 ref	BIRC2	True	True	False
	QAEEMASDDLIR	14 gi	4502141 ref	BIRC2	True	True	False
	TNPYSYAMSTEEAR	14 gi	4502141 ref	BIRC2	True	True	False
	YDFSCELYR	9 gi	4502141 ref	BIRC2	True	True	False
	YIPTEDVSGLSLEEQLR	17 gi	4502141 ref	BIRC2	True	True	False
	STEEAR	6 gi	4502141 ref	BIRC2;GPI	False	False	True
	AGFYIIGPGDR	11 gi	4502141 ref	BIRC3;BIRC2	False	False	True
	ELIDTILVK	9 gi	4502141 ref	BIRC3;BIRC2	False	False	True
	MSTYSTFPAGVPVSR	16 gi	4502141 ref	BIRC3;BIRC2	False	False	True
	VACFACGGK	9 gi	4502141 ref	BIRC3;BIRC2	False	False	True
VDAC1	AVPPTYADLGK	11 gi	4507879 ref	VDAC1	True	True	False
	AVPPTYADLGKSARDVFTK	19 gi	4507879 ref	VDAC1	True	True	False
	AVPPTYADLGKSAR	14 gi	4507879 ref	VDAC1	True	True	False
	EHINLGCDMDFDIAGPSIR	19 gi	4507879 ref	VDAC1	True	True	False
	GALVLGYEGWLAGYQMNFETAK	22 gi	4507879 ref	VDAC1	True	True	False
	GLKLTDFSFSFNTGKK	17 gi	4507879 ref	VDAC1	True	True	False
	GYGFGLIK	8 gi	4507879 ref	VDAC1	True	True	False
	GYGFGLIKLDLK	12 gi	4507879 ref	VDAC1	True	True	False
	IKTGYK	6 gi	4507879 ref	VDAC1	True	True	False
	IKTGYKR	7 gi	4507879 ref	VDAC1	True	True	False
	KLETAVNLAWTAGNSNTR	18 gi	4507879 ref	VDAC1	True	True	False
	LETAVNLAWTAGNSNTR	17 gi	4507879 ref	VDAC1	True	True	False
	LTFDSSFSPNTGK	13 gi	4507879 ref	VDAC1	True	True	False
	LTFDSSFSPNTGKK	14 gi	4507879 ref	VDAC1	True	True	False
	LTLSALLDGK	10 gi	4507879 ref	VDAC1	True	True	False
	LTLSALLDGKNVNAGGHK	18 gi	4507879 ref	VDAC1	True	True	False
	NVNAGGHK	8 gi	4507879 ref	VDAC1	True	True	False
	NVNAGGHKLGLGLEFQA	17 gi	4507879 ref	VDAC1	True	True	False
	REHINLGCDMDFDIAGPSIR	20 gi	4507879 ref	VDAC1	True	True	False
	SENGLEFTSSGSANTETTK	19 gi	4507879 ref	VDAC1	True	True	False
	SENGLEFTSSGSANTETTKVTGSLET	27 gi	4507879 ref	VDAC1	True	True	False
	SRVTQSNFAVG	13 gi	4507879 ref	VDAC1	True	True	False
	SRVTQSNFAVGKYTDEFQLHTNVNDGTEFGGS	36 gi	4507879 ref	VDAC1	True	True	False
	TDEFQLHTNVNDGTEFGGSYQK	23 gi	4507879 ref	VDAC1	True	True	False
	TDEFQLHTNVNDGTEFGGSYQKV	26 gi	4507879 ref	VDAC1	True	True	False
	TKSENGLEFTSSGSANTETTK	21 gi	4507879 ref	VDAC1	True	True	False
	TKSENGLEFTSSGSANTETTKVTGSLET	29 gi	4507879 ref	VDAC1	True	True	False
	VNNSSLIGLGYTQLKPGIK	20 gi	4507879 ref	VDAC1	True	True	False
	VTGSLET	8 gi	4507879 ref	VDAC1	True	True	False
	VTGSLETKYR	10 gi	4507879 ref	VDAC1	True	True	False
	VTQSNFAVG	11 gi	4507879 ref	VDAC1	True	True	False
	VTQSNFAVGKYTDEFQLHTNVNDGTEFGGSYQ	34 gi	4507879 ref	VDAC1	True	True	False
	VTQSNFAVGKYTDEFQLHTNVNDGTEFGGSYQ	37 gi	4507879 ref	VDAC1	True	True	False
	WNTDNTLGTEITVEDQLAR	19 gi	4507879 ref	VDAC1	True	True	False
	WTEYGLTFTEK	11 gi	4507879 ref	VDAC1	True	True	False
	WTEYGLTFTEKWNTDNTLGTEITVEDQLAR	30 gi	4507879 ref	VDAC1	True	True	False
	YQIDPDACFSAK	12 gi	4507879 ref	VDAC1	True	True	False
	YRWTEYGLTFTEK	13 gi	4507879 ref	VDAC1	True	True	False
	FGIAAK	6 gi	42476281 ref	VDAC3;VDAC2;VDAC1	False	False	True
Caspase 9	DHGFEVASTSPEDSPGSNPEPDATPFQEGLR	32 gi	14790124 ref	CASP9	True	False	True
	ELFRPHMIEDIQR	13 gi	14790124 ref	CASP9	True	True	False
	GNADLAYILSMPEPCGHCLINN	27 gi	14790124 ref	CASP9	True	False	True
	KPEVLRPETPRPVDIGSGGFGDVG	30 gi	14790124 ref	CASP9	True	False	True
	FFIIQACGGEQK	12 gi	14790124 ref	CASP9	True	False	True
	LSKPTLENLTPVVL	19 gi	14790124 ref	CASP9	True	False	True
	QLIIDLETR	9 gi	14790124 ref	CASP9	True	True	False
	VANAVSVK	8 gi	14790124 ref	CASP9	True	False	True
Caspase 8	AQISAYR	7 gi	15718704 ref	CASP8	True	False	True
	CKLDDDMNLLDIFIEMEK	18 gi	15718704 ref	CASP8	True	False	True
	CPSLAGKPK	9 gi	15718704 ref	CASP8	True	False	True
	DALMLFQR	8 gi	15718704 ref	CASP8	True	False	True
	EQDSESQTL	11 gi	15718704 ref	CASP8	True	False	True
	FLLQEEISK	9 gi	15718704 ref	CASP8	True	False	True
	FLSLDYIPQR	10 gi	15718704 ref	CASP8	True	False	True
	GDDILTILTEVN	22 gi	15718704 ref	CASP8	True	False	True
	GDDILTILTEVN	18 gi	15718704 ref	CASP8	True	False	True
	GIYGTDGQEAPIVELTSQFTGLK	24 gi	15718704 ref	CASP8	True	False	True
	GIPVETDSEEQPYLEMDLSSPQTR	24 gi	15718704 ref	CASP8	True	False	True
	GYCLII	13 gi	15718704 ref	CASP8	True	False	True
	IINDYEEFSKER	12 gi	15718706 ref	CASP8	True	False	True
	IINDYEEFSK	10 gi	15718704 ref	CASP8	True	False	True
	INRLDLLITYLNTR	14 gi	15718704 ref	CASP8	True	False	True
	KQEPIKDALMLFQR	14 gi	15718704 ref	CASP8	True	False	True
	LDDDMNLLDIFIEMEK	16 gi	15718704 ref	CASP8	True	False	True
	LGDSETAMVPGK	12 gi	122056476 ref	CASP8	True	True	False
	MLEESNLSFLK	11 gi	15718704 ref	CASP8	True	False	True
	NLYDIGEQLDSEDLASLK	18 gi	15718704 ref	CASP8	True	False	True
	NPAEGTWYIQSLCQSLR	17 gi	15718704 ref	CASP8	True	False	True
	QEPIKDALMLFQR	13 gi	15718704 ref	CASP8	True	False	True
	QMPQPTFTLR	10 gi	15718704 ref	CASP8	True	False	True
	QTSGILSDHQSSQFCK	16 gi	15718712 ref	CASP8	True	True	False
	VCAQINK	7 gi	15718704 ref	CASP8	True	False	True
	VFFIQACQGDNYQK	14 gi	15718704 ref	CASP8	True	False	True
	VILGEGK	7 gi	15718704 ref	CASP8	True	False	True
	VMLYQISEEVS	12 gi	15718704 ref	CASP8	True	False	True

Footnote: peptides marked in red were excluded from analysis due to insufficient specificity.

Table S2: Mass spectrometry peptide details (Related to Figure 1).

Protein	Total peptides analyzed	Total gene-specific peptides analyzed	Total gene-specific peptides detected (all tissues)	Total gene-specific peptides detected (Adult B Cells)
BAX	19	18	17	12
BAK	12	12	9	6
BCL-2	7	6	6	5
BCL-XL	8	7	4	0
MCL-1	6	4	4	0
BIM	5	5	4	3
BID	12	12	12	9
APAF-1	54	50	38	16
Caspase 3	23	23	20	7
XIAP	20	20	14	2
CIAP	11	6	3	0
VDAC1	39	38	35	16
Caspase 9	8	8	4	3
Caspase 8	28	28	26	18

A**B**

Sham

8 Gray

Sham

8 Gray

Sham

8 Gray

Sham

8 Gray

P0

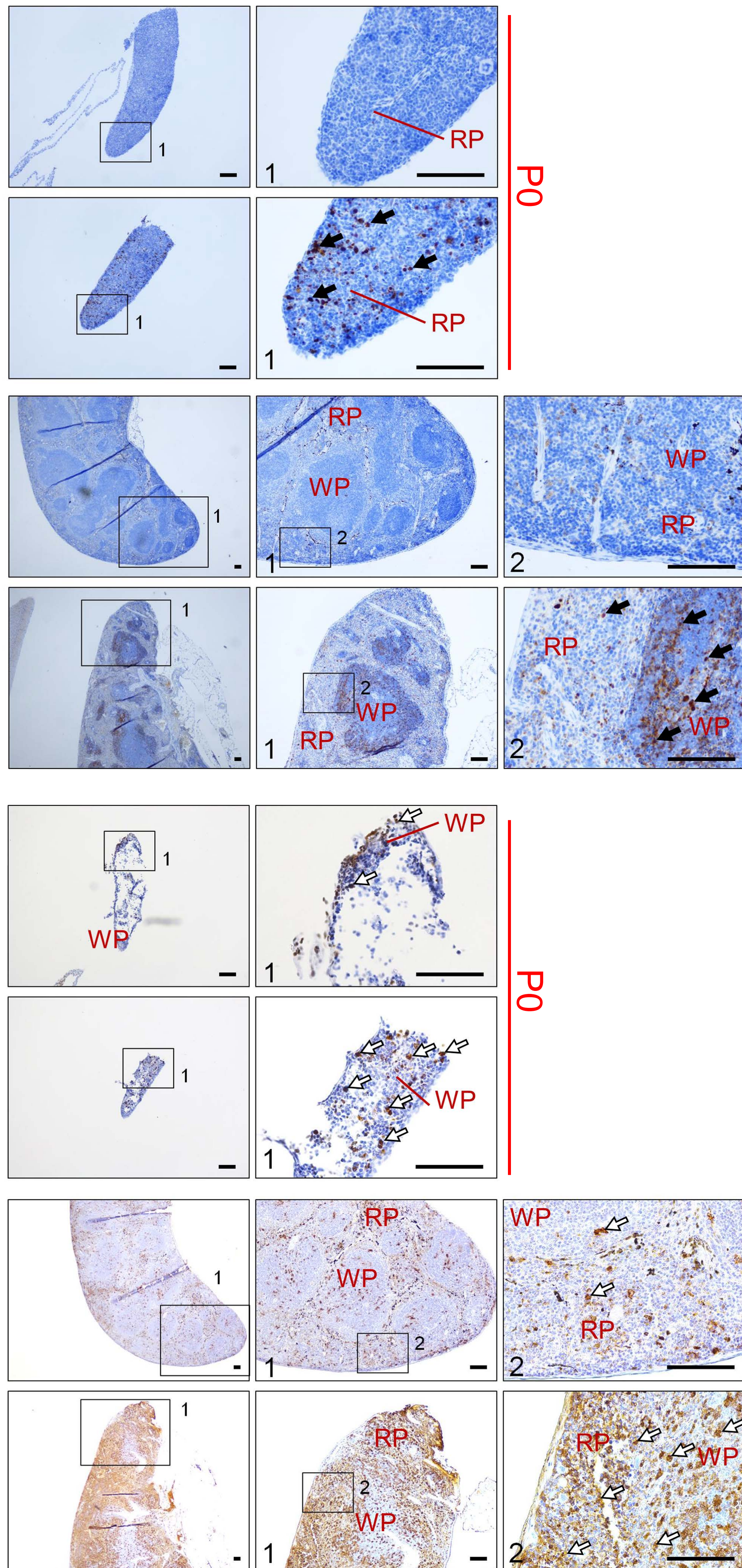
Adult

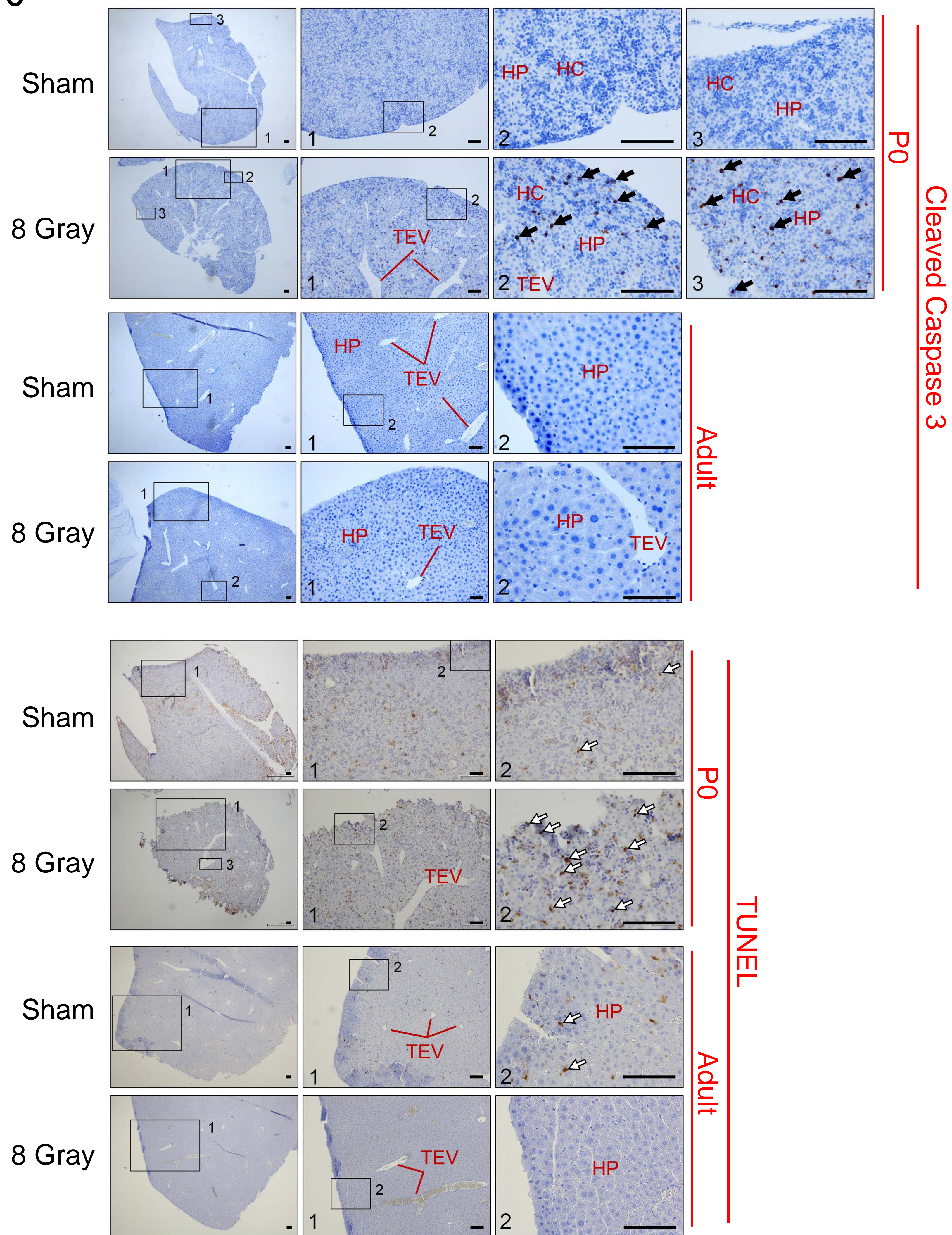
Cleaved Caspase 3

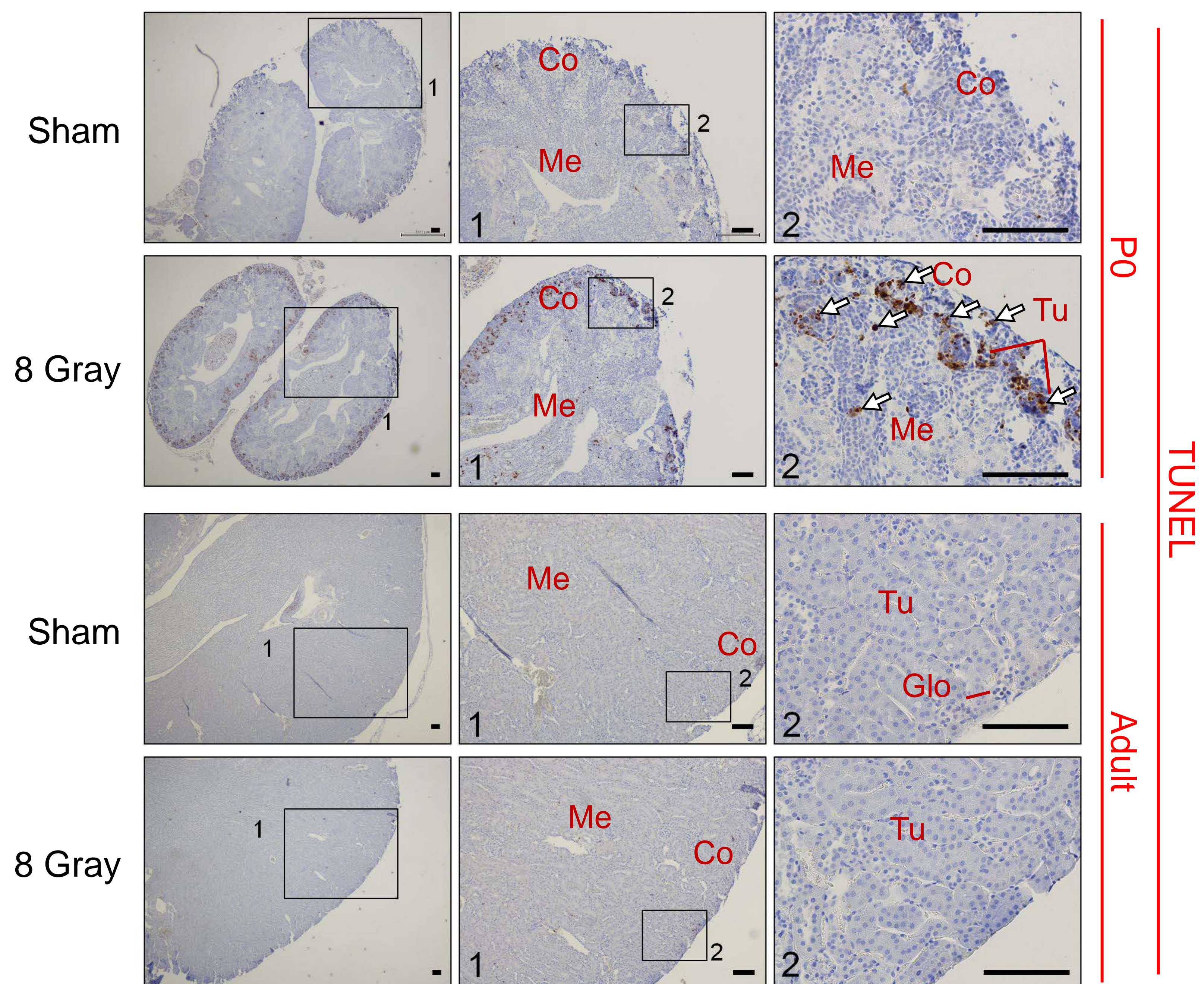
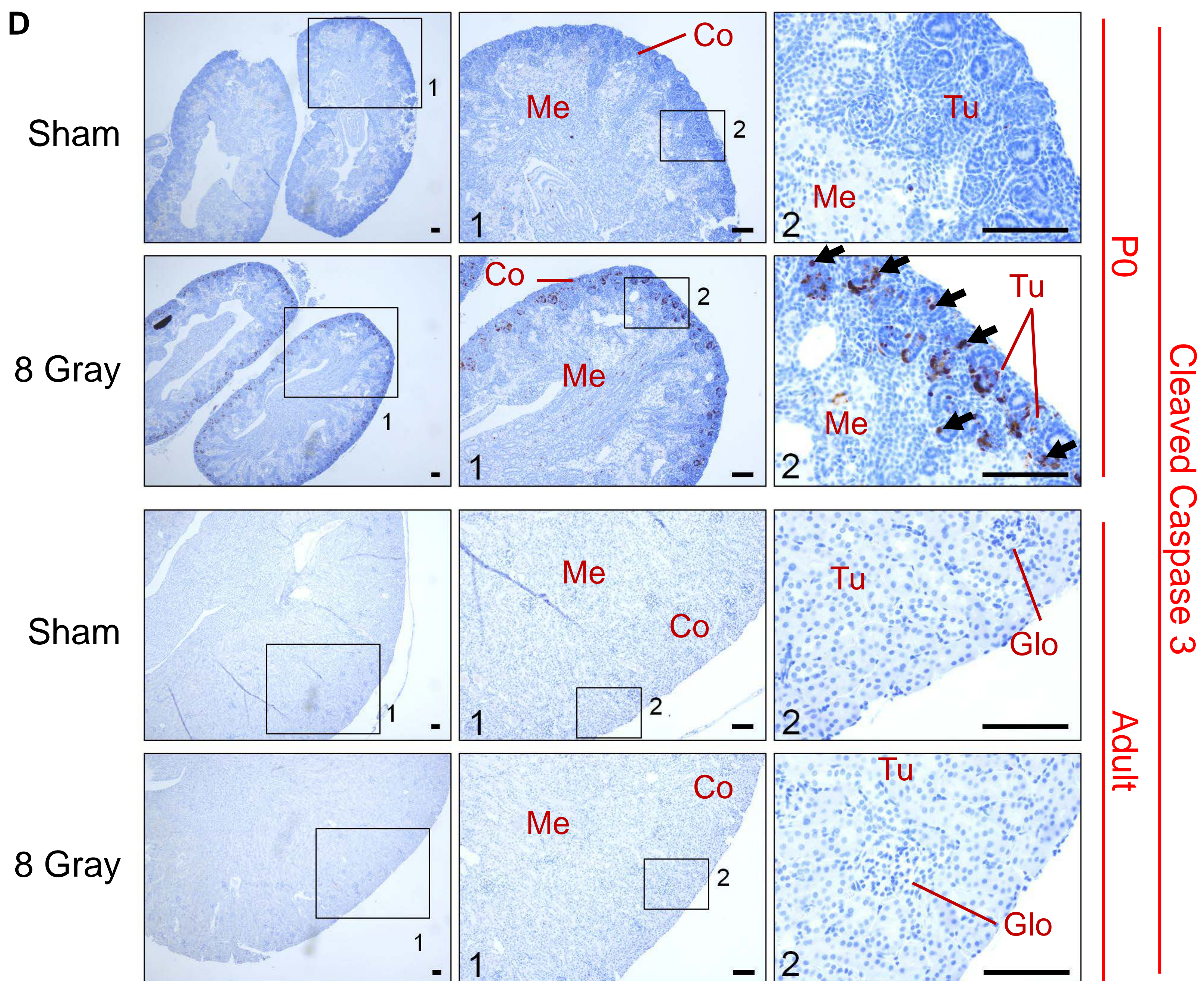
P0

Adult

TUNEL

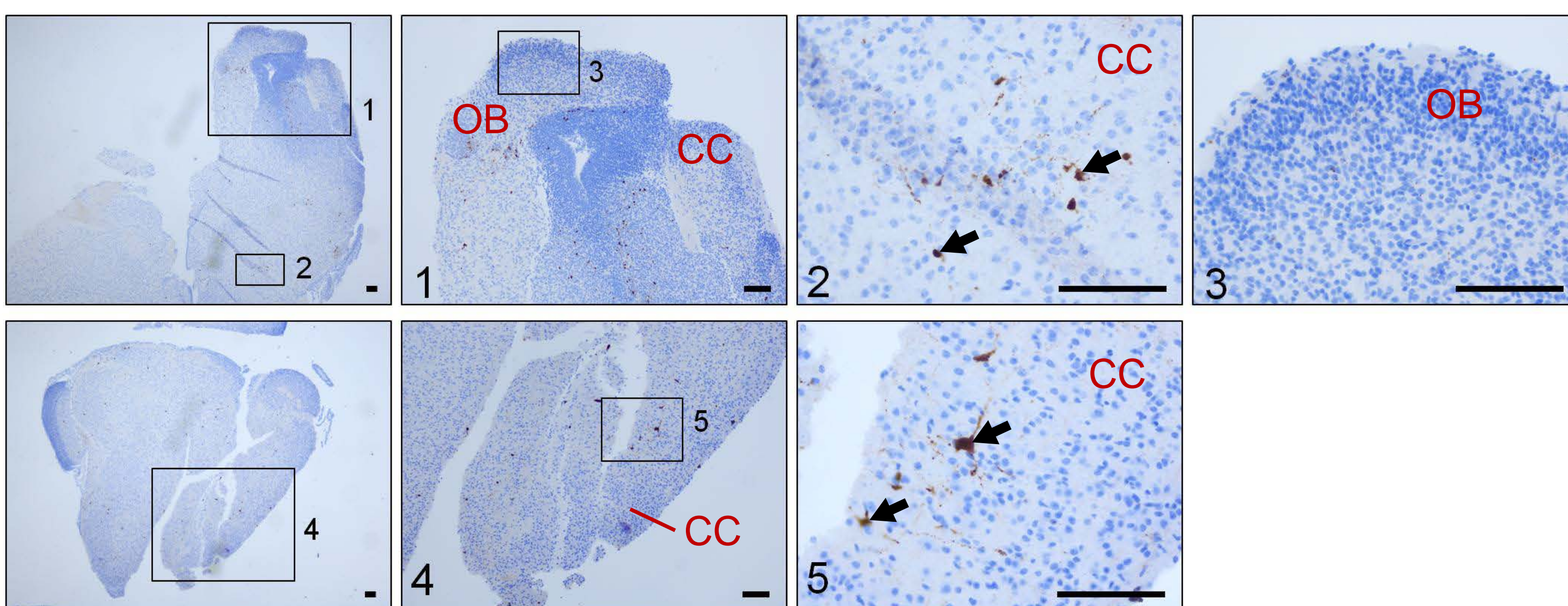


C

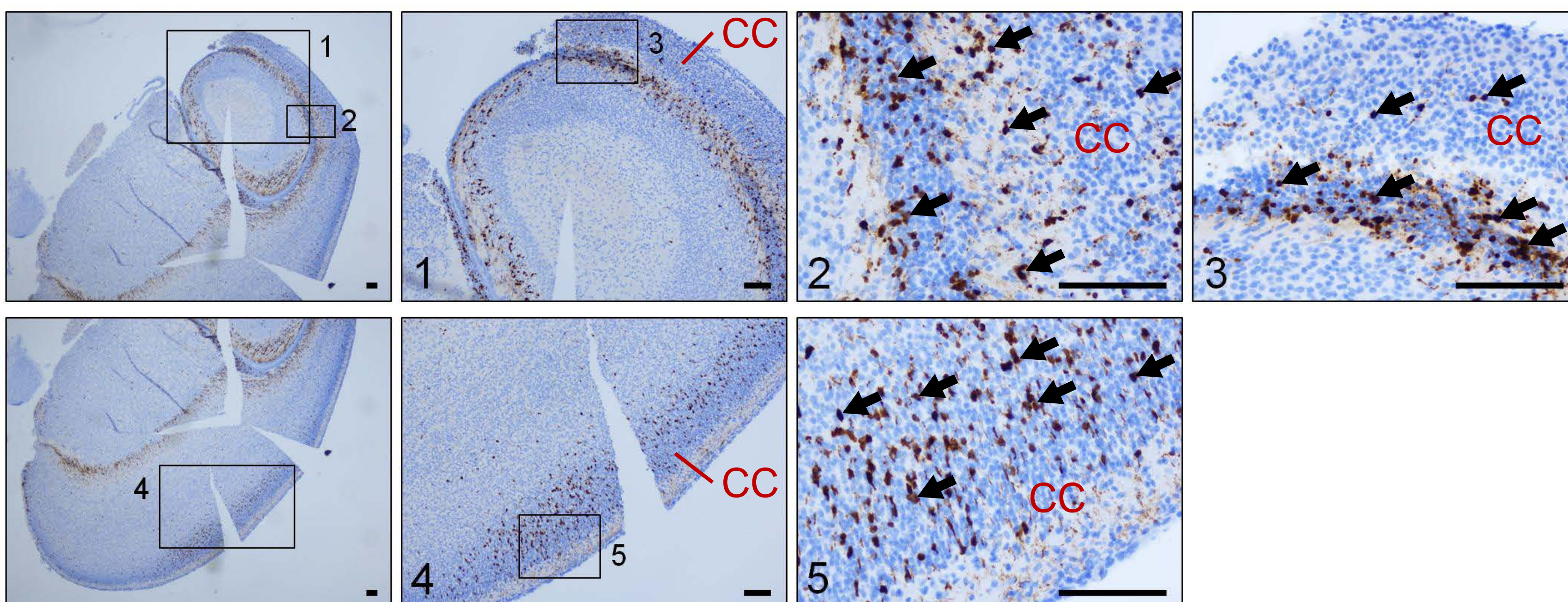


E

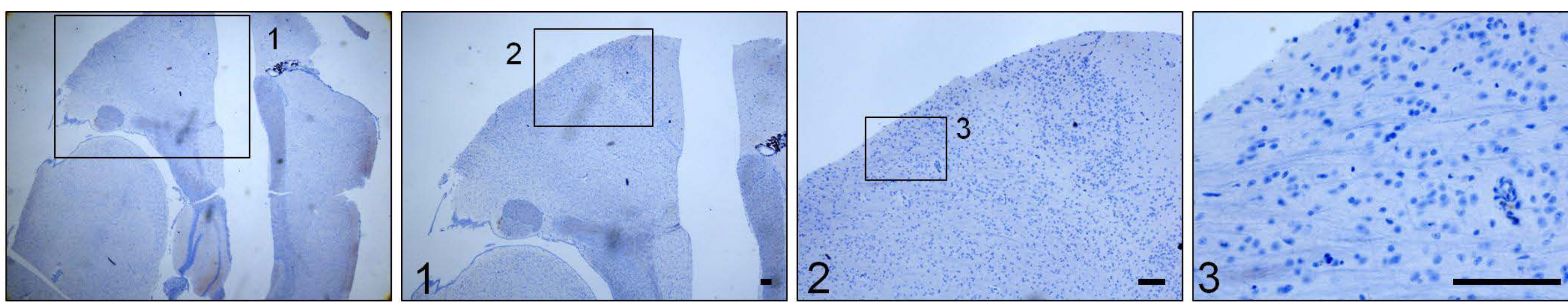
Sham



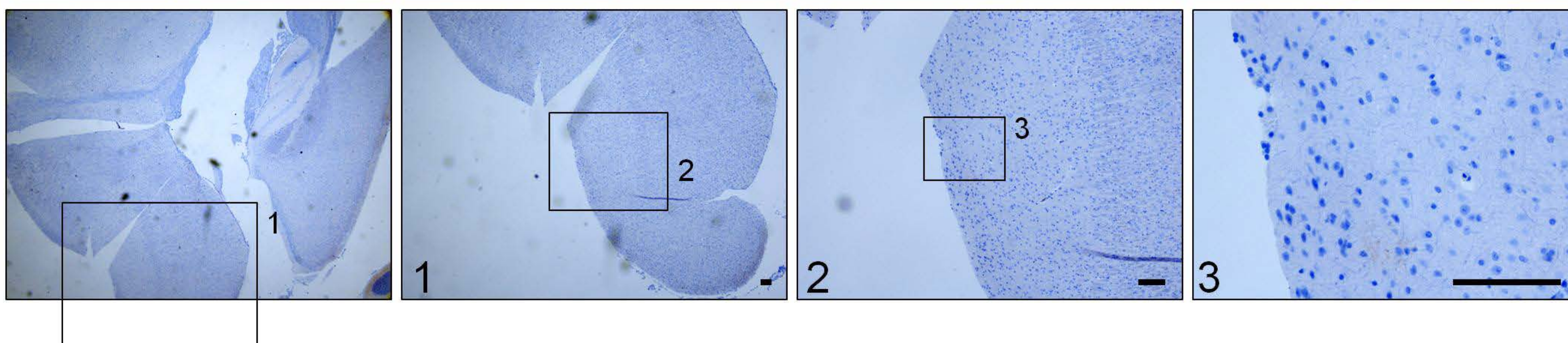
8 Gray



Sham



8 Gray



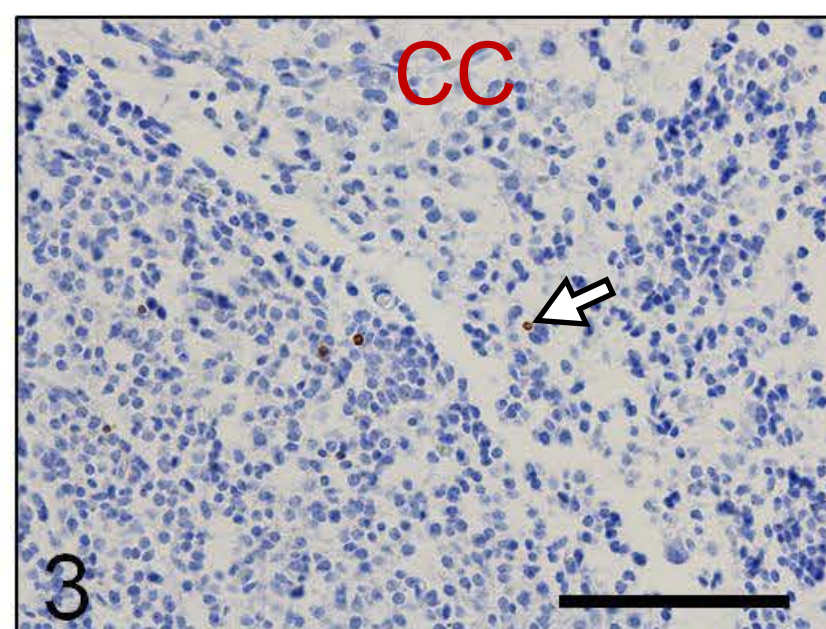
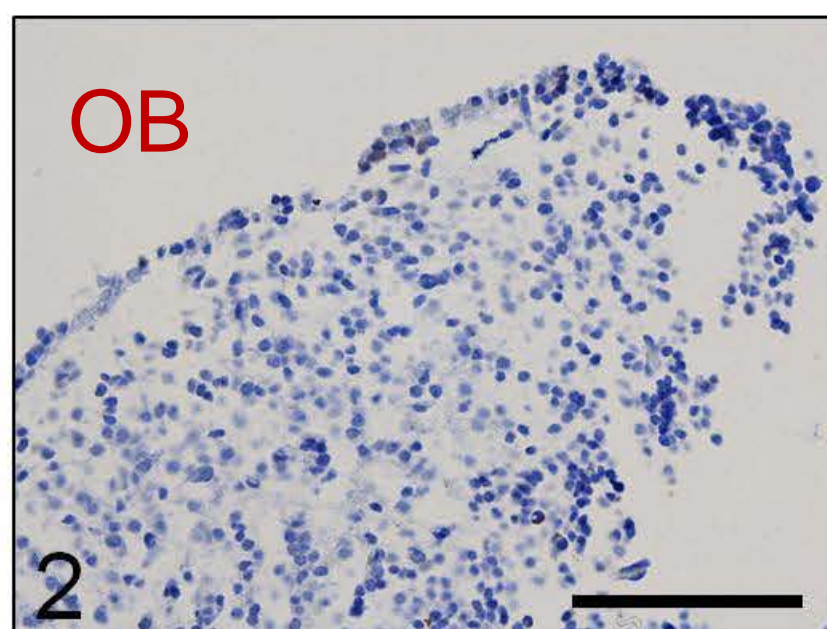
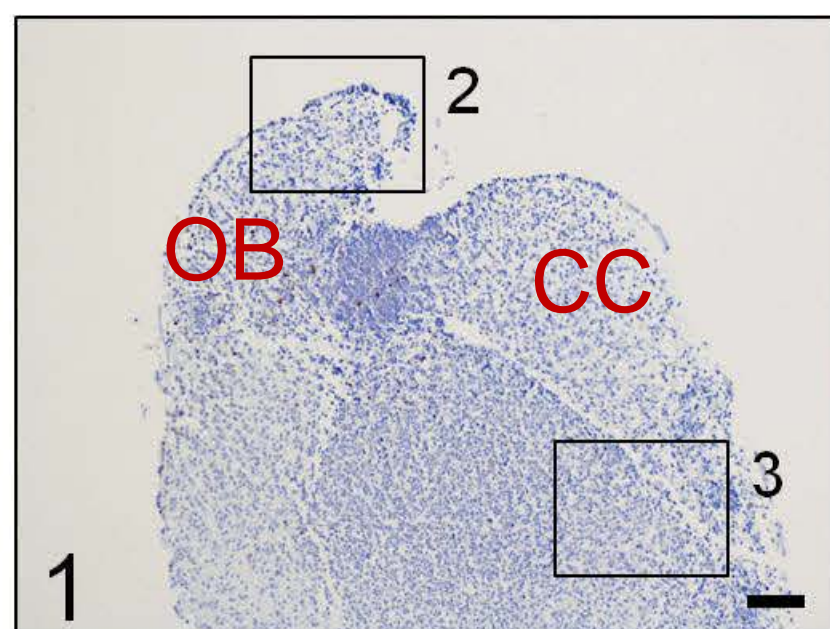
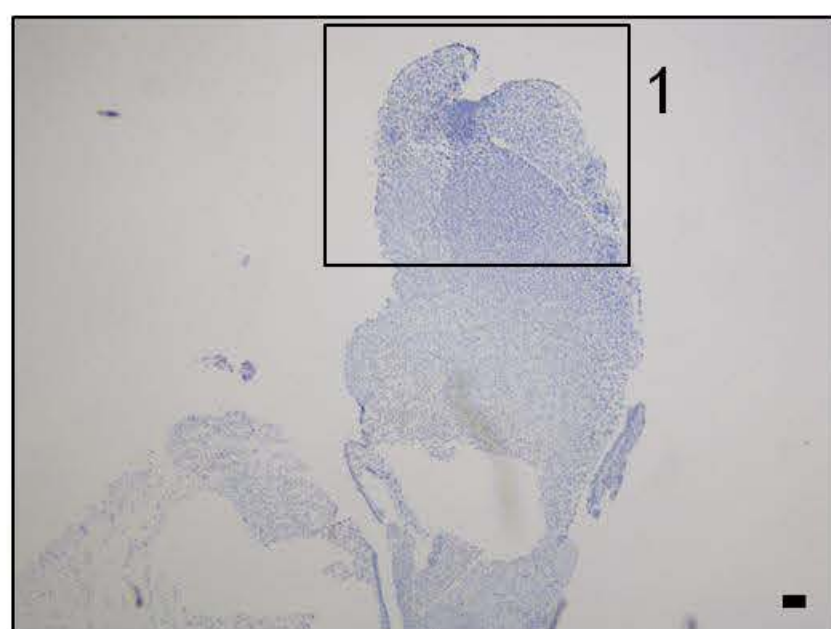
P0

Adult

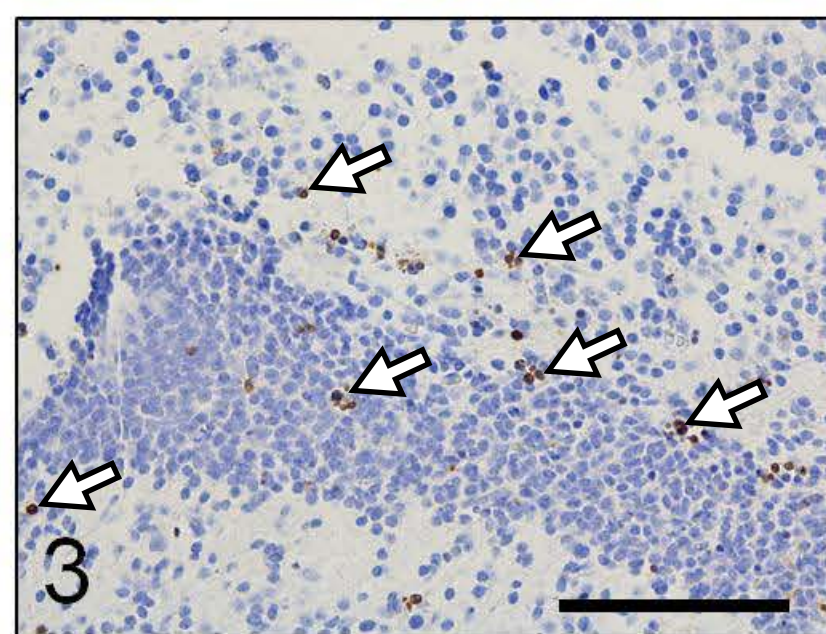
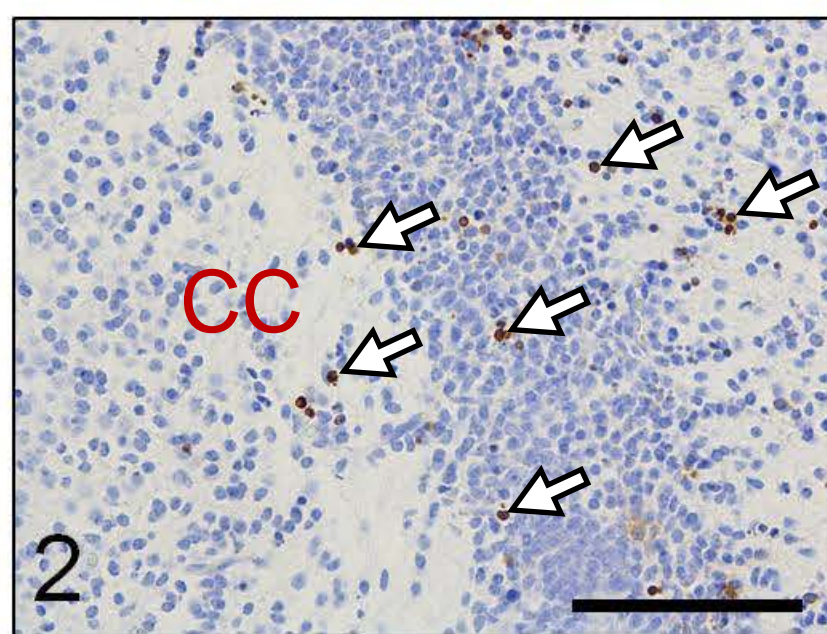
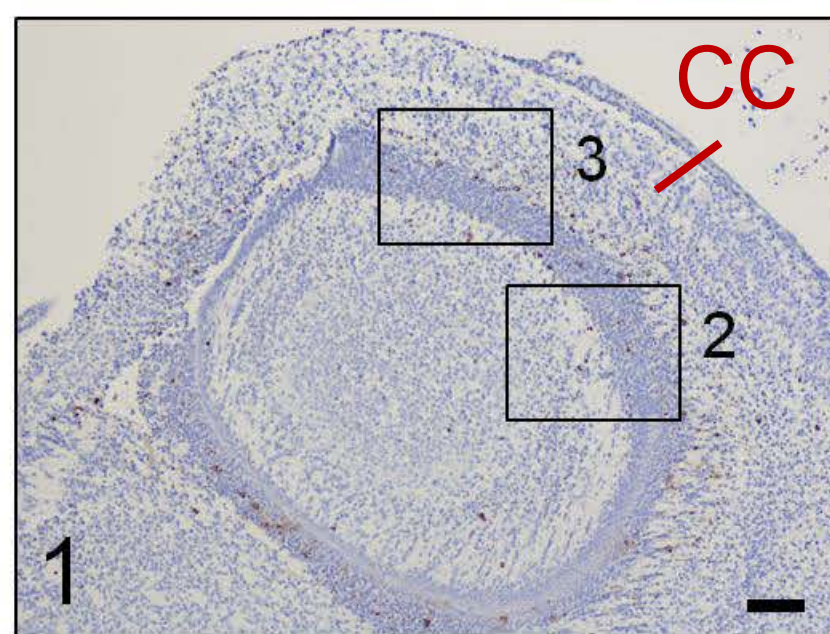
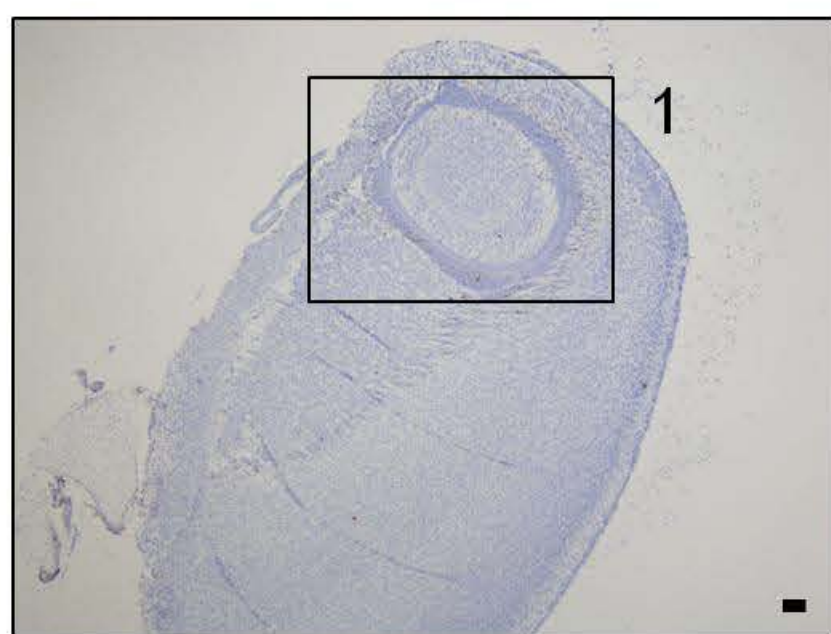
Cleaved Caspase 3

E

Sham



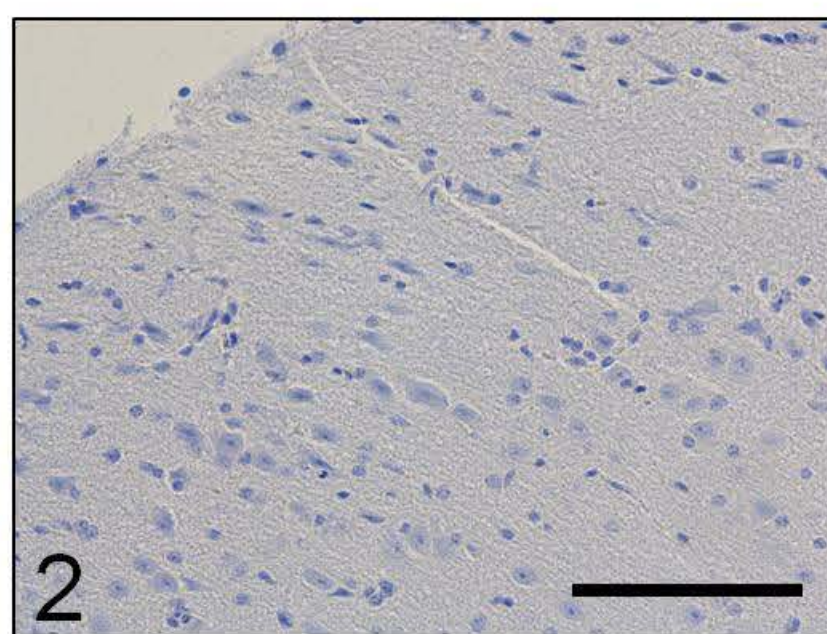
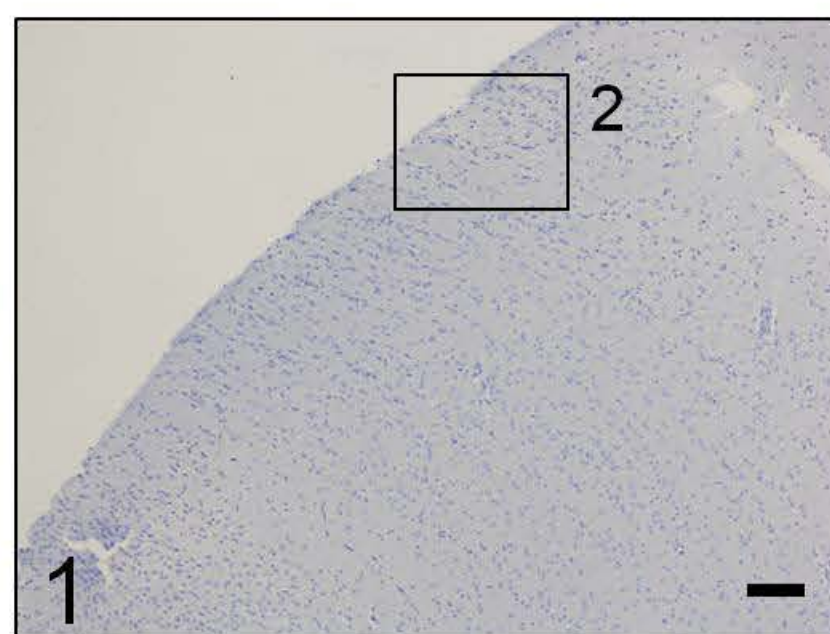
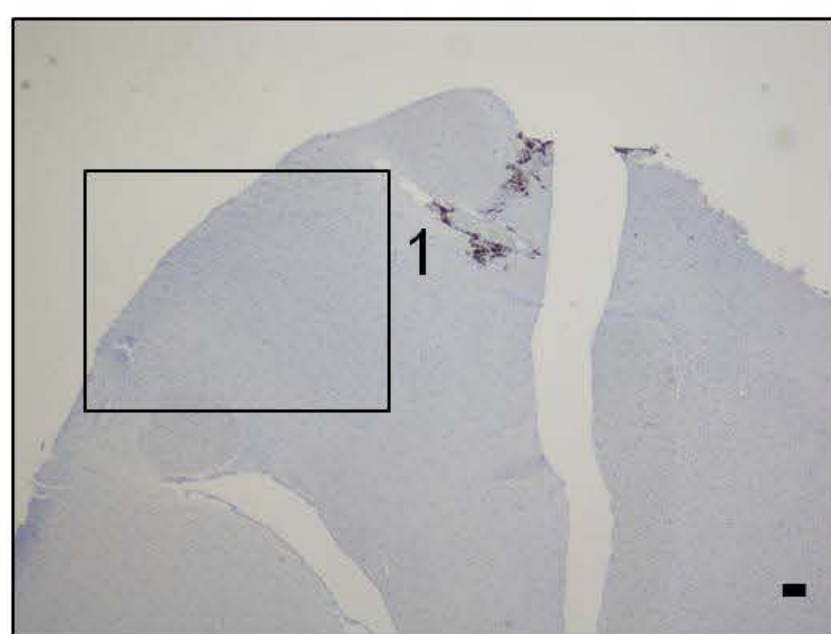
8 Gray



P0

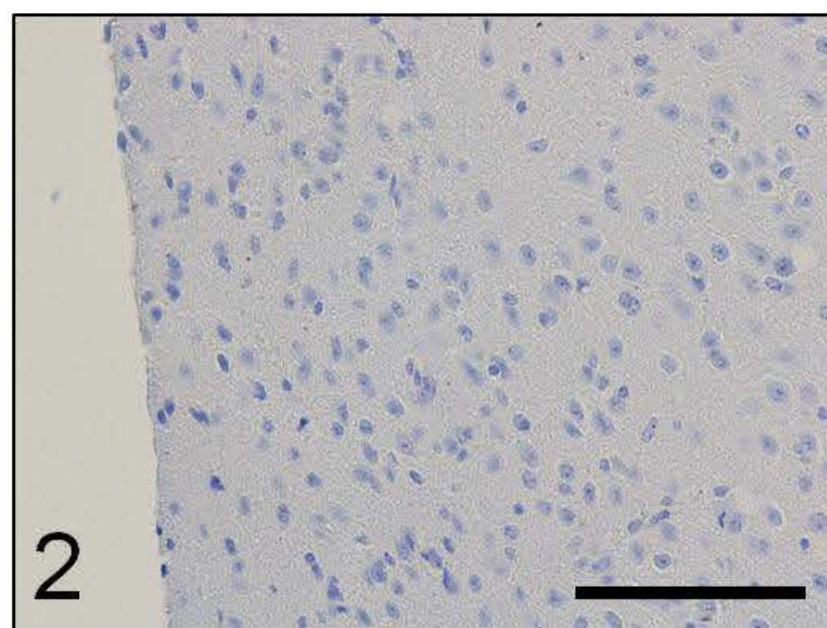
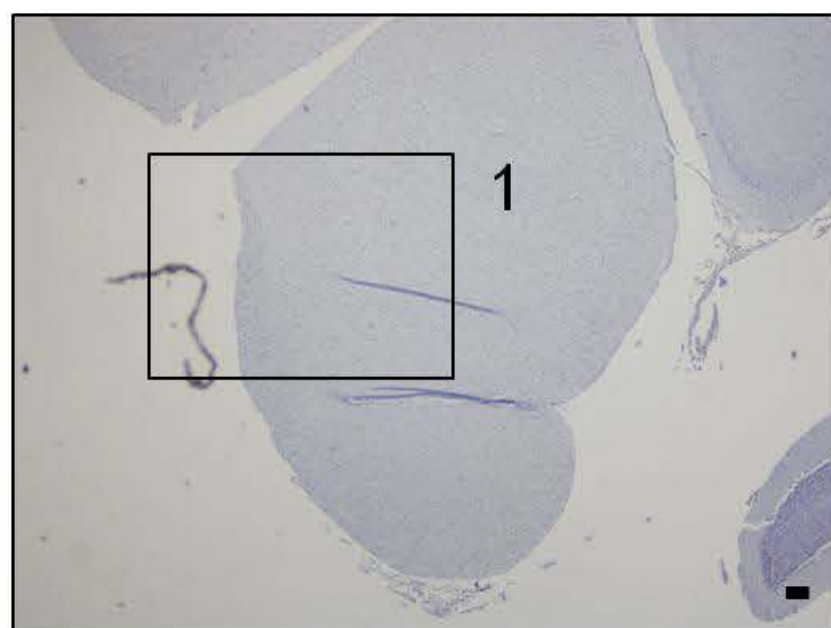
TUNEL

Sham



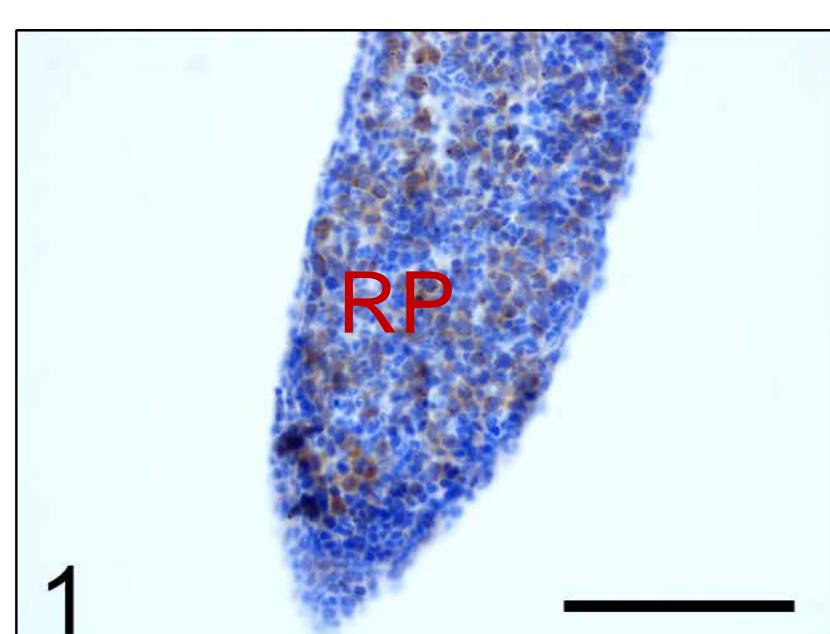
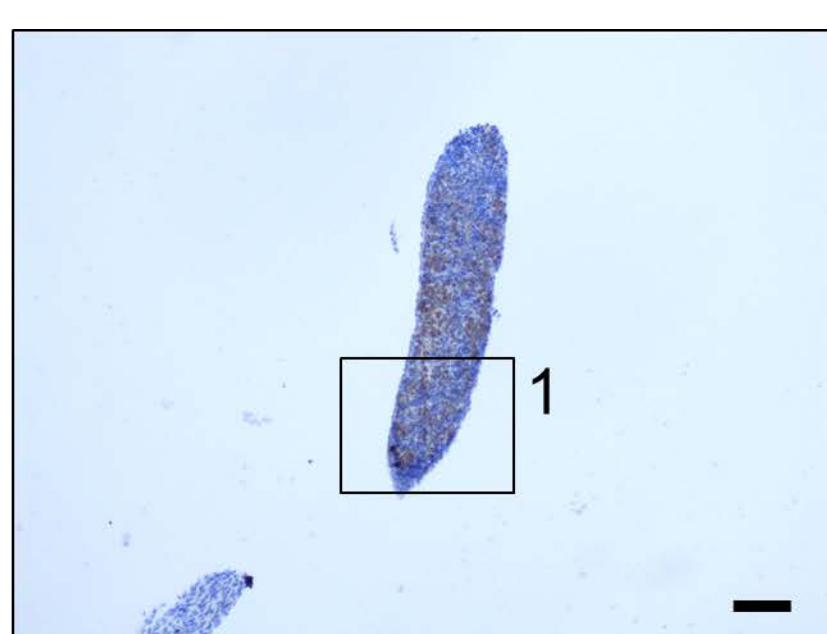
Adult

8 Gray



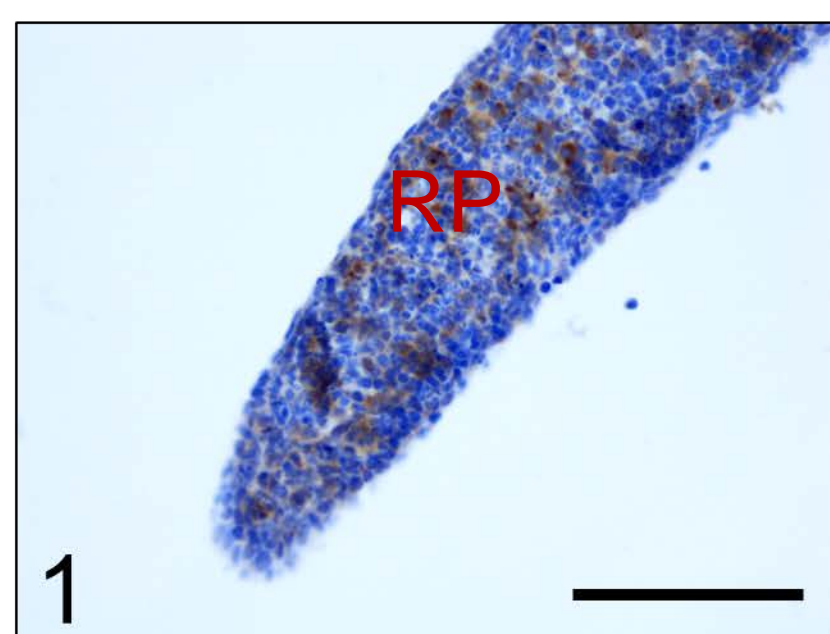
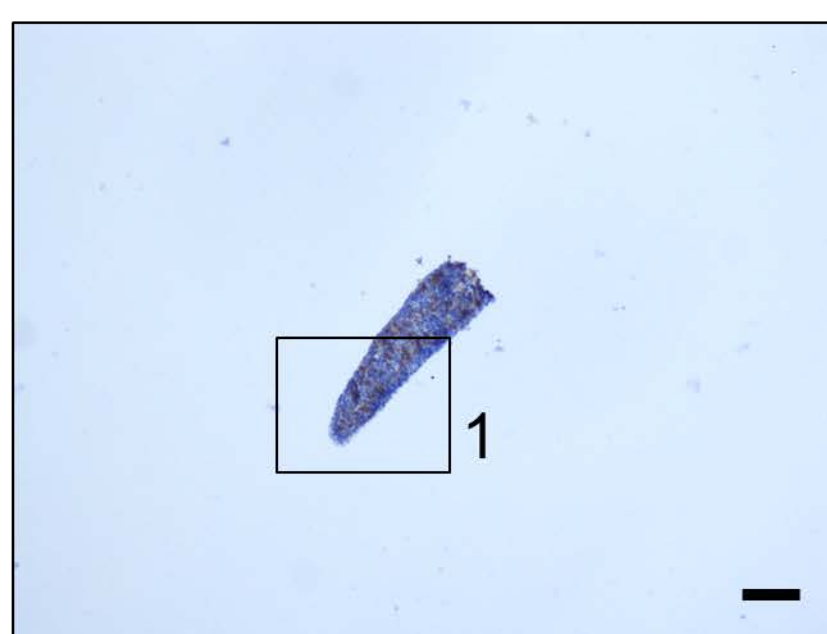
A

Sham

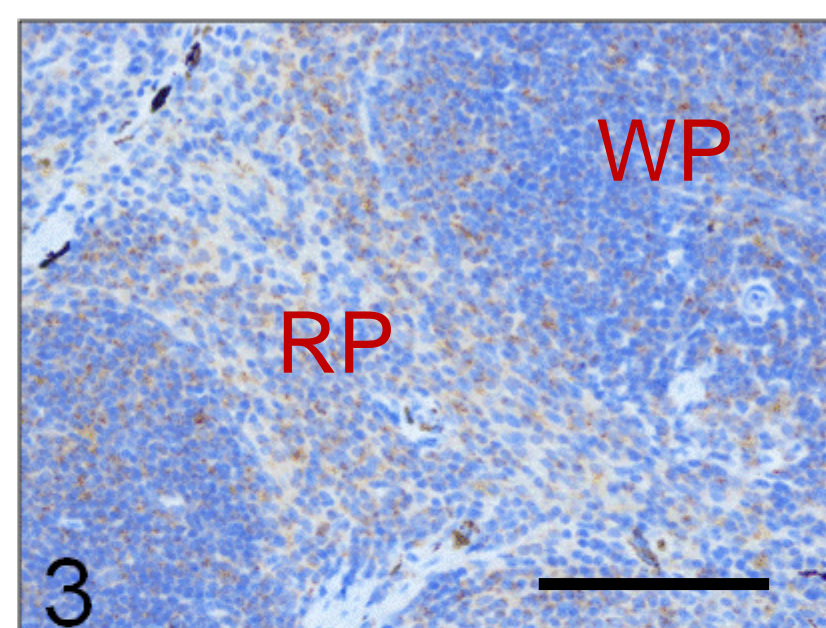
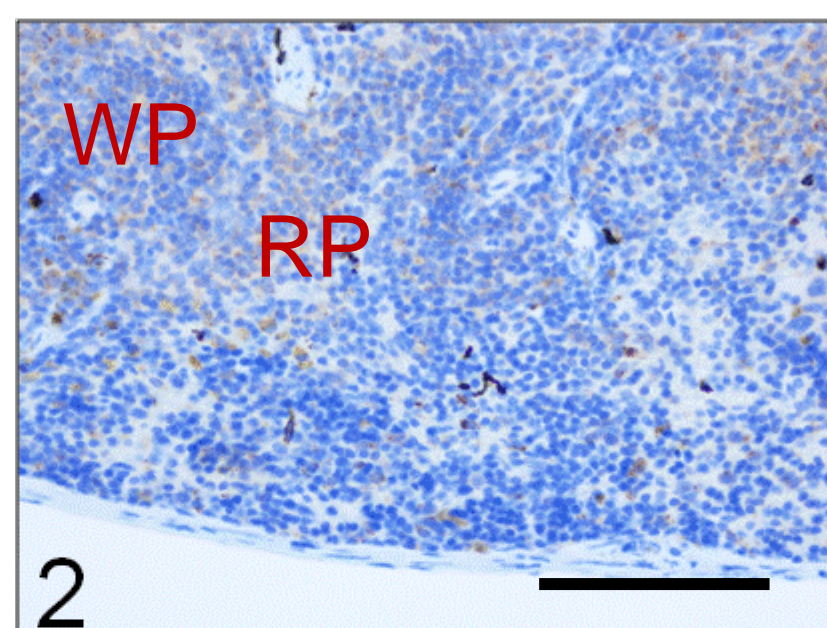
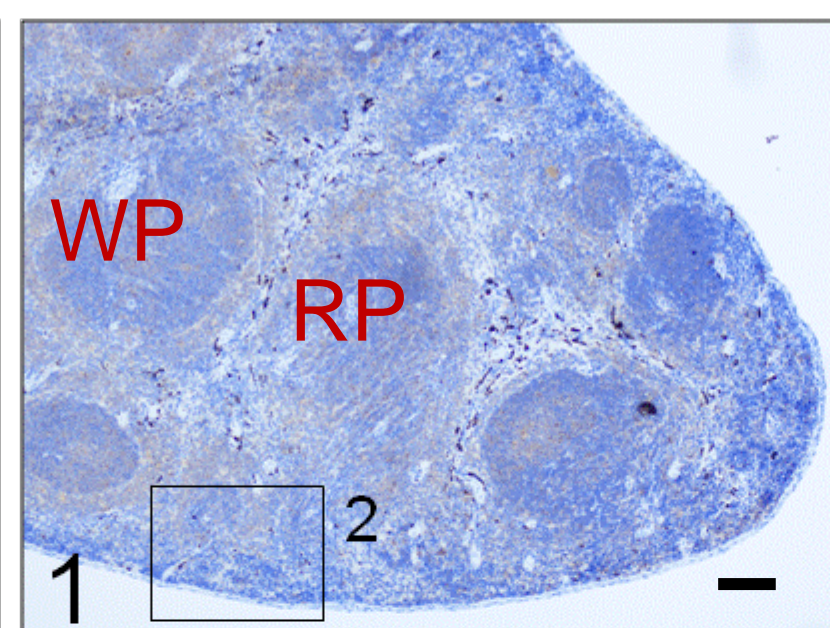
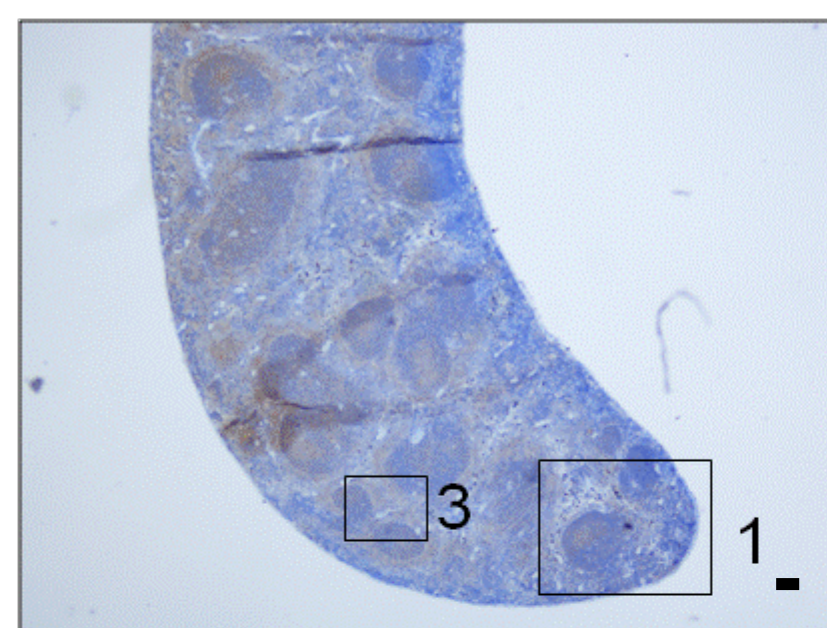


P0

8 Gray



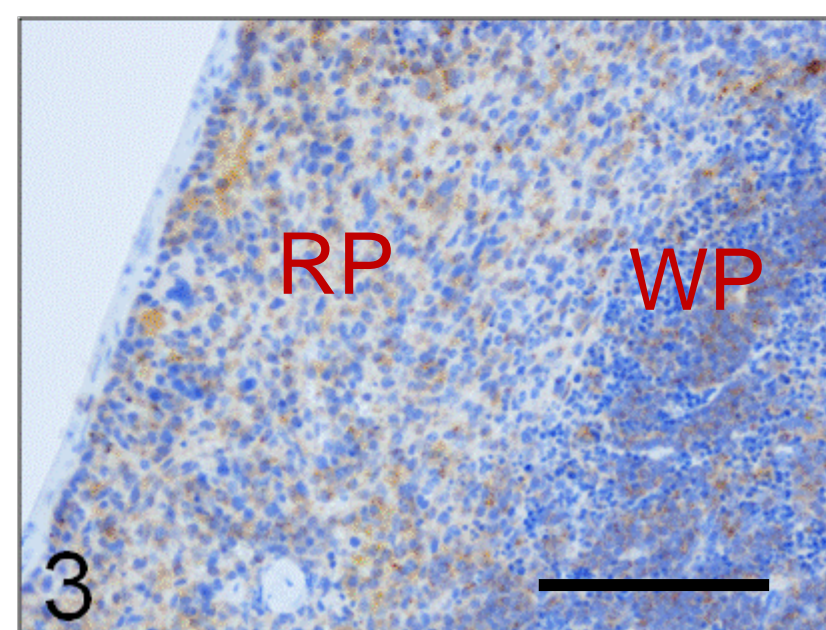
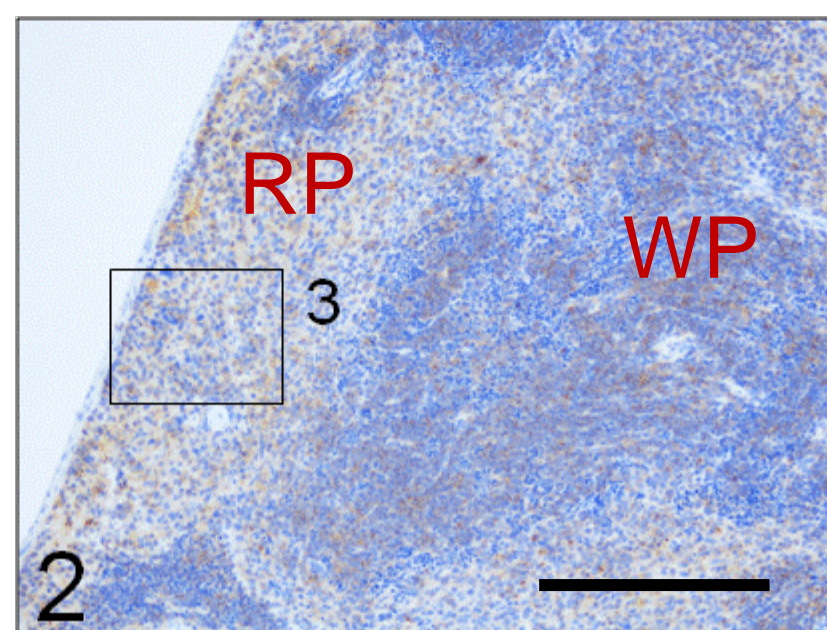
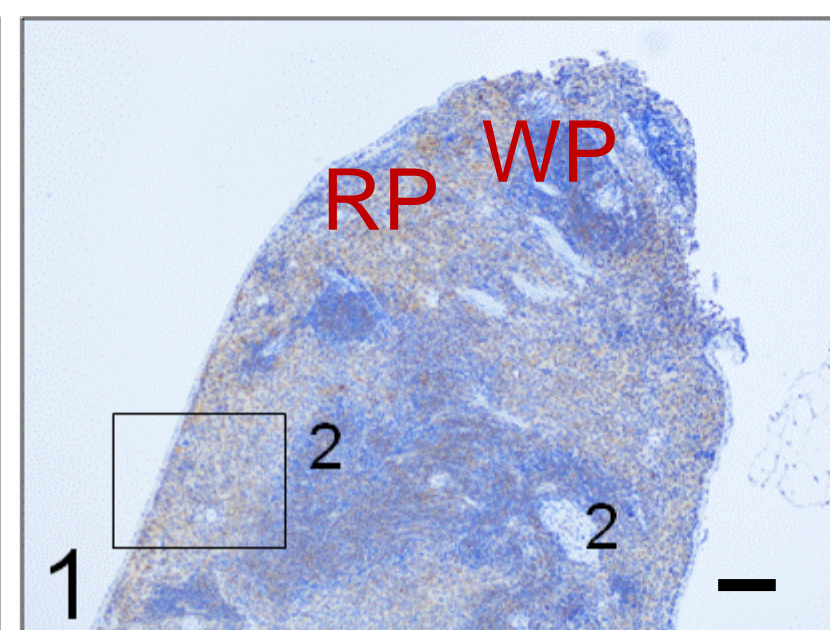
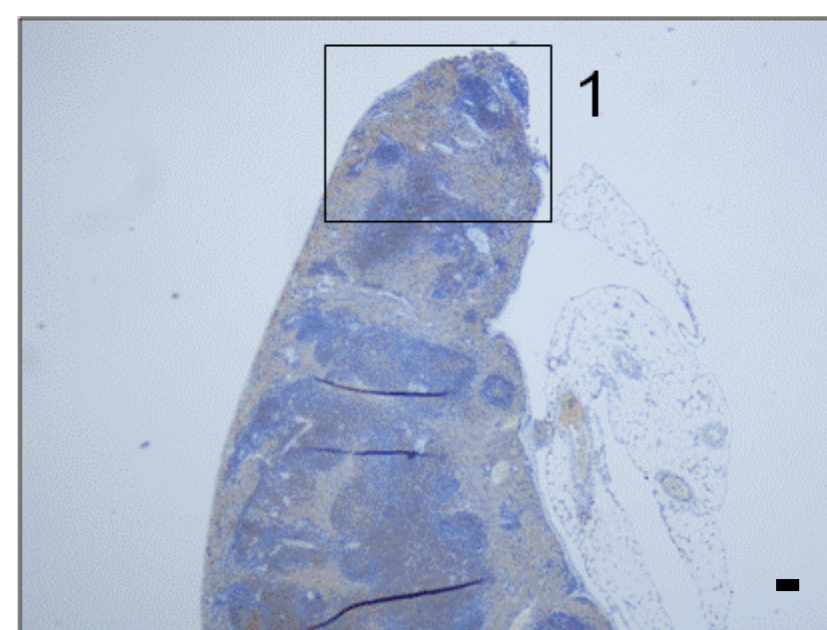
Sham



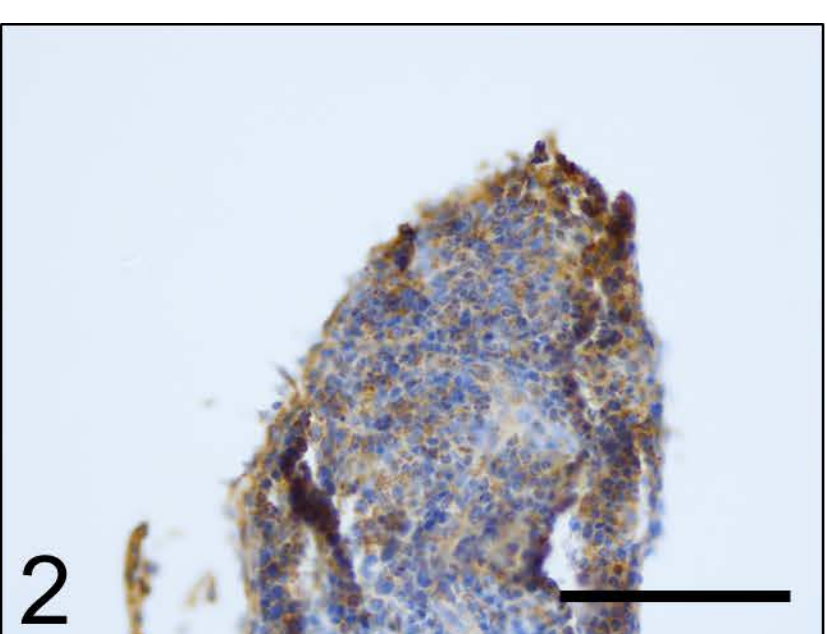
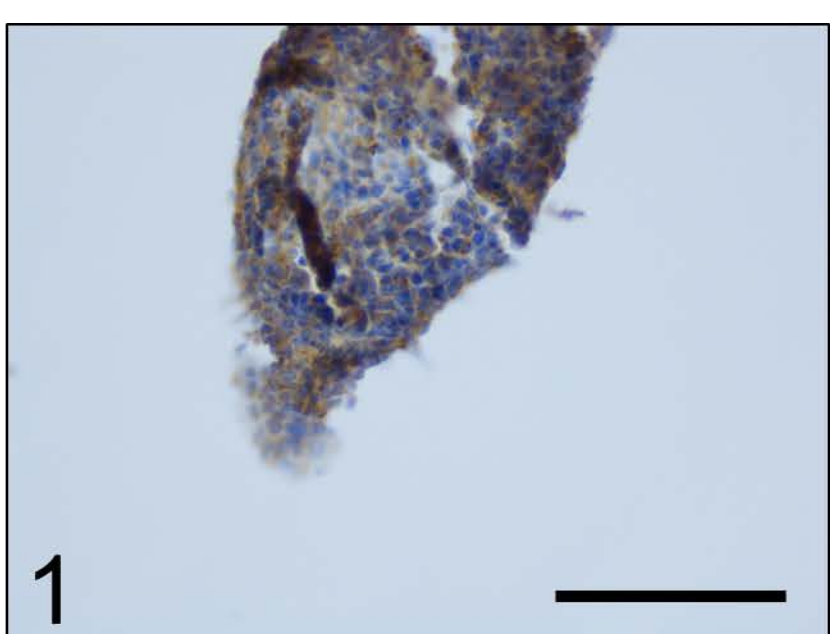
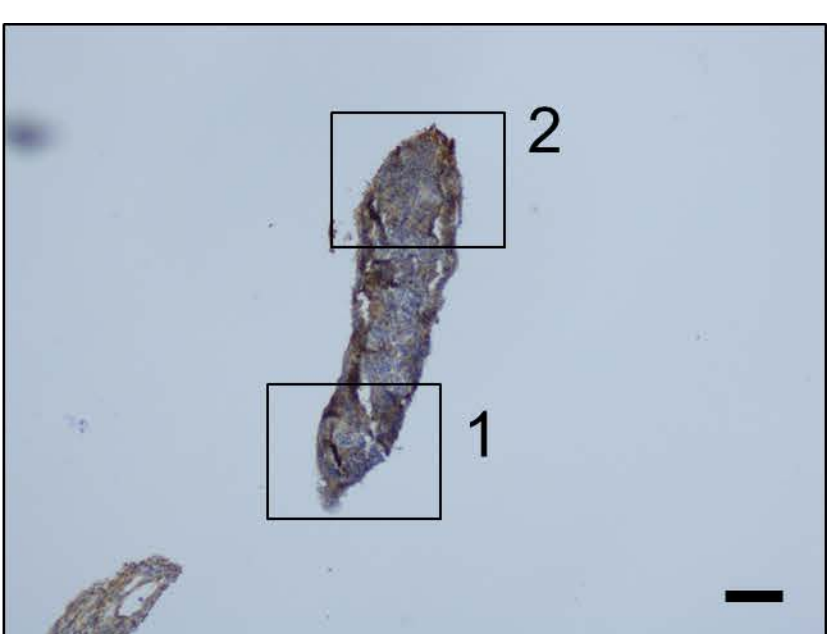
Adult

BAX

8 Gray

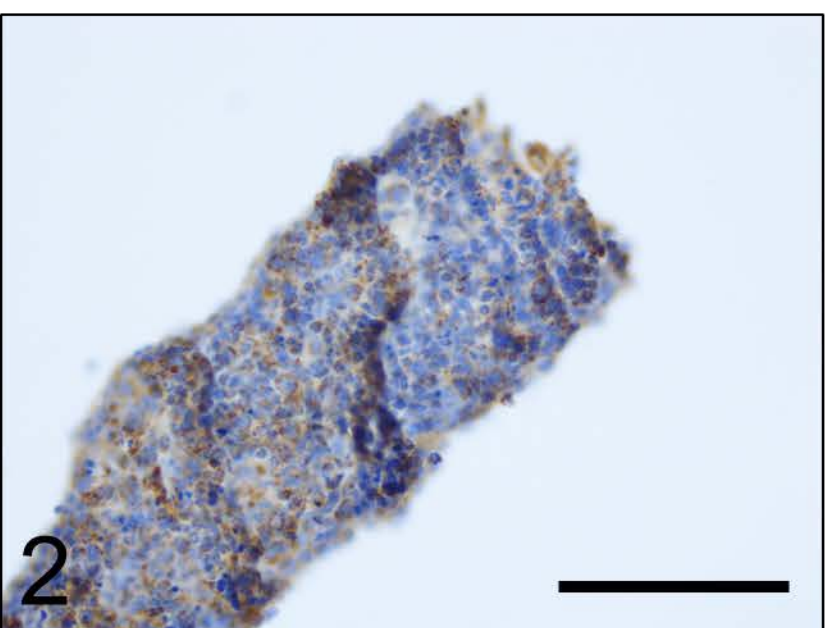
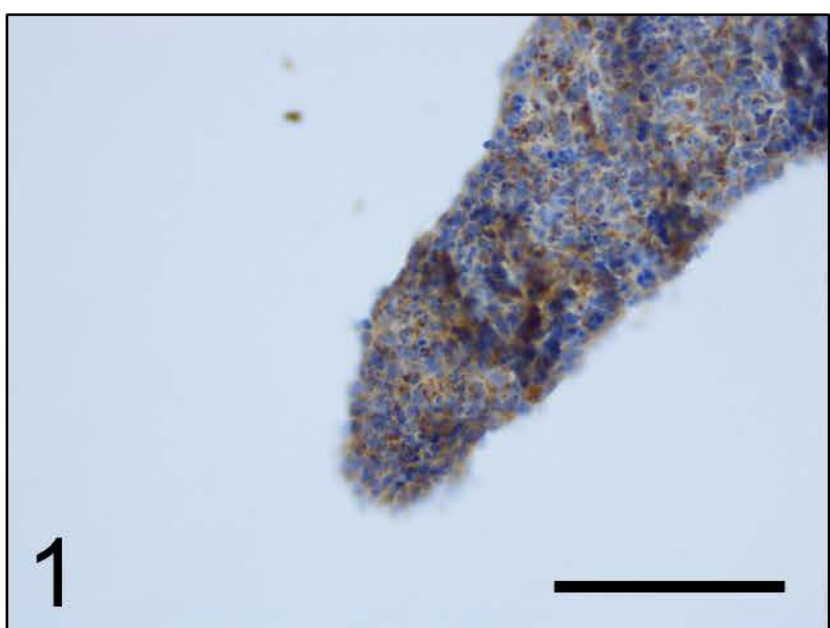


Sham



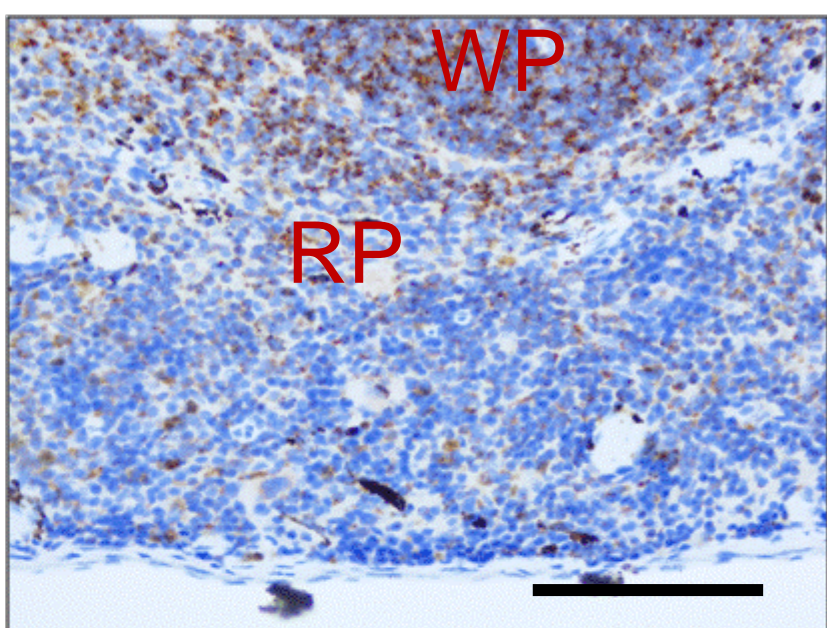
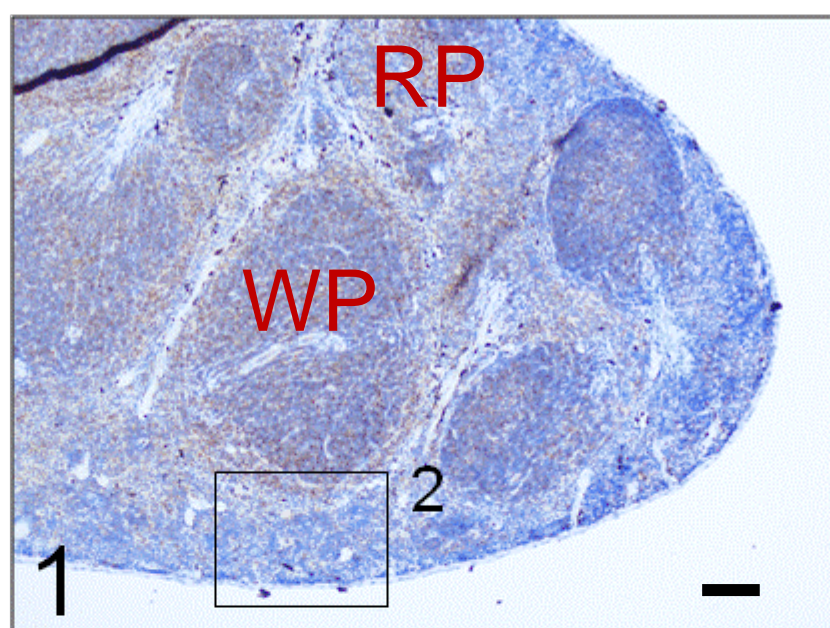
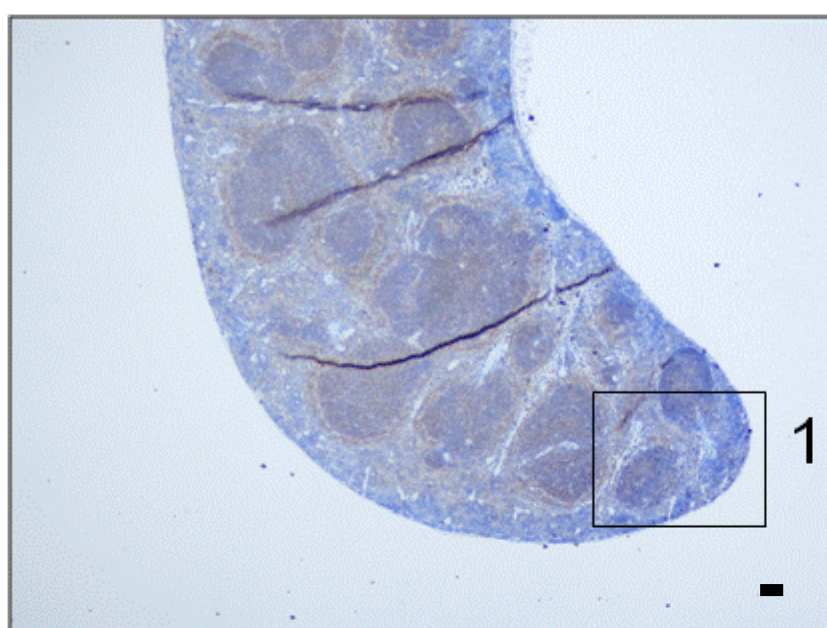
P0

8 Gray



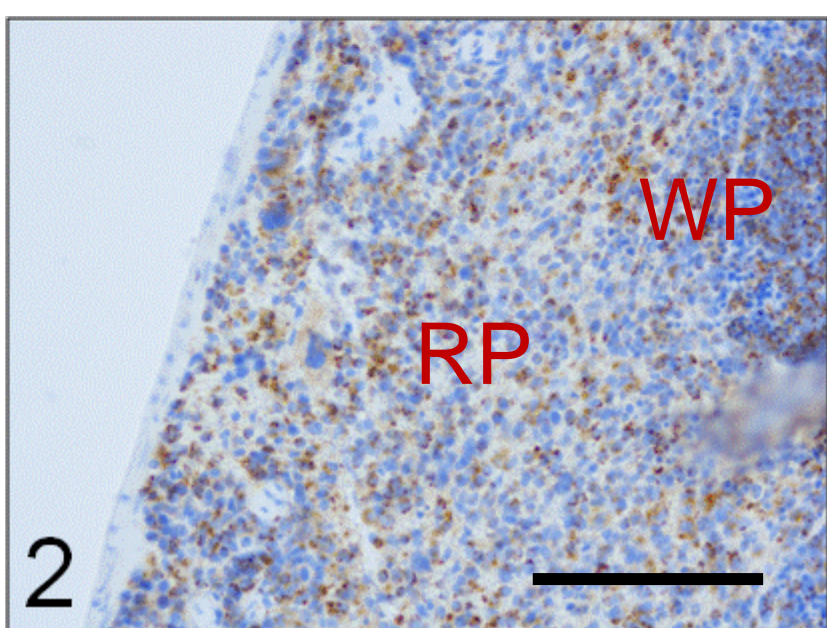
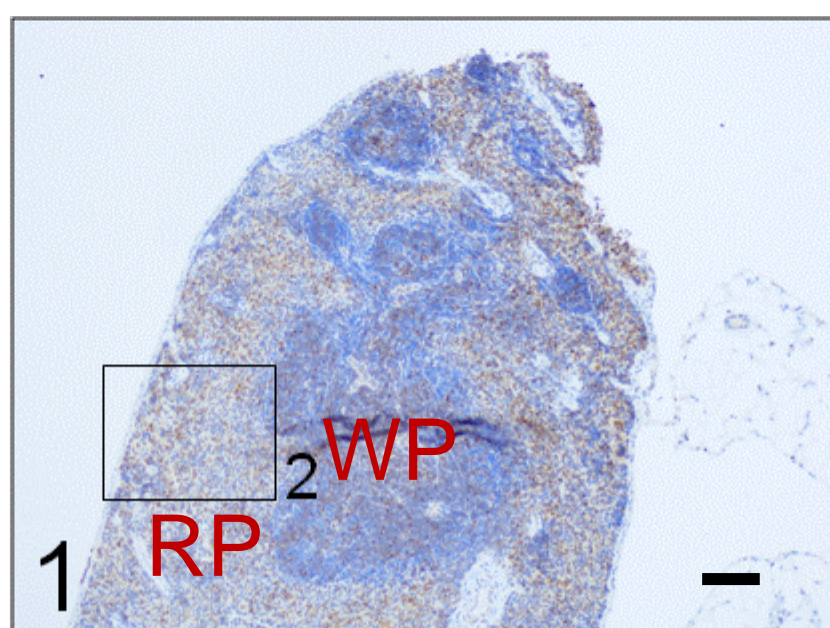
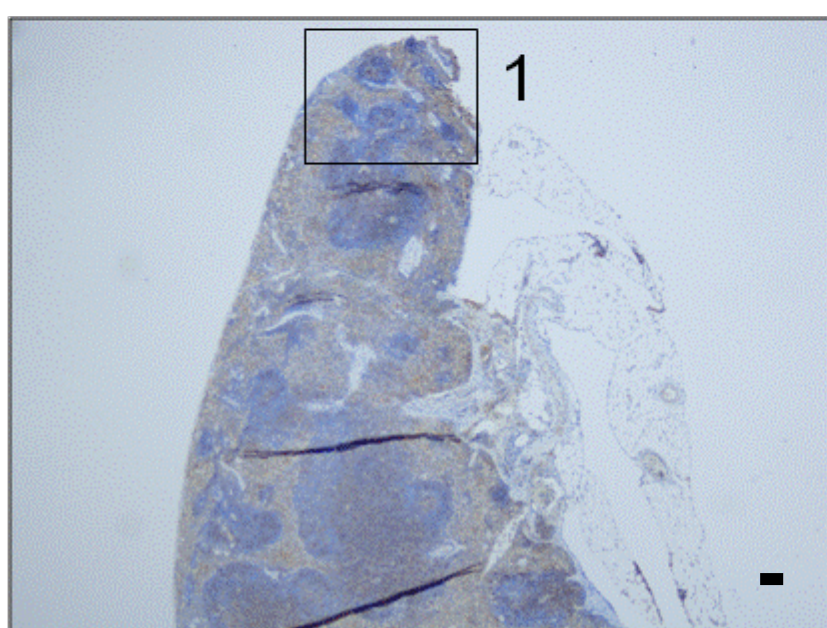
BAK

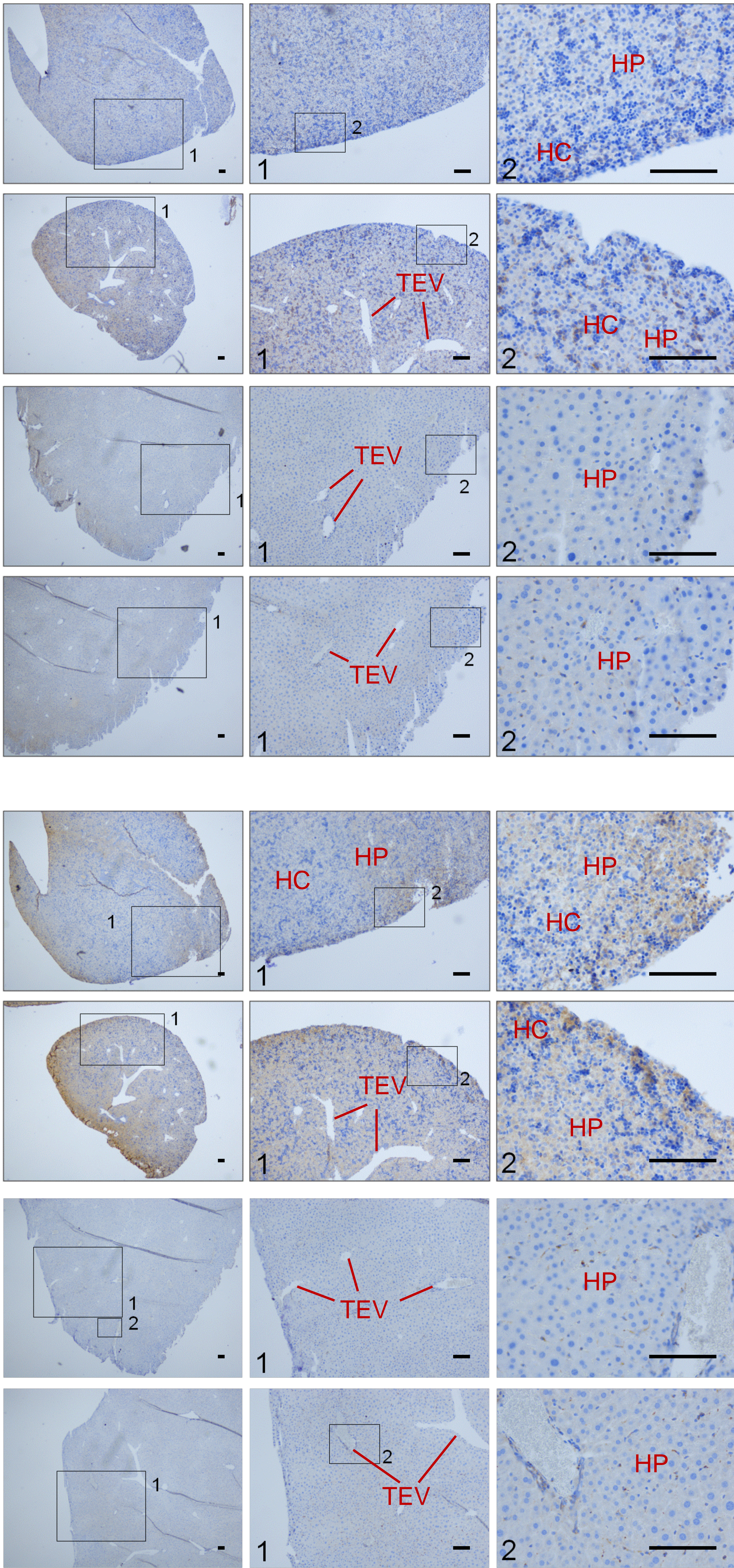
Sham



Adult

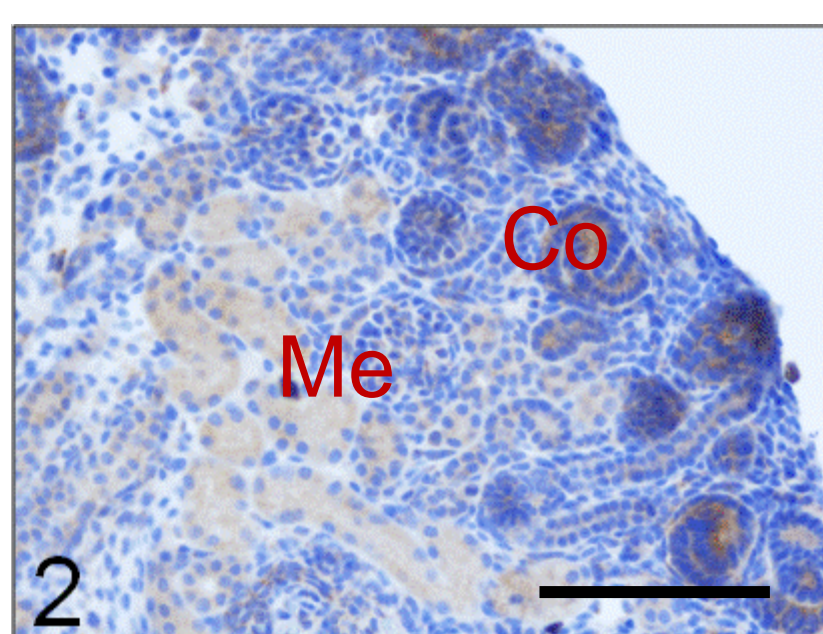
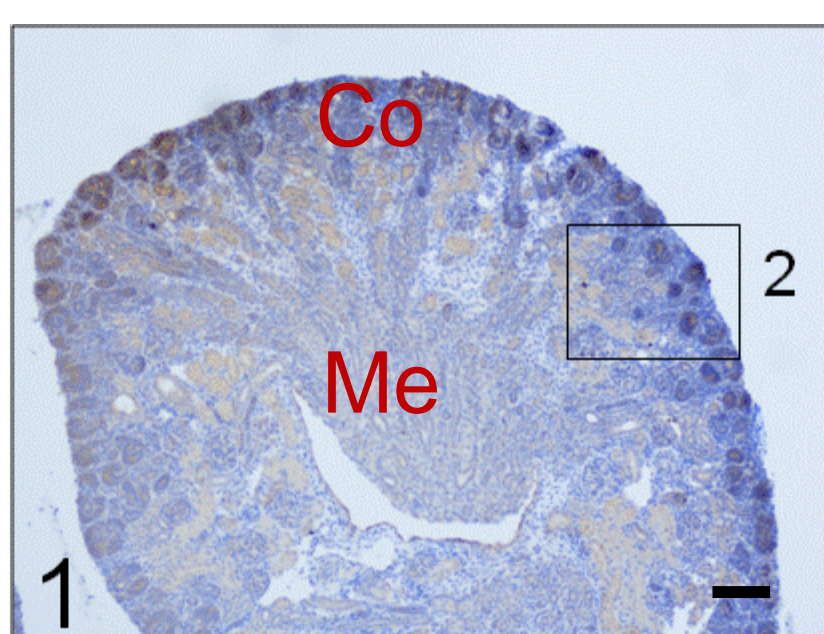
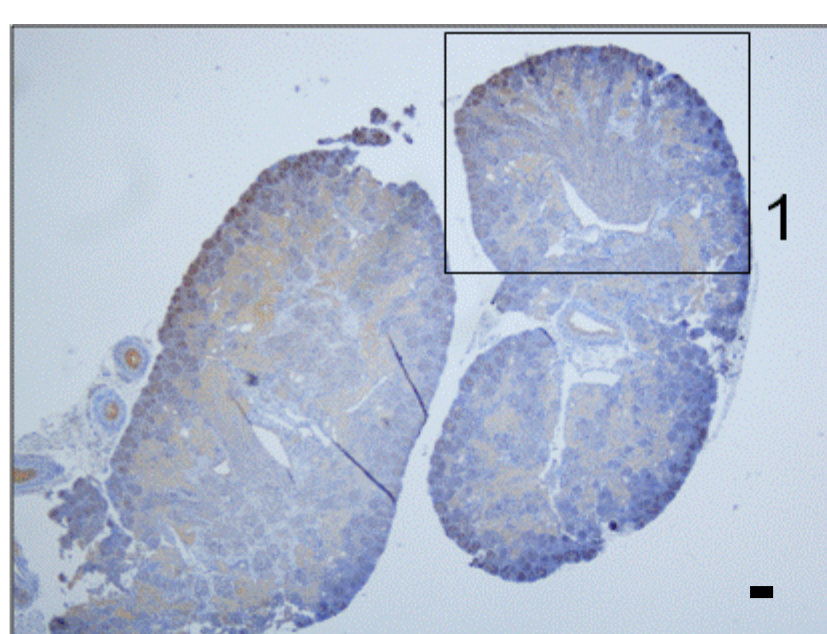
8 Gray





C

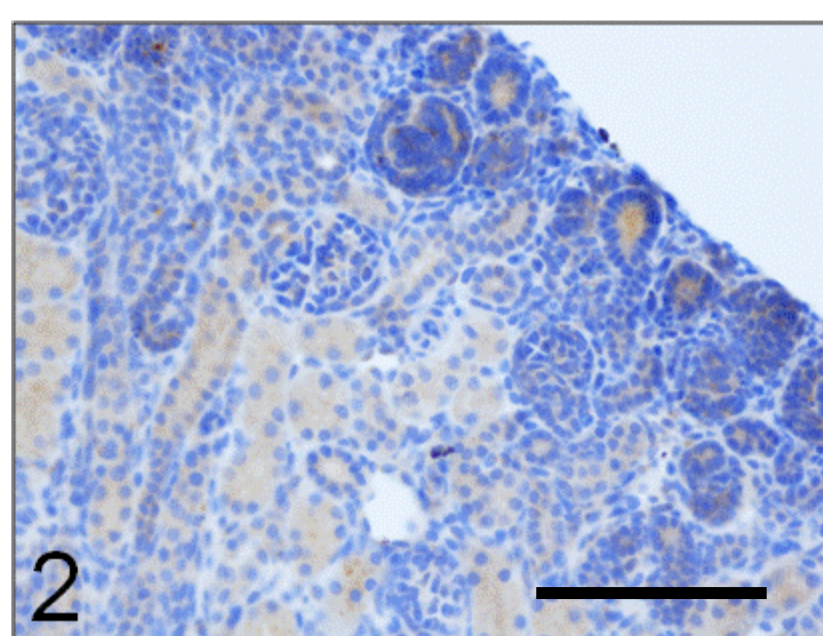
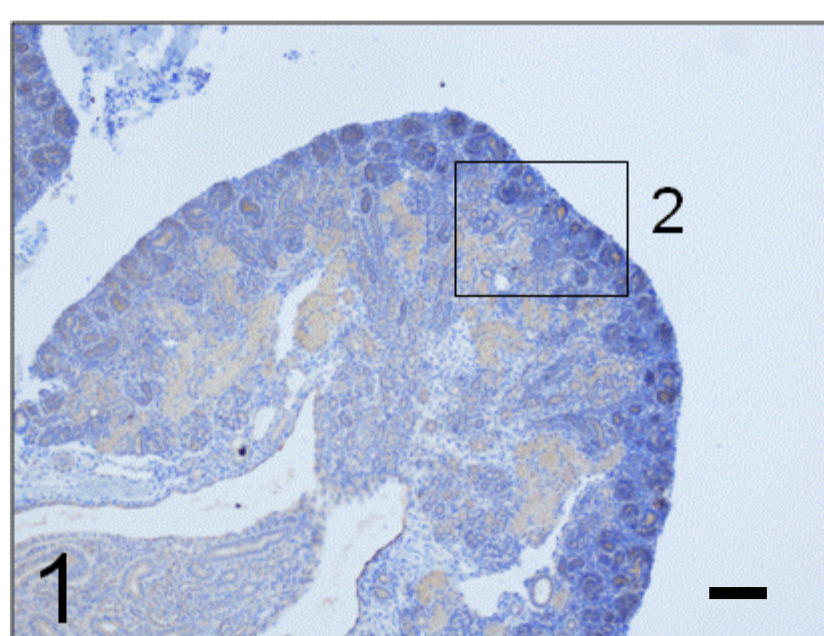
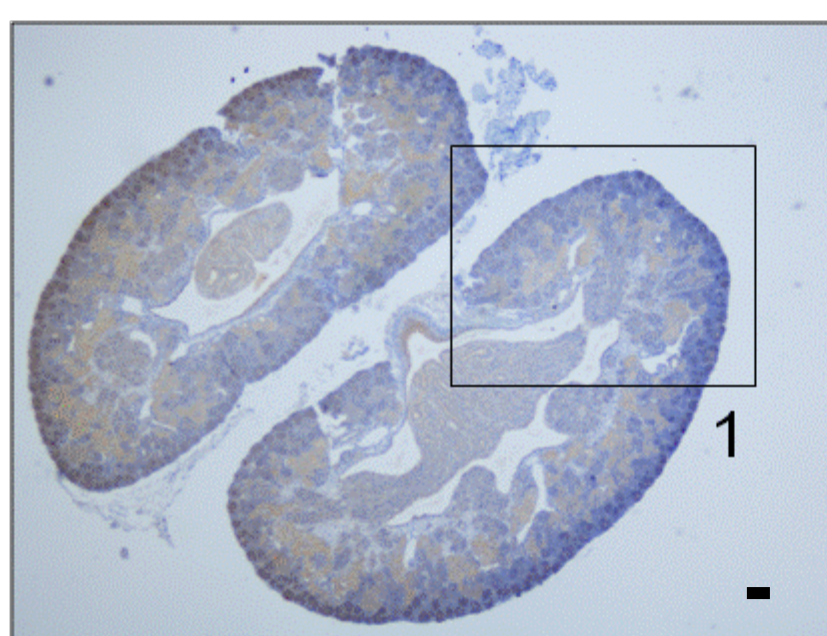
Sham



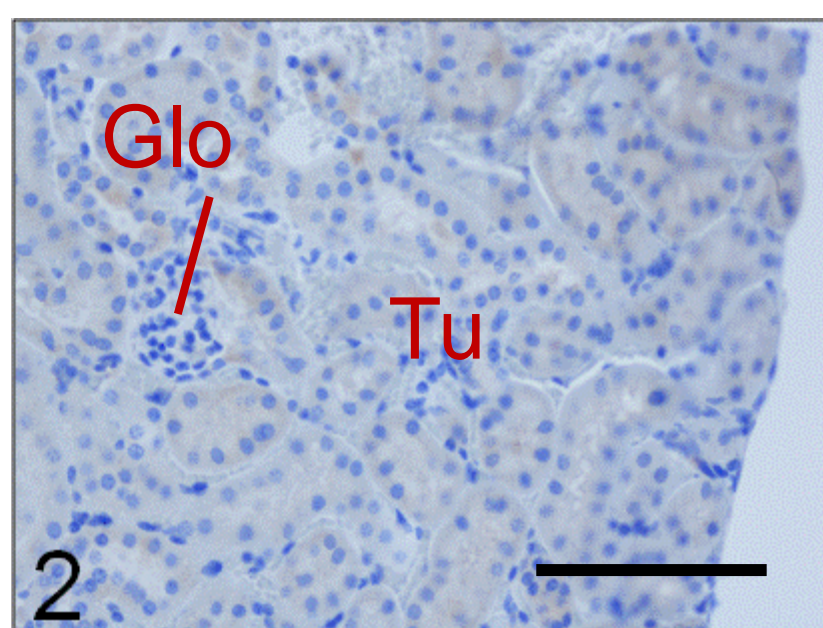
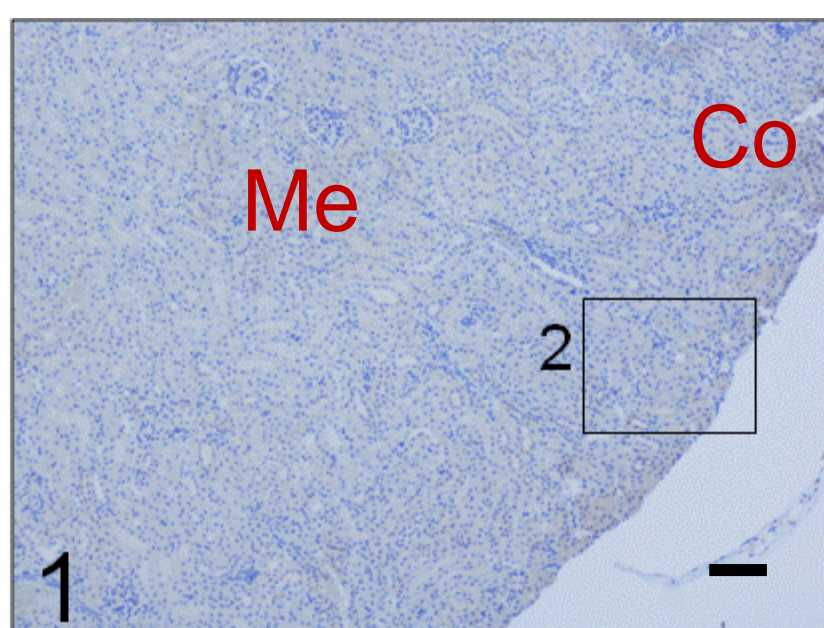
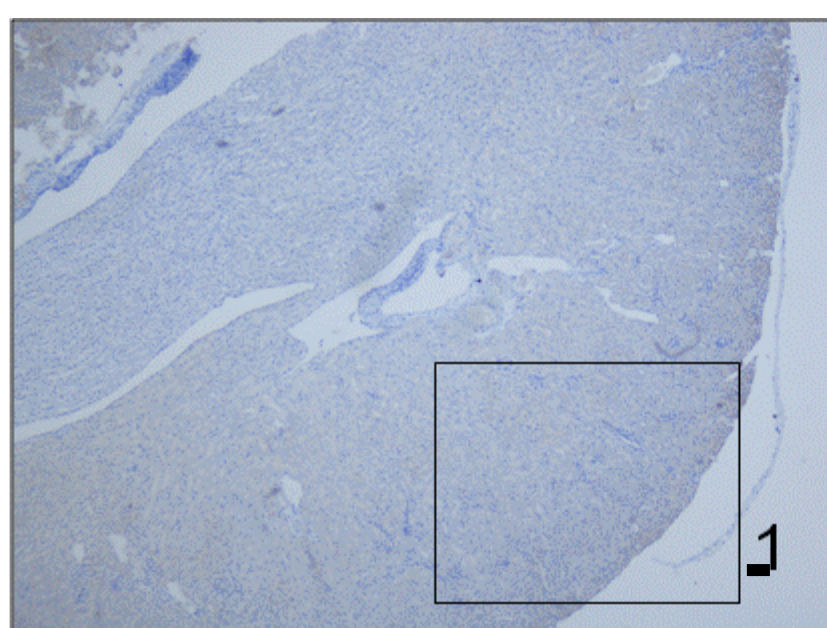
P0

BAX

8 Gray

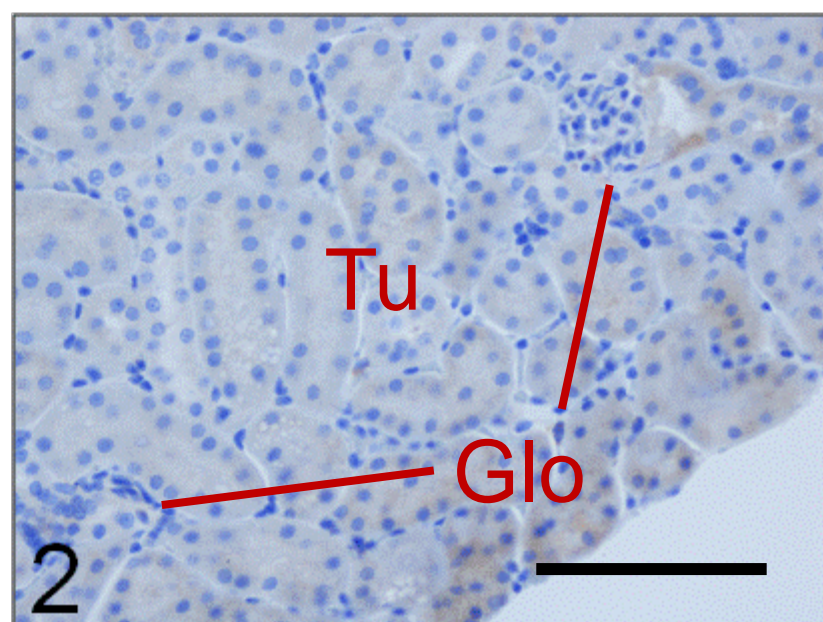
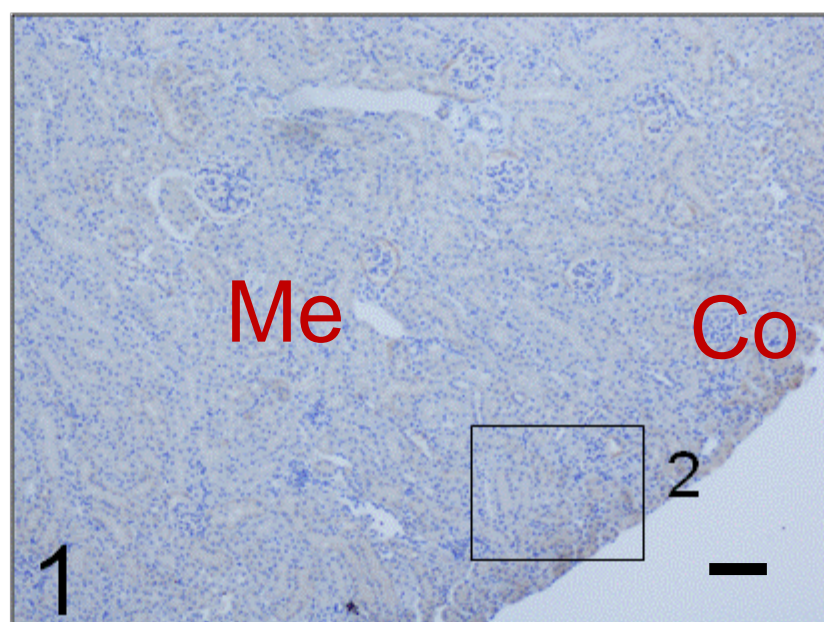
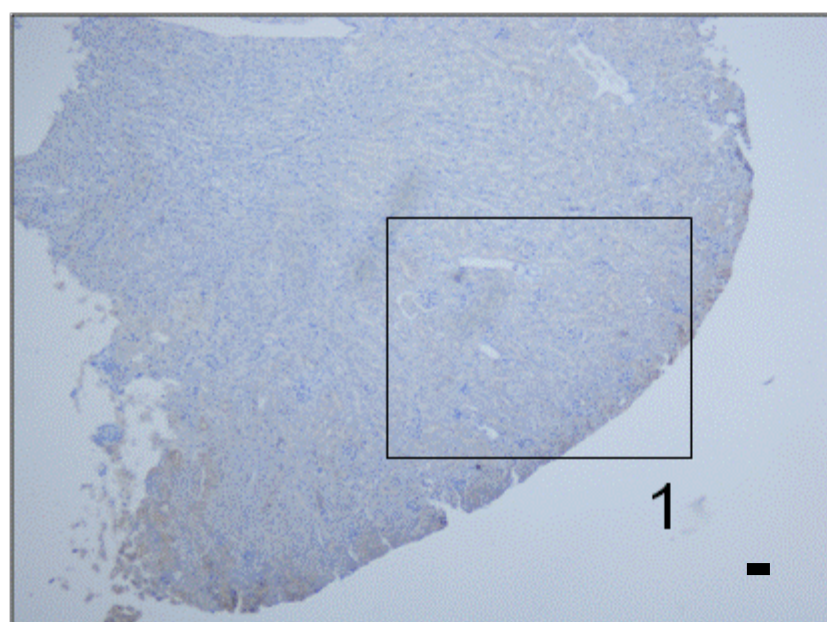


Sham

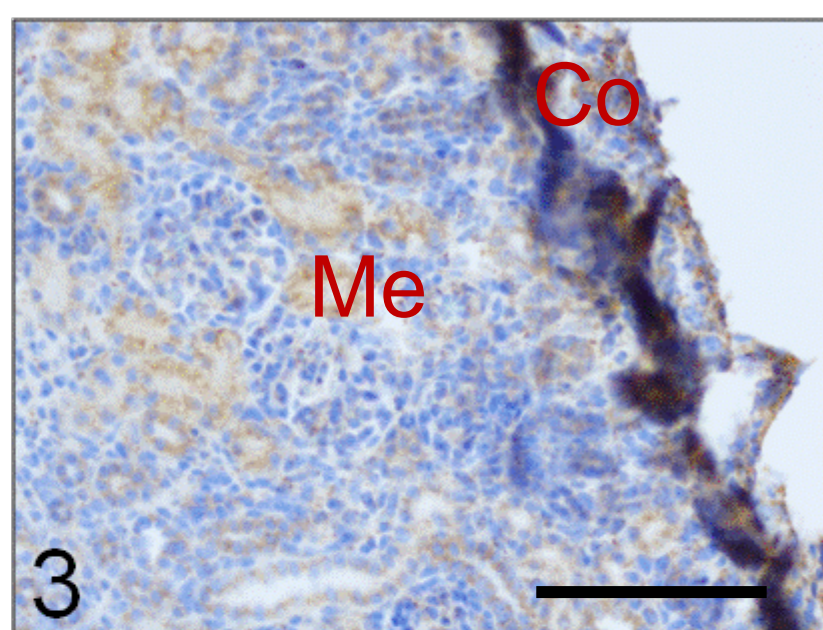
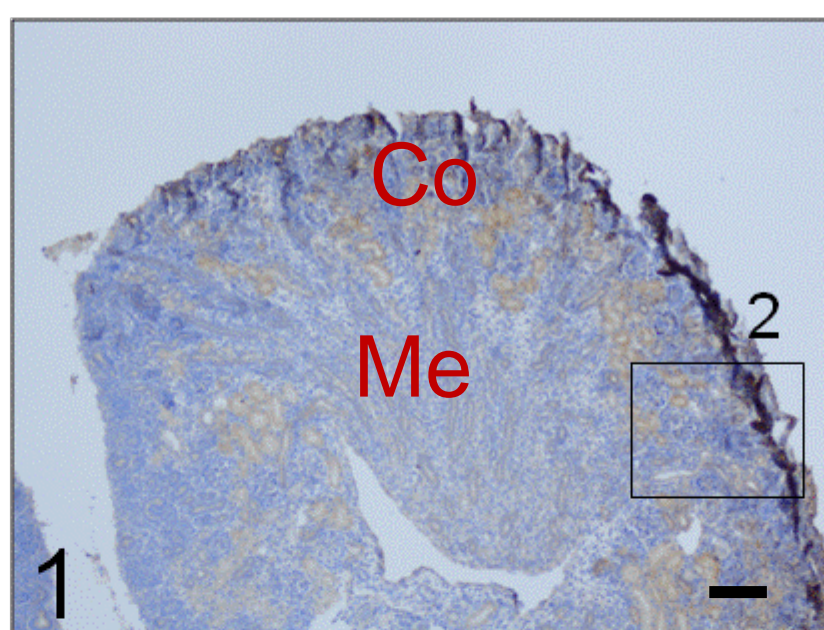
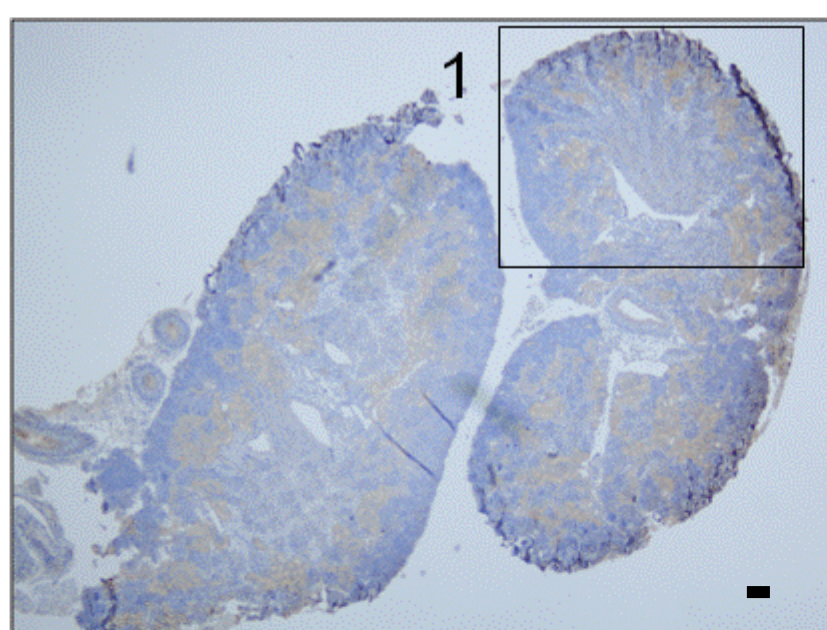


Adult

8 Gray



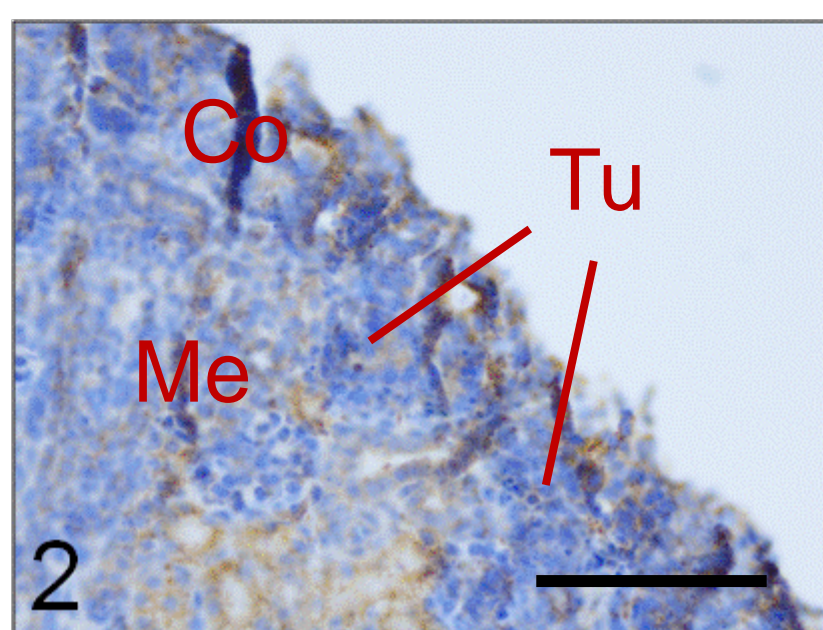
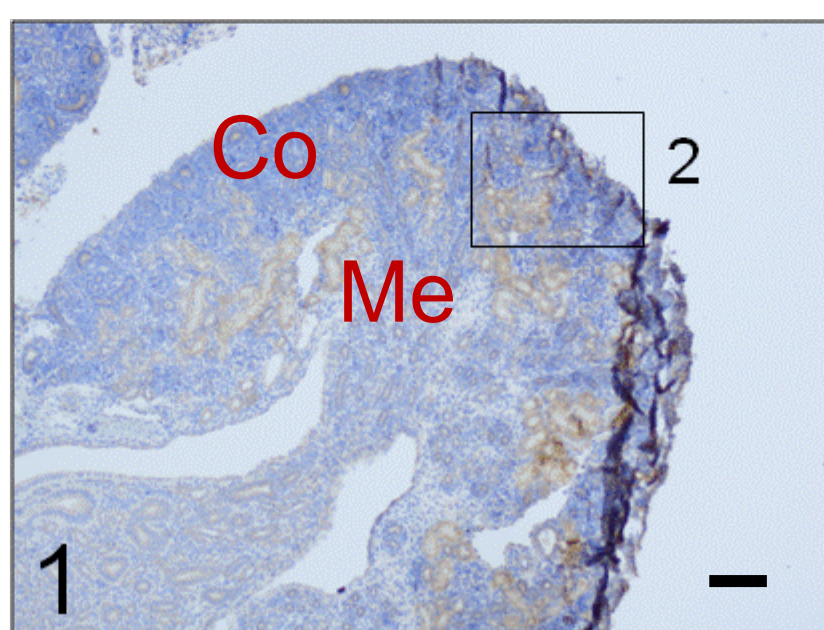
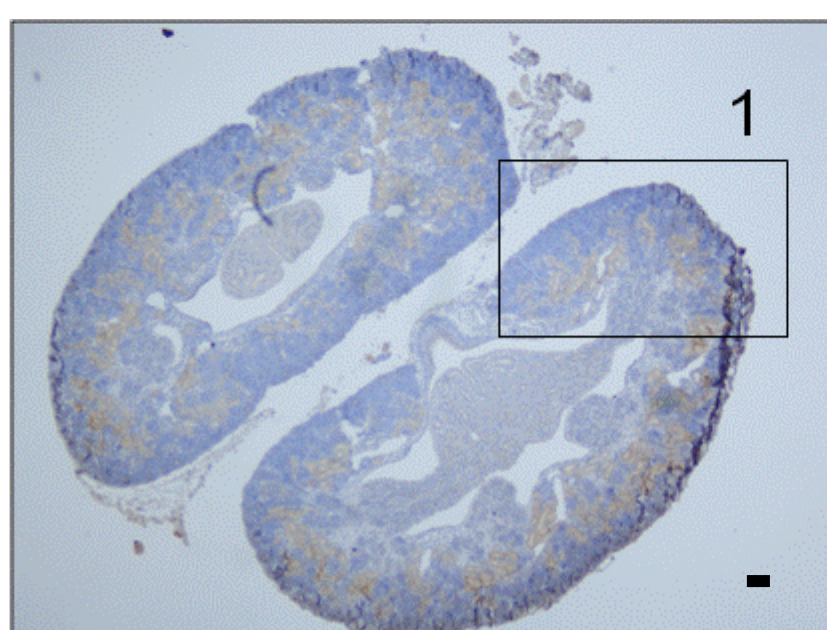
Sham



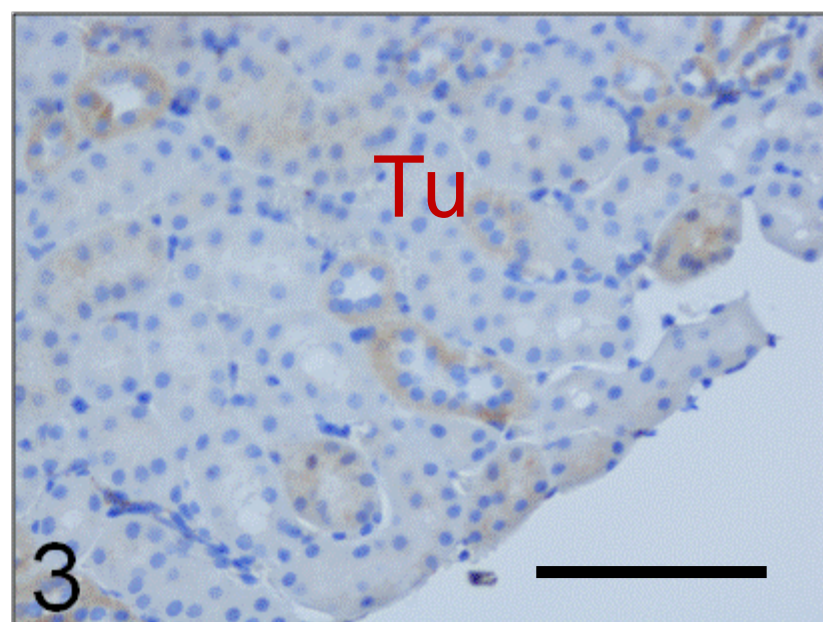
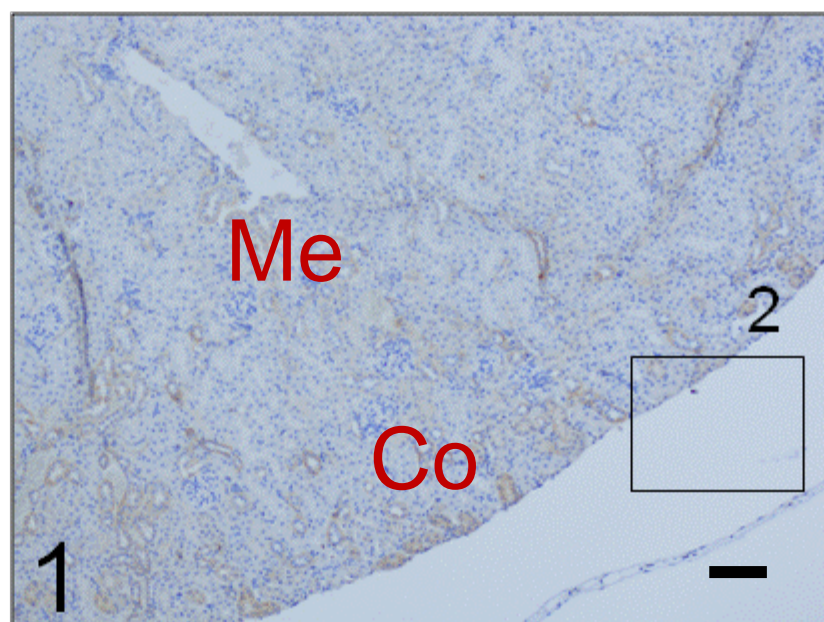
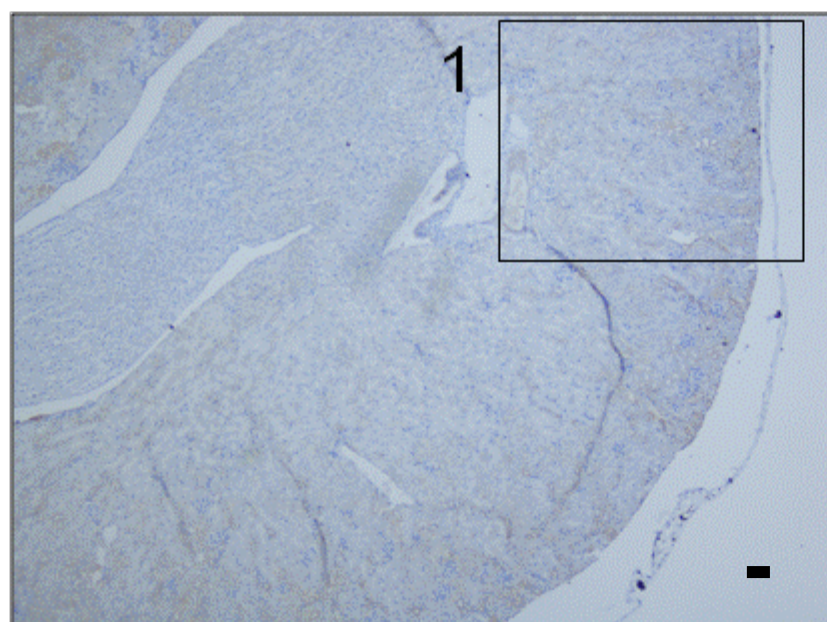
P0

BAK

8 Gray

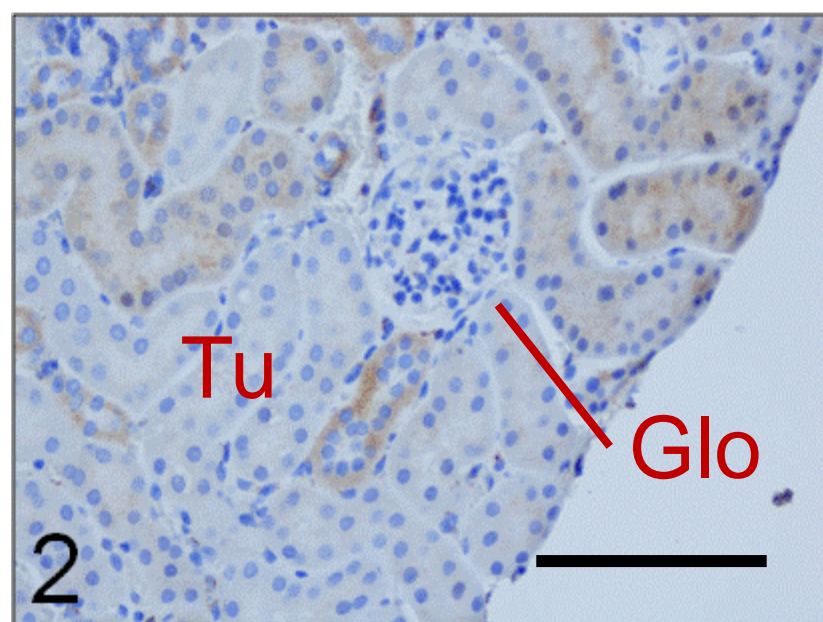
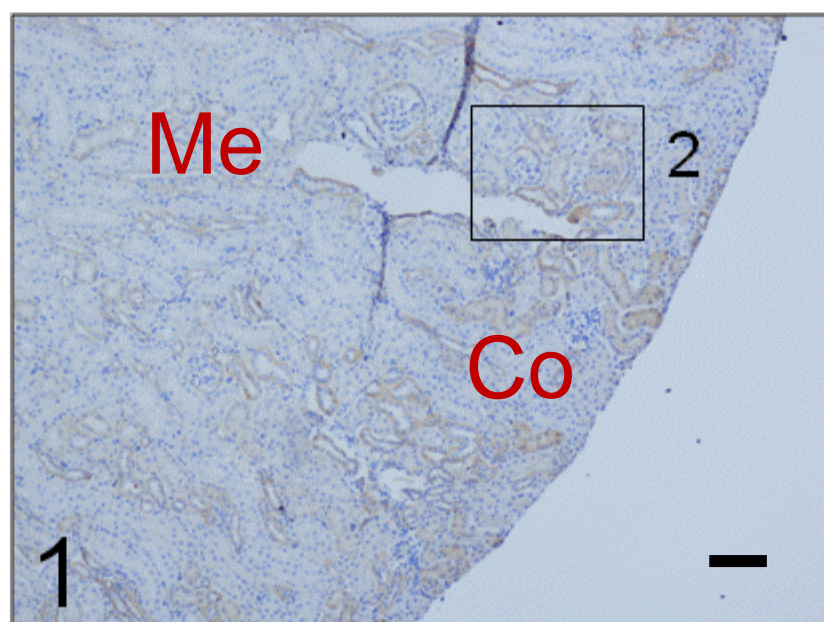
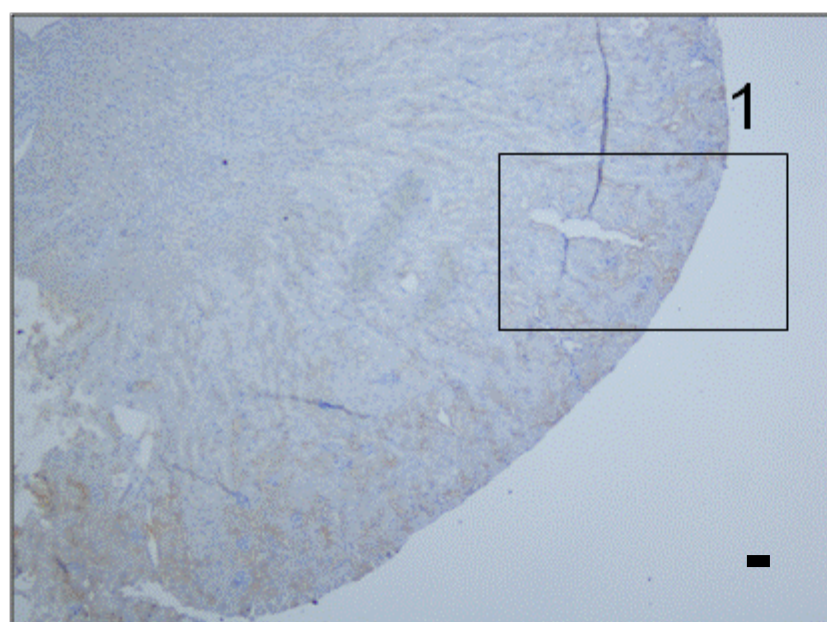


Sham



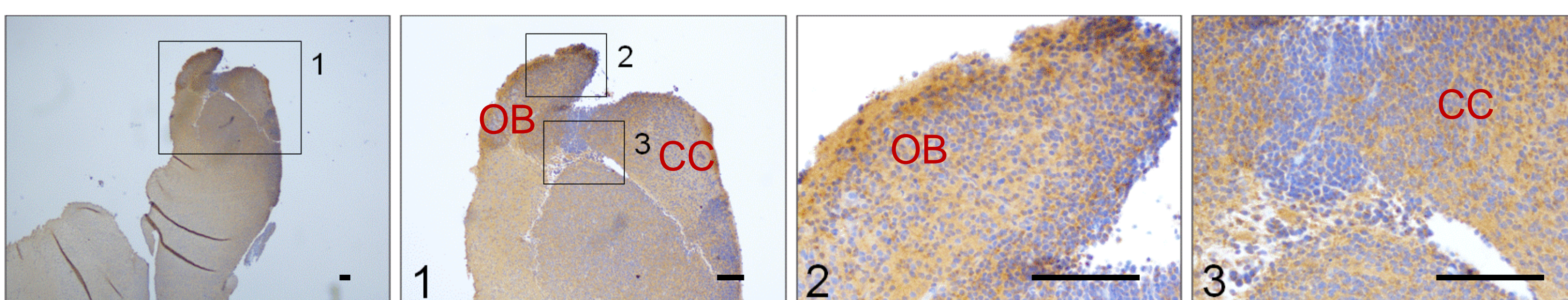
Adult

8 Gray



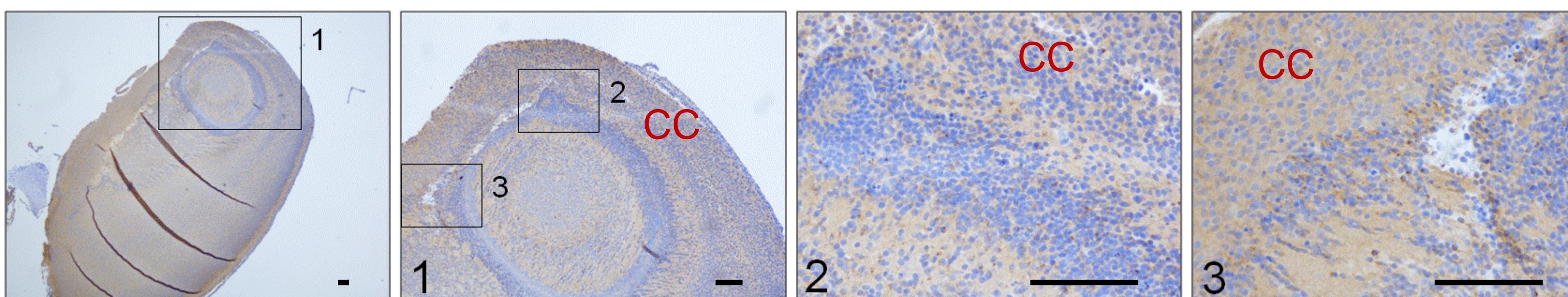
D

Sham



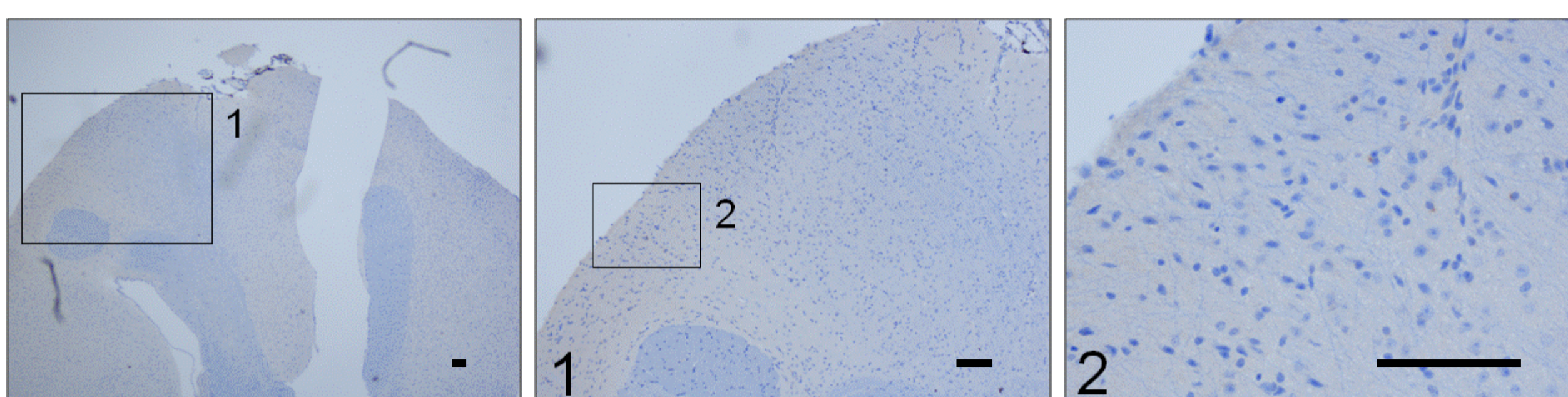
P0

8 Gray



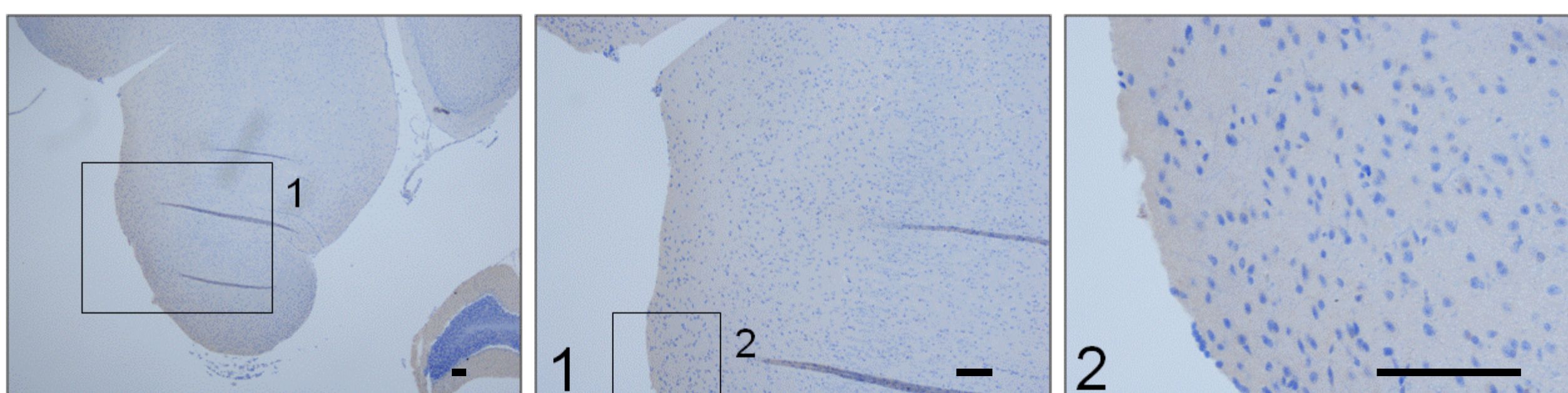
BAX

Sham

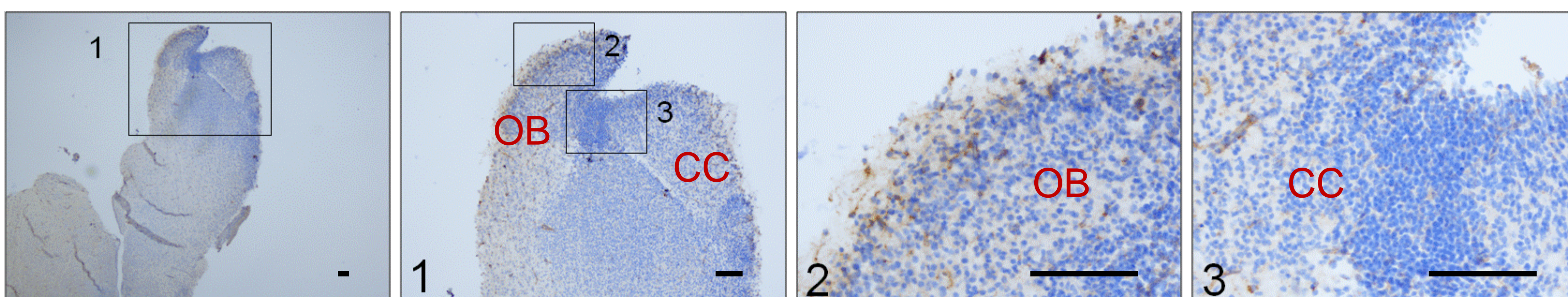


Adult

8 Gray

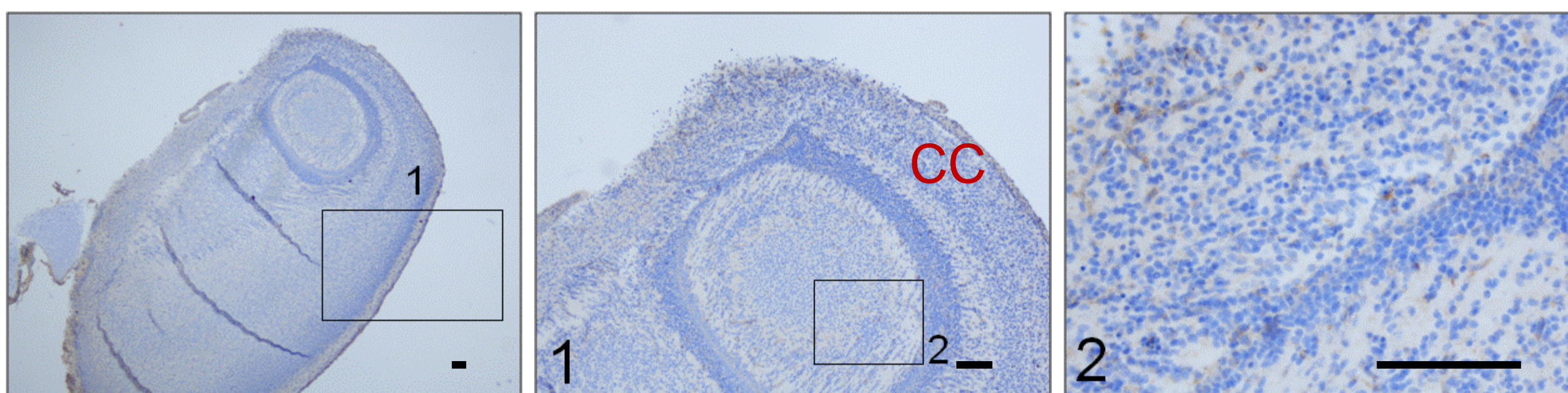


Sham



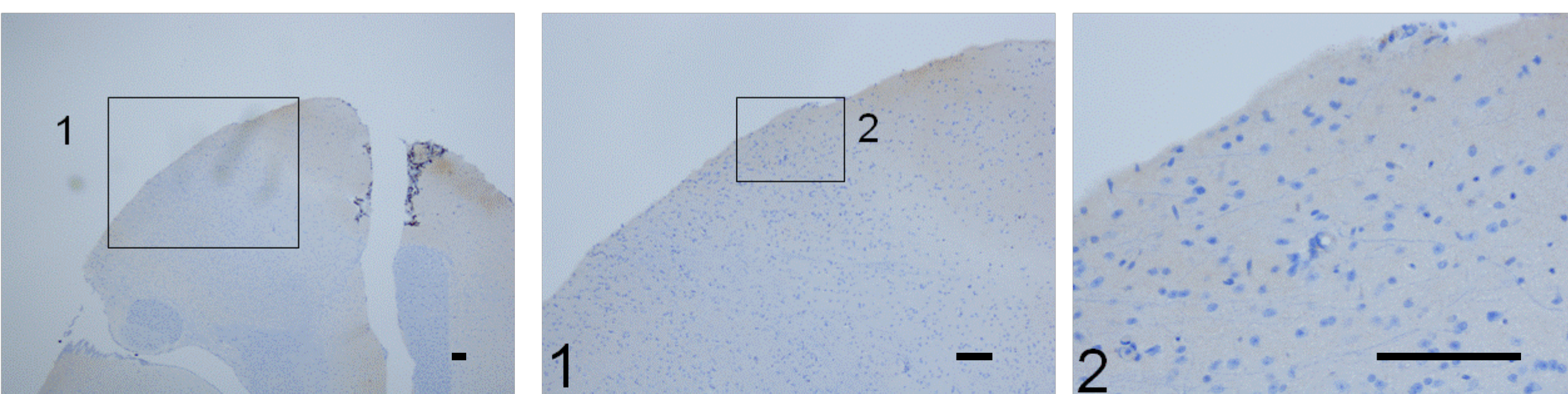
P0

8 Gray



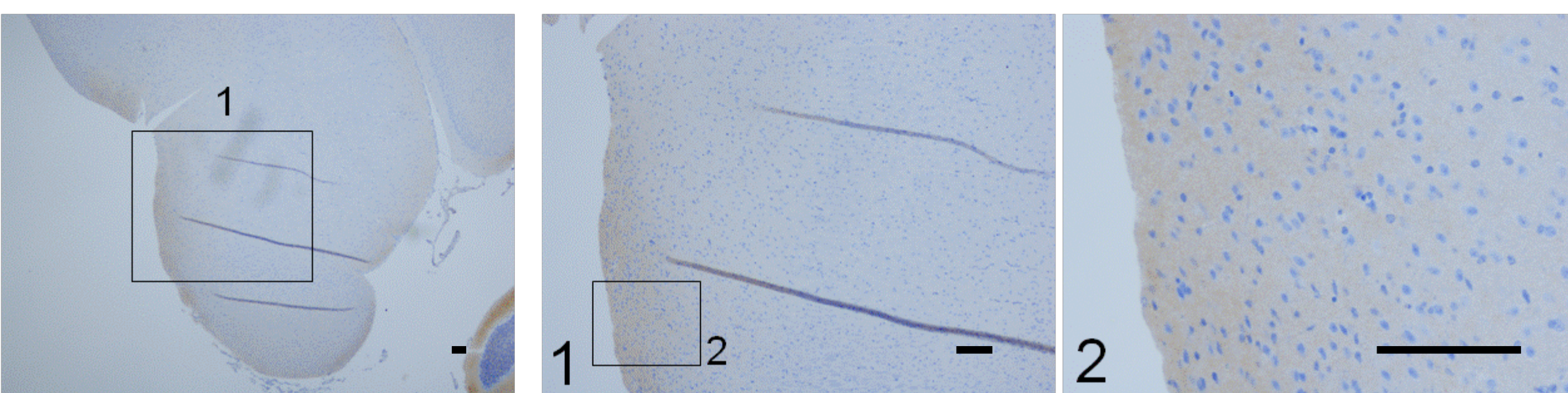
BAK

Sham



Adult

8 Gray



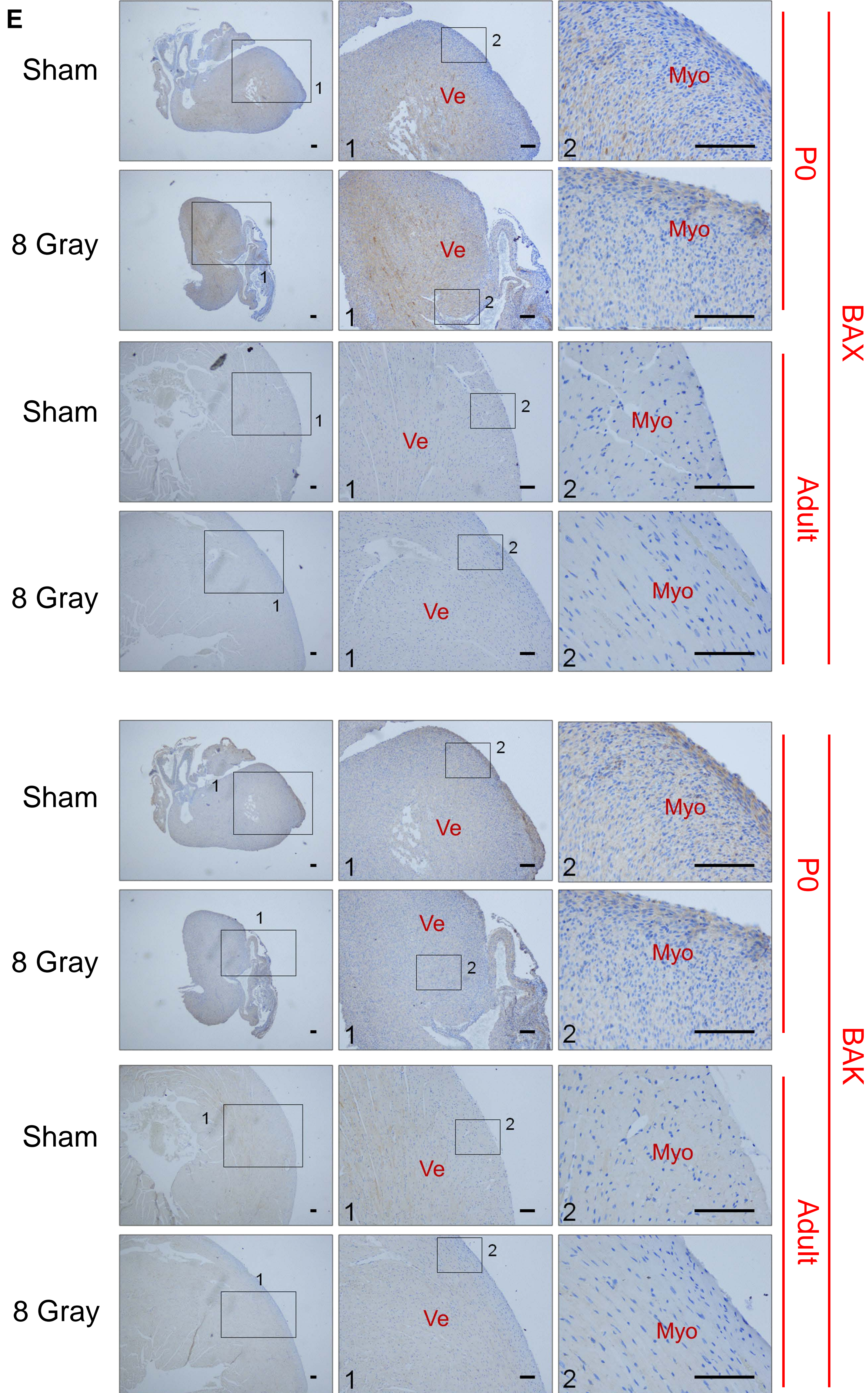
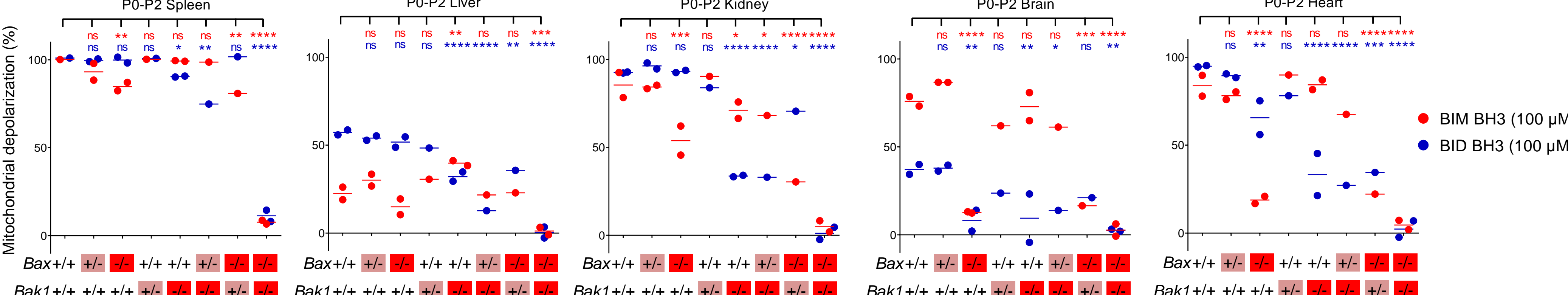


Figure S3: Detection of BAX and BAK in sham treated or irradiated tissue from adult or early postnatal mice (Related to Figure 4). After whole body irradiation, BAX and BAK were stained in the spleen (A), liver (B), kidney (C), brain (D) and heart (E). Brown staining indicates detection of the indicated protein. (A) “RP” designates red pulp while “WP” designates white pulp within spleen. (B) “TEV” designates terminal hepatic venule; “HP” designates hepatocyte plates; “HC” designates hematopoietic cells. (C) “Co” designates kidney cortex; “Me” designates kidney medulla; “Tu” designates tubules; “Glo” designates Glomerulus. (D) “OB” designates olfactory bulb while “CC” designates cerebral cortex. (E) “Ve” designates ventricle while “Myo” designates myocardium. All images are representative of two independent experiments. Scale bars are 200 μ m.

A



B

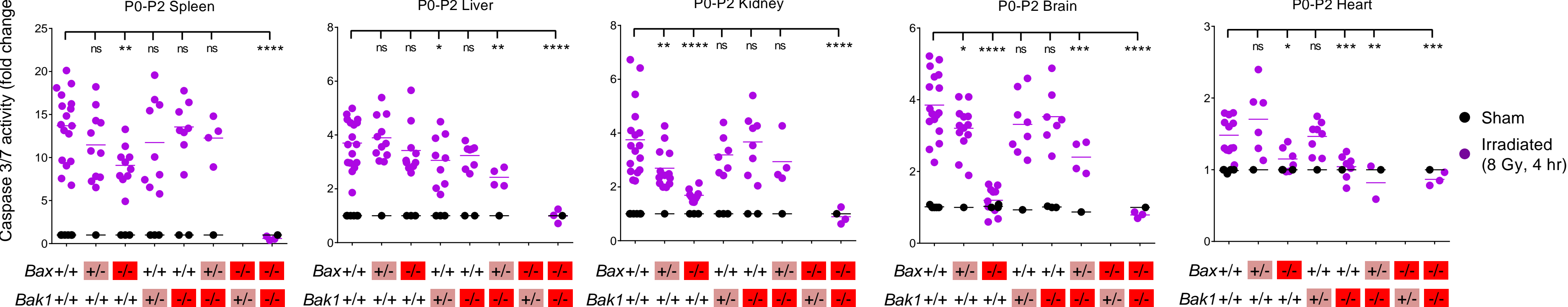
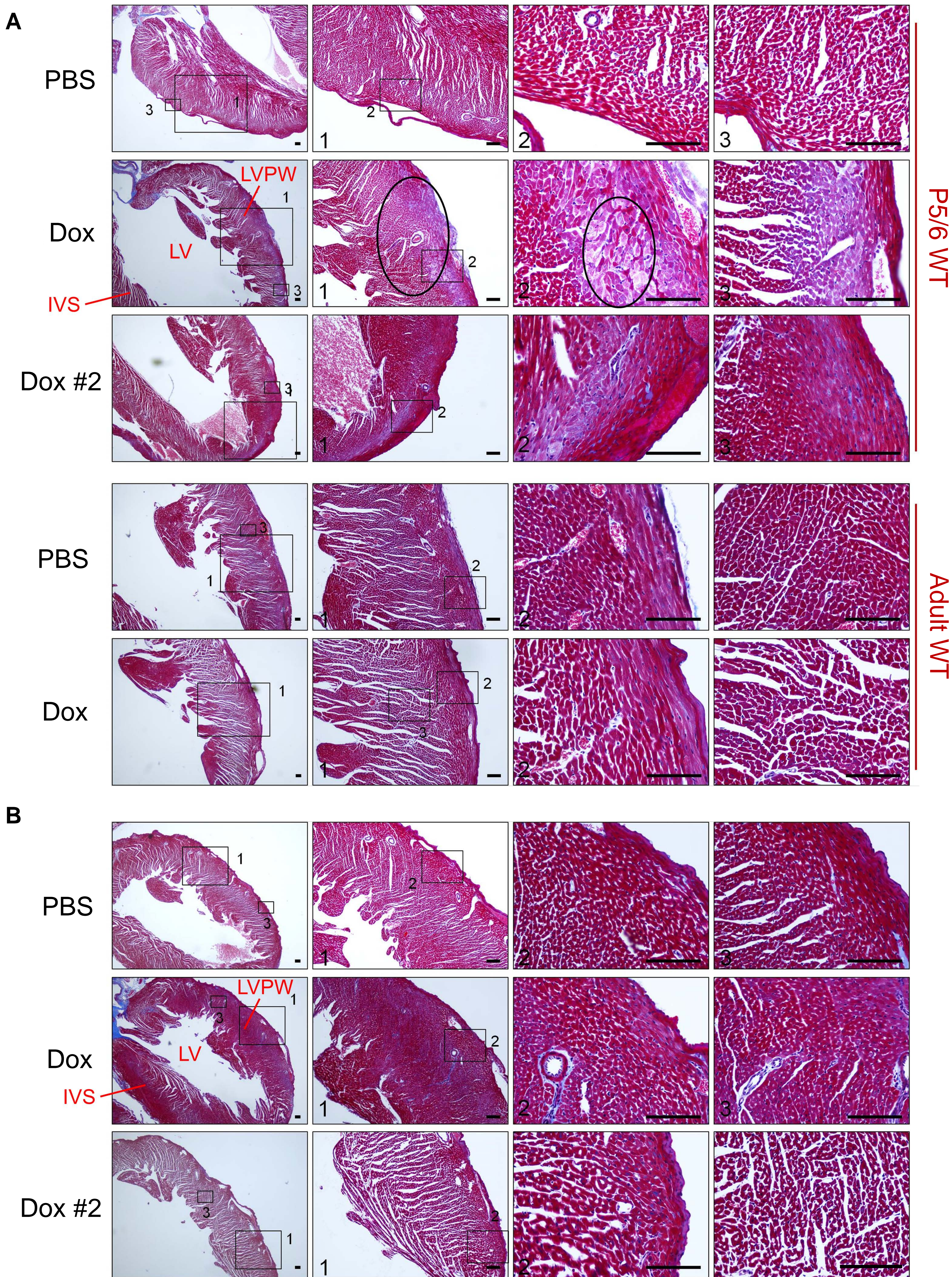


Figure S4: BAX and BAK dependence in early postnatal mouse tissues (Related to Figure 5). (A) Summary BH3 Profiling data from P0-P2 mouse tissues of indicated genotypes. Each point represents the mean of 3 measurements in each tissue across 4 IEs. Horizontal bars represent means. (B) Summary caspase 3 activity data from P0-P2 mouse tissues after whole body irradiation. Each point represents an average of 3 measurements in each tissue across 11 IEs. Horizontal bars represent means.



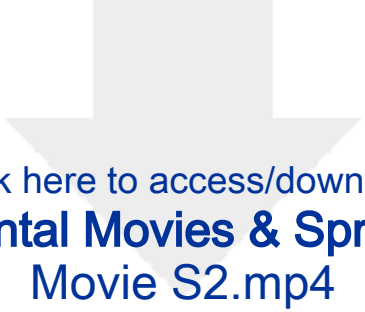
Movie S1: Echocardiogram of WT mouse treated with PBS starting at P5 (Related to Figure 6). Provided as a movie in supplemental materials. A WT mouse was treated with three doses of PBS on day 0, 4, and 7, starting at postnatal day 5 (P5). Echocardiogram was performed at day 14. Movie depicts parasternal long-axis view of beating heart. Normal interventricular septal wall and posterior wall thickness can be observed, along with normal ejection fraction (measurement of how much blood the left ventricle pumps out with each contraction).

Movie S2: Echocardiogram of WT mouse treated with doxorubicin starting at P5 (Related to Figure 6). Provided as a movie in supplemental materials. A WT mouse was treated with three doses of doxorubicin (5mg/kg) on day 0, 4, and 7, starting at postnatal day 5 (P5). Echocardiogram was performed at day 14. Movie depicts parasternal long-axis view of beating heart. Reduced interventricular septal wall and posterior wall thickness can be observed, along with reduced ejection fraction (measurement of how much blood the left ventricle pumps out with each contraction).



[Click here to access/download](#)

Supplemental Movies & Spreadsheets
Movie S1.mp4



[Click here to access/download](#)

Supplemental Movies & Spreadsheets
Movie S2.mp4




Table S3: Human brain specimen details (Related to Figure 7).

Sample ID	Secondary ID (if applicable)	Age	Months post conception	Diagnosis	Laterality	Brain Region	Surgery	BIM BH3 (100μM)	BID BH3 (100μM)
25	N/A	0 years, 4 months	14	Diffuse cortical dysplasia	Right	Temporal lobe	Temporal lobectomy	35.4%	47.5%
4	N/A	0 years, 9 months	19	Sturge-Weber syndrome	Left	Anterior temporal lobe	Functional hemispherectomy	36.2%	32.9%
23	A	0 years, 9 months	19	Perinatal stroke	Left	Medial temporal lobe	Functional hemispherectomy	22.3%	16.6%
23	B	0 years, 9 months	19	Perinatal stroke	Left	Lateral temporal lobe	Functional hemispherectomy	27.5%	13.9%
24	N/A	0 years, 11 months	21	Focal cortical dysplasia	Left	Hippocampus	Anterior temporal lobectomy	26.9%	22.6%
8	N/A	1 year, 0 months	22	Tuberous sclerosis	Left	Temporal lobe	Anterior temporal lobectomy	21.3%	26.7%
3	N/A	1 year, 0.5 months	22.5	Perinatal stroke	Left	Hippocampus	Hemispheric disconnection	24.5%	40.1%
8	N/A	1 year, 7 months	29	Tuberous sclerosis	Left	Lateral temporal lobe	Temporal lobectomy	26.5%	19.3%
14	N/A	1 year, 7 months	29	Focal cortical dysplasia; not otherwise specified	Right	Frontal lobe	Hemispheric disconnection	25.4%	28.4%
18	N/A	1 year, 7 months	29	Focal cortical dysplasia; not otherwise specified	Left	Frontal lobe	Frontal resection	15.6%	16.3%
11	N/A	1 year, 9 months	31	Focal cortical dysplasia IIa	Left	Frontal lobe	Frontal resection	25.9%	26.5%
12	N/A	2 years, 6 months	40	Focal cortical dysplasia; not otherwise specified	Left	Frontal lobe	Functional hemispherectomy with posterior disconnection	20.4%	22.9%
2	N/A	3 years, 10 months	56	Malformation of cortical development	Right	Lateral temporal lobe	Modified perisylvian functional hemispherectomy	22.1%	16.0%
16	B	5 years, 3.5 months	73.5	Focal cortical dysplasia IIa	Left	Intermdiate temporal lobe	Temporal lobectomy	22.6%	19.9%
16	C	5 years, 3.5 months	73.5	Focal cortical dysplasia IIa	Left	Lateral temporal lobe	Temporal lobectomy	17.6%	11.8%
17	A	5 years, 7 months	77	Focal cortical dysplasia Ia	Left	Lateral temporal lobe	Anterior temporal lobectomy	11.5%	6.5%
17	B	5 years, 7 months	77	Focal cortical dysplasia Ia	Left	Hippocampus	Anterior temporal lobectomy	7.7%	8.3%
17	C	5 years, 7 months	77	Focal cortical dysplasia Ia	Left	Parahippocampus	Anterior temporal lobectomy	12.9%	12.2%
7	N/A	5 years, 11 months	81	Rasmussen Encephalitis	Left	Lateral temporal lobe	Functional hemispherectomy	17.2%	21.2%
6	N/A	6 years, 11 months	93	Focal cortical dysplasia IIb	Right	Frontal lobe	Frontal resection	4.7%	19.1%
13	N/A	9 years, 4 months	122	Polymicrogyria	Left	Frontal lobe	Frontotemporal resection	13.8%	10.3%
15	B	14 years, 9 months	187	Stroke - gliosis	Left	Hippocampus	Functional hemispherectomy	2.0%	5.2%
15	C	14 years, 9 months	187	Stroke - gliosis	Left	Parietal lobe	Functional hemispherectomy	6.7%	2.0%
19	A	15 years, 8 months	198	prior tumor - gliosis	Right	Temporal lobe	Anterior temporal lobectomy	8.0%	7.0%
19	B	15 years, 8 months	198	prior tumor - gliosis	Right	Medial temporal lobe	Anterior temporal lobectomy	12.0%	10.0%
1	N/A	18 years, 10 months	236	Focal cortical dysplasia IIb	Left	Frontal lobe	Frontal resection	2.2%	13.8%
9	N/A	19 years, 1 month	239	Gliosis	Left	Temporal lobe	Anterior temporal lobectomy	7.8%	12.9%
10	N/A	21 years, 0 months	262	Trauma - gliosis	Right	Temporal lobe	Anterior temporal lobectomy	0.1%	5.9%
20	N/A	21 years, 0 months	262	Focal cortical dysplasia; not otherwise specified	Left	Temporal lobe	Temporal lobe resection	6.8%	0.3%

Supplemental Experimental Procedures

Mouse strains, breeding and treatments: The following mouse strains were used:

C57BL/6J (WT) (Jackson Laboratories #000664, Bar Harbor ME)

B6.129X1-Bax^{tm1}Sjk/J (*Bax* Knockout) (Jackson Laboratories #002994)

B6.129-Bak1^{tm1}Thsn/J (*Bak1* Knockout) (Jackson Laboratories #004183)

FVB/N-Gt(ROSA)26Sor^{tm1.1}(MYC/ERT2)^{Gev} (Rosa26-MycER^{T2}) (available upon request from Gerard Evan, Cambridge University). Heterozygous male and female mice were bred to produce WT, heterozygous and KO litter-matched animals for analysis. To produce double knockout mice (*Bax*^{-/-}, *Bak1*^{-/-}) (DKO), male and female *Bax*^{+/-}, *Bak1*^{-/-} mice were bred (DKO males and females as well as *Bax*^{-/-} males are sterile). DKO mice were born at Mendelian frequencies, as previously reported (Lindsten et al., 2000), but experienced frequent perinatal lethality, with only a subset surviving to adulthood. Genotypes were confirmed with PCR of DNA samples from tail snips (Transnetyx, Cordova TN). For irradiation experiments, litter-matched mice were placed in an acrylic irradiation pie cage (Braintree Scientific, Braintree MA) and irradiated in a Gammacell 40 “Extractor” (Best Theratronics Ltd., Ottawa, ON Canada) for the time required to deliver the desired dose. Acute doxorubicin (Sigma-Aldrich) treatments (to assess levels of apoptosis soon after dosing) were done by injecting litter-matched mice intraperitoneally (IP) with one dose of the agent at 25 mg/kg or an equal volume of saline. Animals were sacrificed 24 hr later and tissues were collected for downstream analysis (see below). Long-term doxorubicin treatments (to assess heart function via echocardiogram) were done by injecting litter-matched P5/6, P11/12 or adult (P60-P90) mice intraperitoneally with 3 doses of the agent at 5 mg/kg or an equal volume of saline on days 0, 4, and 7, followed by echocardiograms (see below) on day 14. For acute activation of MycER^{T2}, tamoxifen dissolved in peanut oil was injected daily at 40 mg/kg.

Human brain specimens: Patients underwent surgery for removal of seizure foci at Boston Children’s Hospital (Table S3) and resected tissues were first delivered to a neuropathologist for evaluation. If available, a de-identified sample (0.2-0.5 g) of brain tissue was provided to study investigators in PBS on ice and was immediately processed for BH3 Profiling. Part of the sample (0.1 g) was excluded for cryopreservation and was subsequently prepared for immunoblotting. The remaining brain tissue was dissociated by repeated pipetting until a single cell suspension was achieved and BH3 Profiled as outlined above.

Tissue isolation from mouse: All mice were euthanized by CO₂ asphyxiation (mice that were less than 14 days old were decapitated following CO₂ administration). To isolate relevant cells from spleen and thymus, organs were mechanically separated in cold PBS using a Potter-ELV tissue grinder (Wheaton, Millville NJ). For bone marrow, femurs were removed and cold PBS was pipetted into one end and allowed to flow through into a collection receptacle and subjected to red blood cell (RBC) lysis using RBC lysis reagent (Qiagen, Germantown MD) according to manufacturer’s instructions. For peripheral blood mononuclear cells (PBMCs), blood was collected from the mouse immediately post mortem, pipetted into cold PBS and subjected to RBC lysis. For heart, kidney, liver, small intestine, large intestine, and lungs, the organ was first coarsely separated and placed into 50 mL of cold PBS, vortexed and then strained through a 70 µM filter to remove leukocytes

and cell debris (flow through). Tissue remaining in the strainer was then mechanically separated using a Potter-ELV tissue grinder. For brain, tissue was placed into cold PBS and repeatedly pipetted (~20 times) until completely dissociated. Aliquots of single cell suspensions were immobilized on a glass slide using cytospin protocol (ThermoFisher Scientific, Waltham MA) stained with Jorvet Dip Quick Stain (Jorgensen Laboratories, Loveland CO), and examined by a trained pathologist (D.R.C.) for >95% purity (less than 5% of cells of hematopoietic origin). In many tissues, all cells analyzed were of the same type, such as hepatocytes in the liver and cardiomyocytes in the heart. Processing time and protocols per tissue type did not differ between neonatal and adult tissues, and total number of tissues processed in batches was limited to ensure processing time was kept below a maximum of 2 hr from time of tissue collection to start of downstream applications including BH3 Profiling or lysate preparation.

Fluorescence-based BH3 Profiling: 15 μ L of BH3 peptides or recombinant proteins (see below for peptide sequences) in T-EB (300 mM Trehalose [Sigma-Aldrich, St. Louis MO], 10 mM Hepes-KOH pH 7.7 [Sigma-Aldrich], 80 mM KCl [Sigma-Aldrich], 1 mM EGTA [Sigma-Aldrich], 1 mM EDTA [Sigma-Aldrich], 0.1% BSA [Sigma-Aldrich], and 5 mM succinate [Sigma-Aldrich]) was deposited into each well in a non-treated, black 384-well plate, 1 treatment per well, in triplicate for each independent experiment. Single cell suspensions were washed once with T-EB before being resuspended at 4X their final density of 6.75×10^5 cells/mL. One volume of the 4X cell suspension was added to one volume of a 4X dye solution containing 4 μ M JC-1 (Enzo Life Sciences, Farmingdale NY), 40 μ g/ml oligomycin (Sigma-Aldrich), 0.02% digitonin (Sigma-Aldrich), and 20 mM 2-mercaptoethanol (Life Technologies) in T-EB. The resulting 2X cell/dye solution was kept at room temperature for 5 min to allow for cell permeabilization and dye equilibration. 15 μ L of the 2X cell/dye mix was then added to each treatment well of the 384-well plate, shaken for 15 seconds inside the plate reader, and the fluorescence at 590 nm was measured every 5 min at 32°C. Peptide treatments that were used corresponded to the BH3 domains of the BCL-2 family proteins, and their respective sequences are as follows: BIM: MRPEIWIAQELRRIGDEFNA; BID: EDIIRNIARHLAQVGDSMDR (New England Peptide, Gardner MA). Relative mitochondrial depolarization was defined as the magnitude of mitochondrial depolarization resulting from BH3 peptide treatment as compared to vehicle DMSO (Sigma-Aldrich) and positive control FCCP (p-trifluoromethoxy carbonyl cyanide phenyl hydrazone) (Sigma-Aldrich). The percentage of mitochondrial depolarization was calculated by comparing the JC1 signal (mitochondrial polarization) in cells treated with each peptide or protein concentration in the following manner:

$$\% \text{ Mitochondrial Depolarization} = [R(t) - F(t)] / [R(t) - \text{FCCP}(t)] * 100$$

where R(t) is the fluorescence value in the reference sample (DMSO), F(t) is the fluorescence value in the test sample (peptide or protein) and FCCP(t) is the fluorescence value in the positive control sample (FCCP) at a time (t) and averaged during the course of the BH3 Profiling assay (from t=20 to 120 min).

Immunoblotting: Immunoblotting was performed as previously described (Montero et al., 2015) Briefly, protein lysates were obtained by cell lysis in Radio Immuno Precipitation Assay (RIPA) buffer (150 mM sodium chloride, 1.0% NP-40, 0.5% sodium deoxycholate,

0.1% sodium dodecyl sulphate, 50 mM Tris, pH 8.0). Protein loading was measured by Protein Assay Dye Reagent (Bio-Rad). Protein samples were electrophoretically separated on NuPAGE 4-12% Bis-Tris polyacrylamide gels (Invitrogen). Heatmaps were generated by normalizing band intensity to loading control (GAPDH). Antibodies used include: BAX (Cell Signaling Technology #2772, Danvers MA); BAK NT (Millipore, Billerica MA); BIM (Cell Signaling Technology #C34C5); BID (clone 11958), BCL-2 3F11 (BD Biosciences, San Jose CA), BCL-X_L (Cell Signaling Technology #2764), MCL-1 (Rockland Immunochemicals, 600-401-394S), APAF-1 (BD Biosciences), Caspase 3 (Cell Signaling Technology #8G10), Caspase 8 (Cell Signaling Technology #4790), Caspase 9 (Cell Signaling Technology #9508), VDAC (Cell Signaling Technology #4661), XIAP (BD Biosciences #610763), CIAP1 (Cell Signaling Technology #4952), c-Myc (Cell Signaling Technology #13987, Santa Cruz Biotechnology #sc-764, Dallas TX), GAPDH (Cell Signaling Technology #5174).

Echocardiograms: Echocardiograms were obtained at 14 days following initiation of sham or doxorubicin treatment with a Vevo 2100 Imaging digital ultrasound system (VisualSonics, Toronto ON Canada) using a 22-55 MHz (MS550D) for adult and 30-70 MHz (MS700) transducer for neonatal mice, as previously described (Bauer et al., 2011). Prior to echocardiography, each mouse chest wall was shaved. Adult and neonatal mice were then placed on a heated platform in the supine position. Echocardiographic analysis was performed on mice receiving oxygen at a heart rate between 400 and 700 beats/min. Data acquisition was initiated with the parasternal cardiac long axis view followed by transition to a short axis view, at the level of mid-papillary muscles. Echocardiographic measurements were obtained from short axis B-mode images. All data were acquired and analyzed in a blinded fashion.

In vitro chemosensitivity assays: For drug-induced, in vitro chemosensitivity assays, neurons were plated in 48-well plates and treated with indicated concentrations of Doxorubicin or Staurosporine (Sigma-Aldrich) for 24 hr. Caspase 3/7 Glo Assay (Promega, Madison WI) was then performed according to manufacturer's instructions and luminescence was measured on a Safire2 microplate reader (Tecan, Männedorf Switzerland). Luminescence readings were normalized to untreated control cells.

Human protein expression data: Fourier-transform mass spectrometry protein expression data in adult and fetal human tissues generated by Kim, et al. (Kim et al., 2014), was downloaded via the humanproteomemap.org website on November 11th, 2014 and again on June 1st, 2015 for local analysis. Expression of relevant proteins in adult and fetal tissues was assessed by examining peptide-level data for each protein, with data excluded from any peptides that were not gene-specific (Table S1 and S2). Spectral counts for all gene-specific peptides were summed and heatmaps were generated by normalizing to the summed spectral count of the tissue displaying the highest expression of each protein analyzed.

Gene expression data in human brain: RNA sequencing (RNA-Seq) data generated across 13 developmental stages in 8-16 brain structures by Miller, et al. (Miller et al., 2014) was downloaded via the brainspan.org website on December 17, 2013 for local analysis. mRNA expression of *BAX* was examined across all brain regions and from the earliest available data (8 weeks post conception) to adulthood (23 years of age). All samples were from

pathologically normal donors. Additional details and documentation is available at brainspan.org.

Statistical analysis: two-way ANOVA (including Fisher's Least Significant Difference [LSD] test for multiple comparisons) was performed using the GraphPad Prism software (GraphPad Software, La Jolla CA). Significance: * $p < 0.05$; ** $p < 0.01$; *** $p < 0.001$; **** $p < 0.0001$.

Rat primary hippocampal neuronal cultures: Neurons were prepared and grown as described previously (Minogue et al., 2009; Walsh et al., 2009). Hippocampi were explanted from E18 Sprague Dawley rat pups in Hank's balanced salt solution and dissociated using 0.25% trypsin (Invitrogen, Carlsbad, CA) for 16 min at 37°C. Neurons were plated at a density of 3×10^4 cells on the inner 24 wells of poly-D-lysine coated 48-well plates and cultivated in Neurobasal medium supplemented with 0.5 mM Glutamax-I (Invitrogen, Carlsbad, CA) and B27 with antioxidants (Invitrogen, Carlsbad, CA). Five days after plating, 20 μ M of 5-fluoro-2'-deoxyuridine was added to reduce glial proliferation. Cultures were kept in a humidified incubator at 37°C and 5% CO₂ and once per week half of the media was replaced with fresh Neurobasal medium containing 0.5 mM Glutamax-I and B27 with antioxidants (Kaeck and Banker, 2006). Every 3 days after plating, cells from a single well were collected using 0.25% trypsin, washed once with phosphate-buffered saline, and BH3 Profiled as outlined above.

Production and purification of cBID, BIML, and BAX: cBID was produced as previously described (Zha, 2000) with these modifications: 1) BID was cloned into pet16b; 2) cBID was eluted from the column with imidazole. For BIML, the cDNA encoding full-length wildtype murine BIML was cloned into pBluescript II KS(+) vector (Stratagene, Santa Clara CA). DNA sequences encoding a polyhistidine tag followed by a TEV protease recognition site (MHHHHHHGGSGGTGGSENLVYFQGT) and an intein/chitin-binding domain were added to the plasmid such that the new plasmid encoded a fusion protein with both an N-terminal His tag and Tev site and an intein/chitin-binding domain at the C-terminus of BIML. The recombinant construct was expressed in SoluBL21 Escherichia coli strain (Genlantis, San Diego CA). Lysis of E. coli was achieved by mechanical disruption with a French press. After affinity chromatography with a chitin column, intein self-cleavage and release of BIML from its fusion partner intein-CBD was initiated by incubation with buffer containing 100 mM β -mercaptoethanol for 36 hr. This process leaves no additional amino acid residues on the C-terminus of BIML. The elution fraction from chitin column was then applied to a Nickel-NTA column (Qiagen, Valencia CA) and BIML was eluted from the Ni column with buffer containing 20 mM HEPES (pH 7.4), 100 mM NaCl, 20% glycerol, 0.3% CHAPS, and 300 mM imidazole. The purified BIML protein was dialyzed against 20 mM HEPES (pH 7.4), 100mM NaCl and 20% glycerol, then flash-frozen and stored at -80 °C. Recombinant BAX was produced as previously described (Suzuki et al., 2000).

Immunohistochemistry: Tissues were collected from mice and immediately placed into 8% formaldehyde solution (Electron Microscopy Sciences, Hatfield PA) and incubated on a rotator for 24 hr at 4°C. The formaldehyde was then replaced with cold PBS and incubated for another 24 hr at 4°C and then stored at 4°C until analysis. Tissues were paraffin embedded and cut into 4 μ M-thick sections. Slides were stained on the Leica Bond III

autostaining platform using the Bond Polymer Refine Detection kit (Leica, Chicago, IL). Antigen retrieval was performed online using Bond Epitope Retrieval 1 (Leica, Chicago, IL) for 30 min. Slides were then incubated at room temperature with primary antibodies against Cleaved Caspase 3 (Cell Signaling Technology #9664), BAX (Cell Signaling Technology #2772) for 60 min, or BAK (Cell Signaling Technology #12105) for 30 min diluted in Bond Primary Antibody Diluent (Leica, Chicago, IL). Primary antibodies were detected with Post Primary, followed by Polymer-HRP reagents from the Polymer Refine Detection Kit. Slides were developed in Diaminobenzene for 10 min.

TUNEL: Formalin-fixed paraffin tissue sections were stained for terminal deoxynucleotidyl transferase-mediated dUTP nick end labeling (TUNEL) with the ApopTag Peroxidase In Situ Apoptosis Detection Kit (R&D Systems, Minneapolis MN) according to the manufacturer's instructions. At least five views in each slide were randomly selected and quantified for positive staining. Two animals in each group were studied. Results were presented as TUNEL-positive cells per 40X field of view.

Heart histology: Harvested hearts were arrested in diastole with 3 M KCl and fixed with 8% buffered formaldehyde solution and incubated on a rotator for 24 hr at 4°C. The formaldehyde was then replaced with cold PBS and incubated for another 24 hr at 4°C and then stored at 4°C until analysis. Hearts were then embedded in paraffin for analysis by histology. Samples were sectioned at the Histology Core Facility at Beth Israel Deaconess Medical Center. Masson's trichrome staining (MTS) was performed according to the manufacturer's protocol (Sigma-Aldrich, St Louis MO).

Flow-cytometry based BH3 Profiling with intracellular c-Myc staining: Tissues were collected and added to 500 μ L PBS on ice. To remove blood, samples were crudely separated, and vortexed in fresh, cold PBS solution three times. Samples were then removed from solution and mechanically separated until finely dissociated, at which time PBS was added to the sample and pipetted repeatedly for further dissociation. The samples, in solution, were then run through a 45 μ m filter to ensure single cell suspension. Samples were centrifuged for 5 min at 500xg, resuspended in FACS staining buffer (PBS, 2 mM EGTA, 2% FBS), and stained on ice for 15 min with AF594 anti-mouse CD45 antibody at 1:100 dilution (Biolegend #103144). Samples were then centrifuged for 5 min at 500xg and resuspended in Newmeyer buffer (300 mM Trehalose, 10 mM HEPES-KOH, 80 mM KCl, 1mM EGTA, 1 mM EDTA, 0.1% BSA, 5 mM Succinate, ph 7.7). Flow cytometry-based BH3 Profiling was then performed as previously described (Ryan and Letai, 2013). Samples were added to a 96 well, V-bottom plate (Corning #3897) containing titrated doses of the BIM and/or BID BH3 peptide and positive and negative controls, all in 0.02% digitonin. The plate was then incubated at 28°C for 1 hr. Peptide exposure was terminated by adding 8% formaldehyde in PBS at 1:4 ratio (2% final concentration of formaldehyde). After 15 min, formaldehyde was neutralized with N2 buffer (1.7 M Tris base, 1.25 M Glycine, ph 9.1). 4x Intracellular Staining buffer with TritonX-100 (PBS, 1% Saponin, 10% BSA, 20% FBS, 0.02% Sodium Azide, 2% TritonX-100) was added to each well. The following antibodies were added to all wells except for unstained control wells at the dilutions indicated: Cytochrome c at 1:1000 (ThermoFisher, clone 6H2.B4 with AF647 tag), Hoechst 33342 at 1:2000 (Life technologies #H3570), c-Myc at 1:1000 (Cell Signaling Technology #13987 [rabbit mAb]). Plate was sealed with an adhesive cover and left to stain

overnight at 4°C. Plate was then centrifuged at 500xg for 5 min and the wells were aspirated, leaving behind the cell pellet. Cell pellet was washed once in FACS staining buffer, centrifuged again, and resuspended in 4x Intracellular Staining buffer with TritonX-100 containing anti-rabbit IgG secondary antibody with AF488 tag at 1:1000 (Life technologies #A11070). Plate was sealed with an adhesive cover and left to stain overnight at 4°C. Plate was then centrifuged at 500xg for 5 min and washed with FACS staining buffer twice, then cells were resuspended in FACS staining buffer for analysis on a BD Biosciences LSR II flow cytometer (BD Biosciences).

ChIP-qPCR: Analysis of Myc occupancy on enhancer boxes of promoters of genes of interest was carried out using Active Motif's ChIP-IT qPCR Analysis Kit (Active Motif, Carlsbad, CA) according to manufacturer's instructions using 30 ug of mouse tissue chromatin from each organ (P0 spleen, liver, heart, kidney and brain; adult spleen, kidney and brain) and 25 ul of anti-c-Myc antibody (Santa Cruz Biotechnology sc-764). qPCR was performed using one positive control primer pair (Mybbp1a) and a negative control primer pair that amplifies a region in a gene desert on chromosome 6 (Untr6), as well as the regions spanning E-boxes in genes of interest.

Immune-system mediated liver damage: Age-matched adult mice were injected intravenously with Concanavalin A (Sigma-Aldrich) at 15 mg/kg or vehicle. Injections took place 24, 48, 72, 96, and 120 hr before tissue collection. All mice were culled simultaneously and their livers were collected and processed for flow-cytometry based BH3 Profiling as outlined above.

Supplemental References

Bauer, M., Cheng, S., Jain, M., Ngoy, S., Theodoropoulos, C., Trujillo, A., Lin, F.C., and Liao, R. (2011). Echocardiographic speckle-tracking based strain imaging for rapid cardiovascular phenotyping in mice. *Circ. Res.* 108, 908–916.

Kaech, S., and Banker, G. (2006). Culturing hippocampal neurons. *Nat. Protoc.* 1, 2406–2415.

Kim, M.-S., Pinto, S.M., Getnet, D., Nirujogi, R.S., Manda, S.S., Chaerkady, R., Madugundu, A.K., Kelkar, D.S., Isserlin, R., Jain, S., et al. (2014). A draft map of the human proteome. *Nature* 509, 575–581.

Lindsten, T., Ross, a J., King, a, Zong, W.X., Rathmell, J.C., Shiels, H. a, Ulrich, E., Waymire, K.G., Mahar, P., Frauwirth, K., et al. (2000). The combined functions of proapoptotic Bcl-2 family members bak and bax are essential for normal development of multiple tissues. *Mol. Cell* 6, 1389–1399.

Miller, J. a, Ding, S.-L., Sunkin, S.M., Smith, K. a, Ng, L., Szafer, A., Ebbert, A., Riley, Z.L., Royall, J.J., Aiona, K., et al. (2014). Transcriptional landscape of the prenatal human brain. *Nature* 508, 199–206.

Minogue, A.M., Stubbs, A.K., Frigerio, C.S., Boland, B., Fadeeva, J. V, Tang, J., Selkoe,

D.J., and Walsh, D.M. (2009). gamma-secretase processing of APLP1 leads to the production of a p3-like peptide that does not aggregate and is not toxic to neurons. *Brain Res.* 1262, 89–99.

Montero, J., Sarosiek, K.A., DeAngelo, J.D., Maertens, O., Ryan, J., Ercan, D., Piao, H., Horowitz, N.S., Berkowitz, R.S., Matulonis, U., et al. (2015). Drug-Induced Death Signaling Strategy Rapidly Predicts Cancer Response to Chemotherapy. *Cell* 160, 977–989.

Ryan, J., and Letai, A. (2013). BH3 profiling in whole cells by fluorimeter or FACS. *Methods*.

Suzuki, M., Youle, R.J., and Tjandra, N. (2000). Structure of Bax: coregulation of dimer formation and intracellular localization. *Cell* 103, 645–654.

Walsh, D.M., Thulin, E., Minogue, A.M., Gustavsson, N., Pang, E., Teplow, D.B., and Linse, S. (2009). A facile method for expression and purification of the Alzheimer's disease-associated amyloid beta-peptide. *FEBS J.* 276, 1266–1281.

Zha, J. (2000). Posttranslational N-Myristoylation of BID as a Molecular Switch for Targeting Mitochondria and Apoptosis. *Science* (80-.). 290, 1761–1765.